AD-A055 253 EG AND G INC SALEM MASS F/G 9/1
REPETITIVE SERIES INTERRUPTER I:.(U)
APR 78 D V TURNQUIST, R SIMON DAAB07-76-C-1301
UNCLASSIFIED ECOM-76-1301-6 NL

1 OF 2
AD A055253

FOR FURTHER TRAN

See A051 608

(12)

Research and Development Technical Report

(18) (19) ECOM-76-1301-6

REPETITIVE SERIES INTERRUPTER II.

(6)

(10) David V. Turnquist
Robert Simon
EG&G INC.
35 Congress Street
Salem, MA. 01970

(12) 163 p.

(11) April 1978

(9) Sixth Interim Report No. 6 for the Period Jan 1976 to Sept 1977

(16) 1L162705AH94 (17) E1

(15) DAAB07-76-C-1301

Prepared for:

ECOM

US ARMY ELECTRONICS COMMAND FORT MONMOUTH, NEW JERSEY 07703

390 408

NOTICES

Disclaimers

The findings in this report are not to be construed as an official Department of the Army position, unless so designated by other authorized documents.

The citation of trade names and names of manufacturers in this report is not to be construed as official Government indorsement or approval of commercial products or services referenced herein.

Disposition

Destroy this report when it is no longer needed. Do not return it to the originator.

UNCLASSIFIED

SECURITY CLASSIFICATION OF THIS PAGE (When Data Entered)

REPORT DOCUMENTATION PAGE		READ INSTRUCTIONS BEFORE COMPLETING FORM
1. REPORT NUMBER ECOM-76-1301-6	2. GOVT ACCESSION NO.	3. RECIPIENT'S CATALOG NUMBER
4. TITLE (and Subtitle) Repetitive Series Interrupter II		5. TYPE OF REPORT & PERIOD COVERED 6th Interim Technical Report Jan 76 to 30 Sep 77
		6. PERFORMING ORG. REPORT NUMBER
7. AUTHOR(s) David V. Turnquist Robert Simon		8. CONTRACT OR GRANT NUMBER(s) DAAB07-76-C-1301
9. PERFORMING ORGANIZATION NAME AND ADDRESS EG&G Inc., 35 Congress Street Salem, Massachusetts 01970		10. PROGRAM ELEMENT, PROJECT, TASK AREA & WORK UNIT NUMBERS 612705 1L1 62705.AH.94.E1.08
11. CONTROLLING OFFICE NAME AND ADDRESS US Army Electronics Technology & Devices Lab. ATTN: DELET-BG Fort Monmouth, New Jersey 07703		12. REPORT DATE April 1978 13. NUMBER OF PAGES 162
14. MONITORING AGENCY NAME & ADDRESS(if different from Controlling Office)		15. SECURITY CLASS. (of this report) Unclassified 15a. DECLASSIFICATION/DOWNGRADING SCHEDULE

16. DISTRIBUTION STATEMENT (of this Report)

Approved for Public Release; distribution unlimited

17. DISTRIBUTION STATEMENT (of the abstract entered in Block 20, if different from Report)

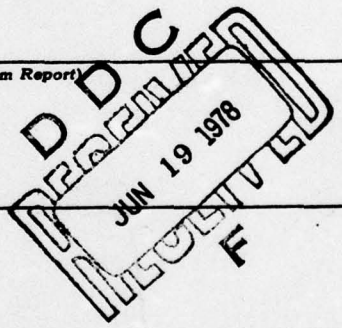

18. SUPPLEMENTARY NOTES

19. KEY WORDS (Continue on reverse side if necessary and identify by block number)

Series Interrupter
Gas Filled Device
Fuse
Thyratron
Magnetic Interaction Region

20. ABSTRACT (Continue on reverse side if necessary and identify by block number)

This report documents development work for the Repetitive Series Interrupter, a hydrogen thyratron modified for opening switch operation. Fault current interruption is provided by the magnetically controlled interaction of a hydrogen discharge with a wall surface in a suitably constructed interaction channel. Investigations herein reported measure the effects on interruption of regular and irregular wall surfaces as well as of the tube parameters of pressure and channel length, diameter, and geometry. Successful

DD FORM 1 JAN 73 1473 EDITION OF 1 NOV 65 IS OBSOLETE

UNCLASSIFIED

SECURITY CLASSIFICATION OF THIS PAGE (When Data Entered)

78 06 12 101

interruptions of 15 kV, 300 ampere fault pulses have been obtained in various chuted channel geometries using an effective magnetic field energy of 5 joules.

Optical observation of the discharge column and a theoretical analysis of the positive column under crossed field conditions have been performed.

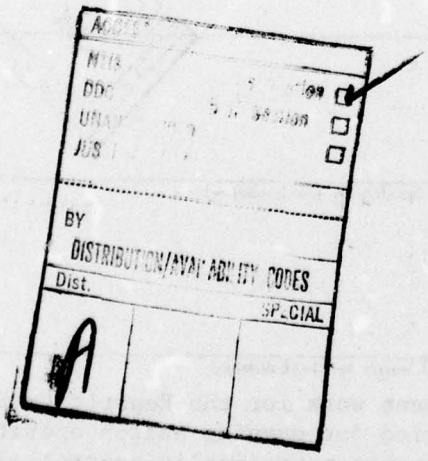

ABBREVIATIONS AND SYMBOLS

Bq	Magnetic field (in kilogauss) required for reducing fault current to zero
Ebb	Main supply voltage for tube under test
Ef	TUT cathode heater filament voltage
egk	Grid to cathode voltage
eic	Interaction channel voltage drop
ξj	Interrupting magnetic field energy within the RSI interaction channel volume
Em	Magnet supply voltage
epy	Instantaneous full voltage across tube under test
Eres	TUT hydrogen reservoir voltage
Eq	Magnet circuit voltage required for quenching fault current
etd	TUT voltage drop during normal pulse operation
ib	Peak RSI-carried current
Ib	Average tube current
im	Magnet current
iRSI	RSI-carried current, as a function of time
L	Length of interaction tube used during test
m	Empirical exponent of proportionality between Bq and 1/L
MCCD	Magnetically-Controlled Charging Diode
N	Number of turns in magnet coil
P	TUT pressure
prr	TUT pulse repetition rate
r	Radius of interaction tube
Rcct	Resistance of magnetic field probe circuit
Rchoke	Resistance of magnetic field probe circuit integrating inductor
Rm	Magnet circuit load resistance
Rl	Pulse-forming network load resistance
Rrc	Fault network load resistance
τD	Time delay between TUT fire and magnet fire
τr	Magnetic field risetime
TUT	Tube under test
β	Empirical exponent of proportionality between Bq and Ebb
δ	Empirical exponent of proportionality between Bq and ib
Δtad	Full range of deviation of delay time drift for tube fire

SYMBOLS USED IN POSITIVE COLUMN ANALYSIS

a	Discharge diameter during magnetic constriction
b	Discharge breadth during magnetic constriction
B	Magnetic field strength
D	Electron diffusion coefficient
e	Electron charge
$\vec{E}$	Electric field
$E_{x,y,z}$	Electric field components
f	Average fraction of energy lost by an electron in a neutral particle collision
f_i	Ionization rate per electron
$\vec{J}$	Current density
$J_{x,y,z}$	Current density components
k	Boltzmann's constant
$L_{x,y,z}$	Positive column dimensions
m_e	Electron mass
$n_{e,i}$	Electron, ion concentration
$T_{e,i}$	Electron, ion temperature
x_*	Position of maximum electron density
$\vec{V}_{e,i}$	Electron, ion velocities
Z	Atomic number of gas species (for hydrogen set = 1)
α,β	Parameters derived in the solution of the equation for n_e
Λ	Characteristic diffusion length
$\mu_{e,i}$	Electron, ion mobility = $\dfrac{e}{m_{e,i}\ \nu_{ce,ci}}$
$\nu_{ce,ci}$	Collision frequency of electrons, ions with neutral hydrogen
ν_i	Electron ionization frequency
Ω_{e,H^+}	Electron, H^+ cyclotron frequencies

TABLE OF CONTENTS

LIST OF ILLUSTRATIONS

LIST OF TABLES

1.0 FOREWORD

This report documents work performed from 26 January 1976 through 30 September 1977 under Phase I of Contract DAAB07-76-C-1301, entitled "Repetitive Series Interrupter II." (RSI 10 series data taken subsequent to 30 September 1977 are also included in this report to provide a complete discussion.) The objective of this program has been to obtain an improved exploratory development model of the 15-kV series interrupter. The efforts herein described were performed by EG&G, Inc., Electronics Components Division, Salem, Massachusetts, for the United States Army Electronics Command, Fort Monmouth, New Jersey.

2.0 INTRODUCTION AND SUMMARY

a. Program Objective

The purpose of the Repetitive Series Interrupter Research and Development Program is to develop a hydrogen thyratron type of device modified to provide current interrupting capability by the application of a transverse magnetic field across an interaction channel contained within the tube. The interrupter is intended to function as a protective device to prevent a high-voltage, high-current fault from causing damage to a circuit component in series with the interrupter such as a traveling wave tube.

The specific objective of Phase I of the program was to investigate the feasibility of the Technical Guidelines, established by the Electronics Technology and Device Laboratory, entitled "Repetitive Series Interrupter II," dated 24 June 1974. Technical Guidelines for Phase II are given in subsection 6.b.

Technical Guidelines for Phase I are:

Open circuit holdoff voltage	Ebb	15 kV minimum
Closed voltage drop	etd	350 volts maximum
Peak fault current	iRSI	300 amps maximum
Normal average current	Ib	0.8 amp minimum
Normal peak current	ib	25 amps maximum
Repetition rate	prr	5,000 Hz maximum
Life	—	1,000 hours minimum
Fault interruptions	—	20,000 minimum
Interruption magnetic field energy	ξj	50 joules maximum

The feasibility of the Technical Guidelines of Phase I has been substantially established, and six prototype devices have in fact been built, five capable of operation at 15 kV, 300 amperes, and one designed (but as yet untested) to operate at 30 kV, 300 amperes. Magnetic fields below 4 kilogauss (magnetic field switching energy of 5 joules) have been shown to be capable of interrupting discharges of 300 amperes at 15 kV in interaction channels producing a column drop of 350 to 450 volts. (Initial results obtained during Phase II have shown that currents as high as 600 amperes at 20 kV can be interrupted with comparable magnetic fields.)

Because the RSI is basically a hydrogen thyratron modified for magnetic current interruption, many long-established techniques for the construction of ceramic-metal hydrogen thyratrons are directly applicable to RSI's. Therefore, no difficulties are expected with other aspects of the Technical Guidelines such as normal average current, pulse repetition rate, etc., since they are well within the capabilities of standard production ceramic-metal tubes.

The extensive experimental and theoretical studies reported here have provided considerable insight into those parameters which are most important to RSI operation, and various trade-offs essential to generate a practical design have been identified.

b. Background

Initial work on a magnetically controlled gas discharge device was performed at EG&G, Inc. from 1964 through 1967 under Contract DA28-043-AMC-00123(E) (13), New Switching Concepts. The feasibility of current interruption at power levels up to 400 amperes at 15 kV was demonstrated in an 11-inch folded linear interaction column at tube pressures generally as low as 0.14 torr, which is considerably below customary thyratron operating pressure levels. No attempt was made in the above study to provide continued voltage holdoff capability after interruption.

Related development efforts continued at EG&G under Contract DAAB07-73-C-0274, 1973 Magnetically Controlled Charging Diode Program. During this program, long, folded interaction channels were appended to the anodes of several production thyratron designs. Problems associated with these tubes included (1) high voltage drop and tube jitter, when operated in a triggered (zero keep-alive) mode; and (2) an apparent operating requirement of high tube pressure and triggering voltage.

The Repetitive Series Interrupter Program began in 1973 at ITT (Contract DAAB07-73-C-0320) (11). A post-anode coaxial interaction channel geometry was studied. Although currents of 200 amperes were interrupted at 15 kV, the use of an air core magnetic field "window coil" over the large coaxial tube volume resulted in an impractically high magnetic switching energy of 1,000 joules (capacitor discharge energy). The present study was therefore directed toward

improving the efficiency of the magnetic switch. The magnetic interaction section was placed between cathode and grid in the expectation of reducing tube drop and improving triggering capability. The decision was made to use a high permeability iron magnet core having an air gap into which the RSI is placed in order to improve the magnetic field efficiency by reducing the total field volume region. Further development of interaction channel geometries and a study of the mechanisms of current interruption were expected to furnish additional means of reducing the magnetic switching requirement.

c. Investigative Approach and Course of Development

To determine the best location for the magnetic interaction section within a thyratron body, i.e., between cathode and grid or between the grid-anode holdoff gap and a second anode (post-anode), tubes RSI 001 and RSI 002 were constructed (Figures 1 and 2). A demonstration of lower voltage drop and greater stability in the RSI 001 led to further development of this approach.

The RSI 003 (Figure 3), a five-section interaction channel tube, was constructed to provide a parametric study of the effects of interaction channel length, Ebb, ib, and tube pressure upon interruption requirements and pulse operation behavior. It was found that long interaction channels are inefficient, since the tube voltage drop increases linearly with channel length while the interrupting magnetic field energy decreases in inverse proportion to the square root of the channel length.

Based on this information, nonlinear interaction channels were examined. A chuted wall surface was devised in the RSI 005 (Figure 5) to allow the greater plasma-wall interaction surface area and the longer effective discharge length to reduce the magnetic switching energy without substantially increasing the tube voltage drop or reducing the stability. The RSI 005 accomplished this at low power operation, where the interrupting magnetic field level was reduced by up to 67%.

The RSI 10 series tubes (Figures 9, 10, and 11) resulted from a continuation of the study of nonlinear channels. A series of varying "plasma chute" depths and widths was designed in ceramic interaction sections. Results from

this series are preliminary, but indicate that an equivalent 67% or higher switching field reduction does again occur. A further reduction occurs in the RSI 10E1 which allows interruption at Ebb = 15 kV, ib = 100 amps at Bq as low as 1 kilogauss.

Simultaneously with the above-mentioned development program, a study was undertaken to determine the character of the interaction channel crossed-field gas discharge. Two components of this study were: 1) a theoretical investigation of plasma behavior in a transverse magnetic field, and 2) an experimental investigation via optical observations of the RSI 004 (Figure 4), a tube having a transparent glass interaction channel. Results of this study indicate agreement between experiment and theory in that a stable magnetically constricted discharge of an approximate dimension was predicted and observed. Certain particulars, however, including electron temperature effects, wall heating and outgassing, and parametric dependences of Bq, could disturb justification for the observed agreement (see subsection 4.b).

In addition to these studies, an empirical investigation of etd versus ξj was performed, indicating the options available for the preferred design result.

Two tests were performed to determine the proper gas fill for RSI operation. Deuterium and hydrogen were compared in the RSI 004 and in the RSI 003 and the MCCD 400D-250. The result indicated that deuterium filling would reduce tube voltage drop, but would also increase the required interrupting magnetic field. The advantage of lower tube drop was overshadowed by the increased switching energy requirement. It was concluded that the lower atomic weight gas (hydrogen) would best serve in the RSI application.

d. Summary of Results

RSI's having a magnetic interaction structure containing chuted channel walls were developed during Phase I of the program. These RSI's operate with a column drop of 350 volts, and are capable of interrupting high voltage, high current (15 kV, 300 amperes) discharges with an interrupting magnetic field level of less than 4 kilogauss (corresponding to a magnetic field switching

energy of 5 joules). The interruption of higher voltages and currents seems feasible with even lower magnetic field energy requirements. Prevention of restriking of the discharge at high Ebb and reduction of the total tube drop are important aspects of the RSI development program and will be considered in detail during Phase II of the program.

Present investigation of magnetically controlled switching yielded considerable information regarding the effects that the various parameters of the interaction channel design exert on interrupting magnetic field requirements. Studies show that interaction channels with chuted wall surfaces and column lengths of minimum practical dimensions are most appropriate for RSI design.

A theoretical investigation was performed which derives a relationship for the constriction of a plasma column in a discharge channel with a transverse magnetic field. This relationship details the extent of constriction as a function of the strengths of the electric and magnetic fields. Experimental observations agree with theoretical predictions to the extent that a constricted (thin) discharge is observed at the discharge channel walls. The precise mechanism which causes current interruption is not identified, but is expected to be energy loss of the discharge to the channel wall, charged particle loss by recombination at the channel wall, or charged particle loss by a reduction of the plasma column volume with a consequent reduction in ion formation from electron-neutral hydrogen scattering.

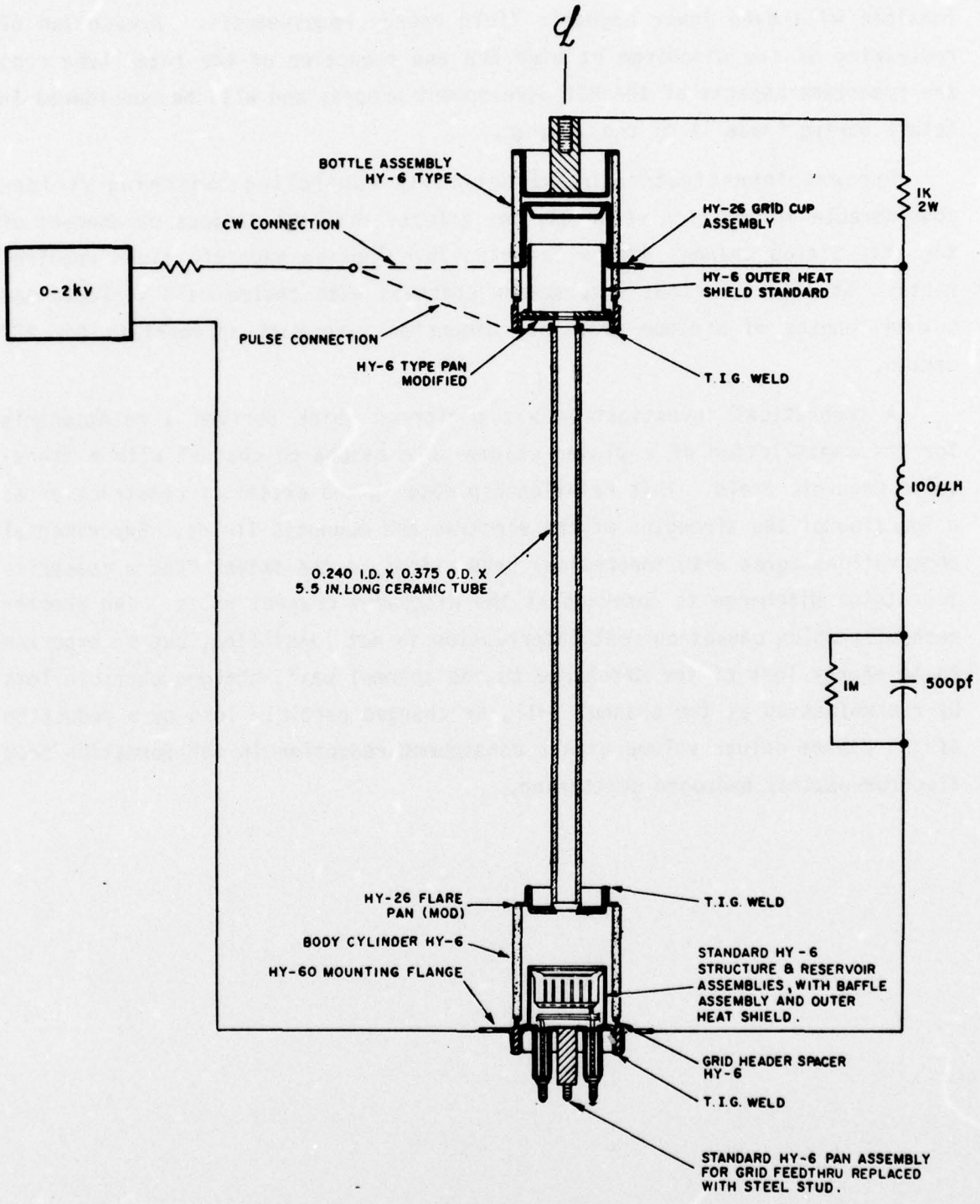

Figure 1. Tube RSI 001 and connections.

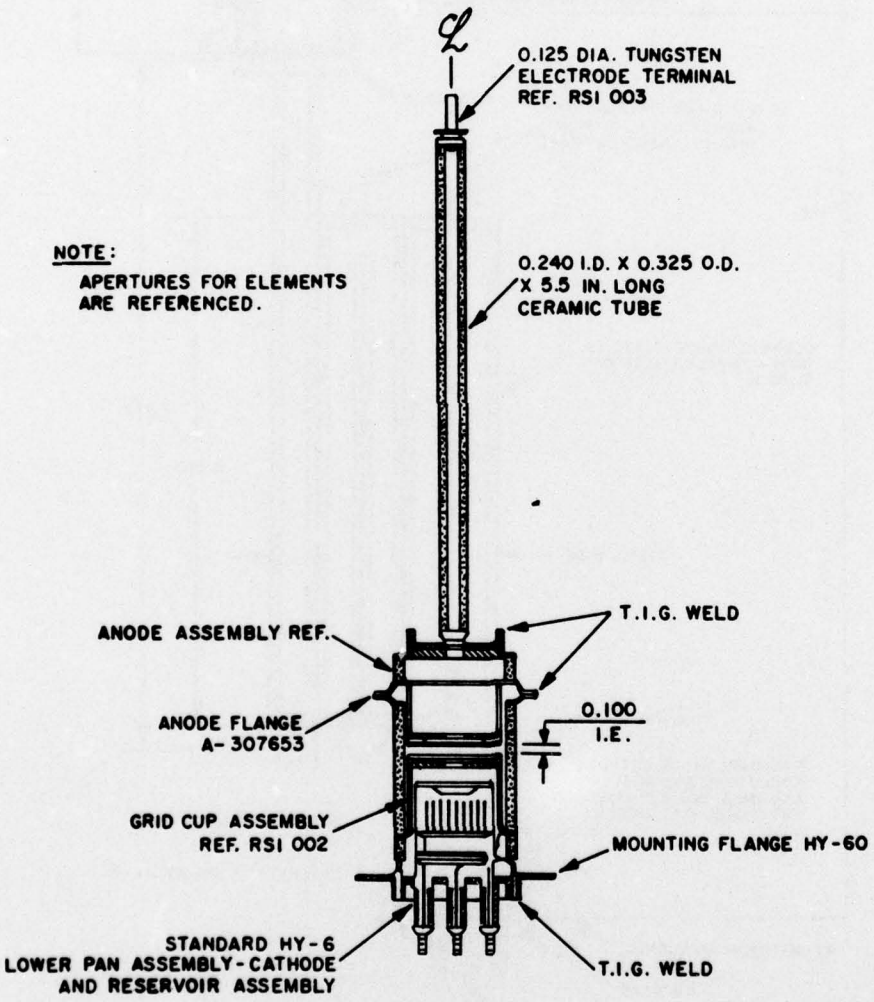

Figure 2. Tube RSI 002.

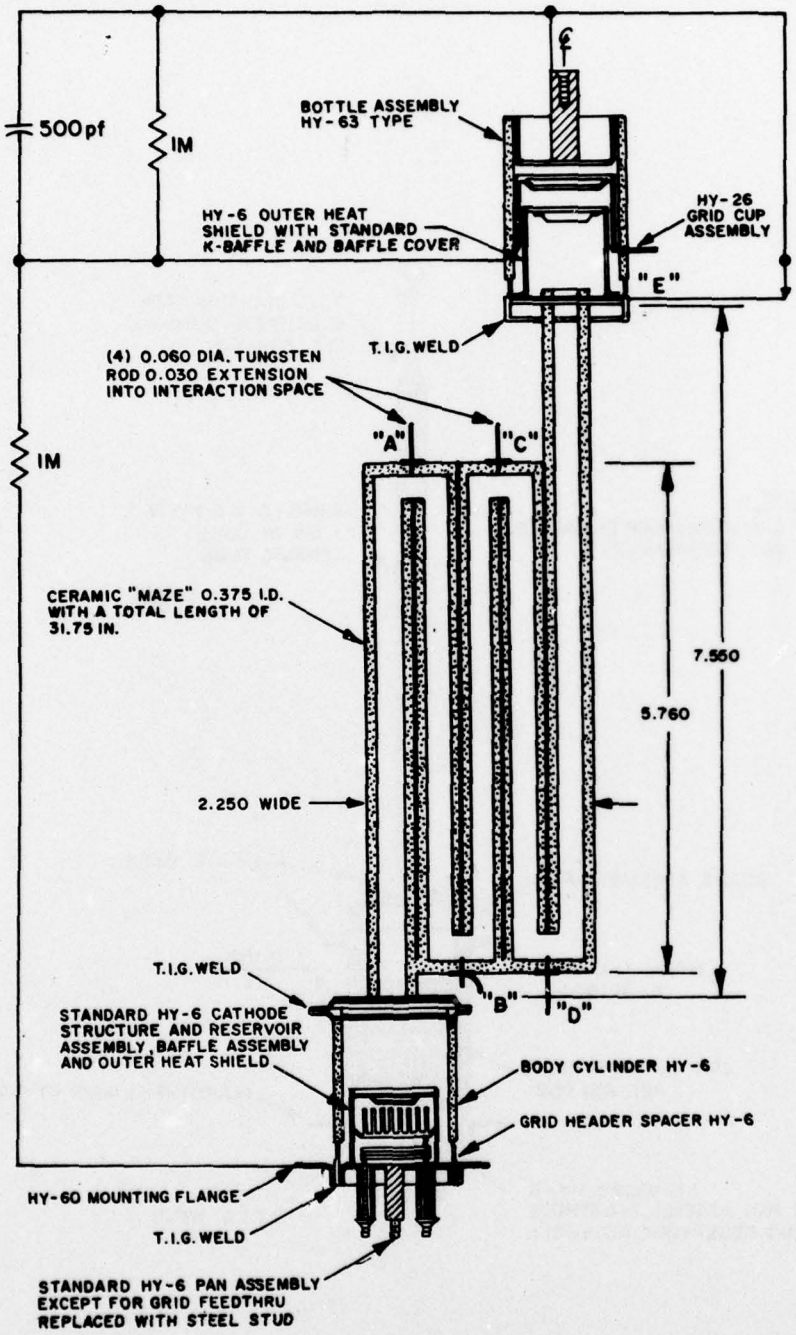

Figure 3. Tube RSI 003 and connections.

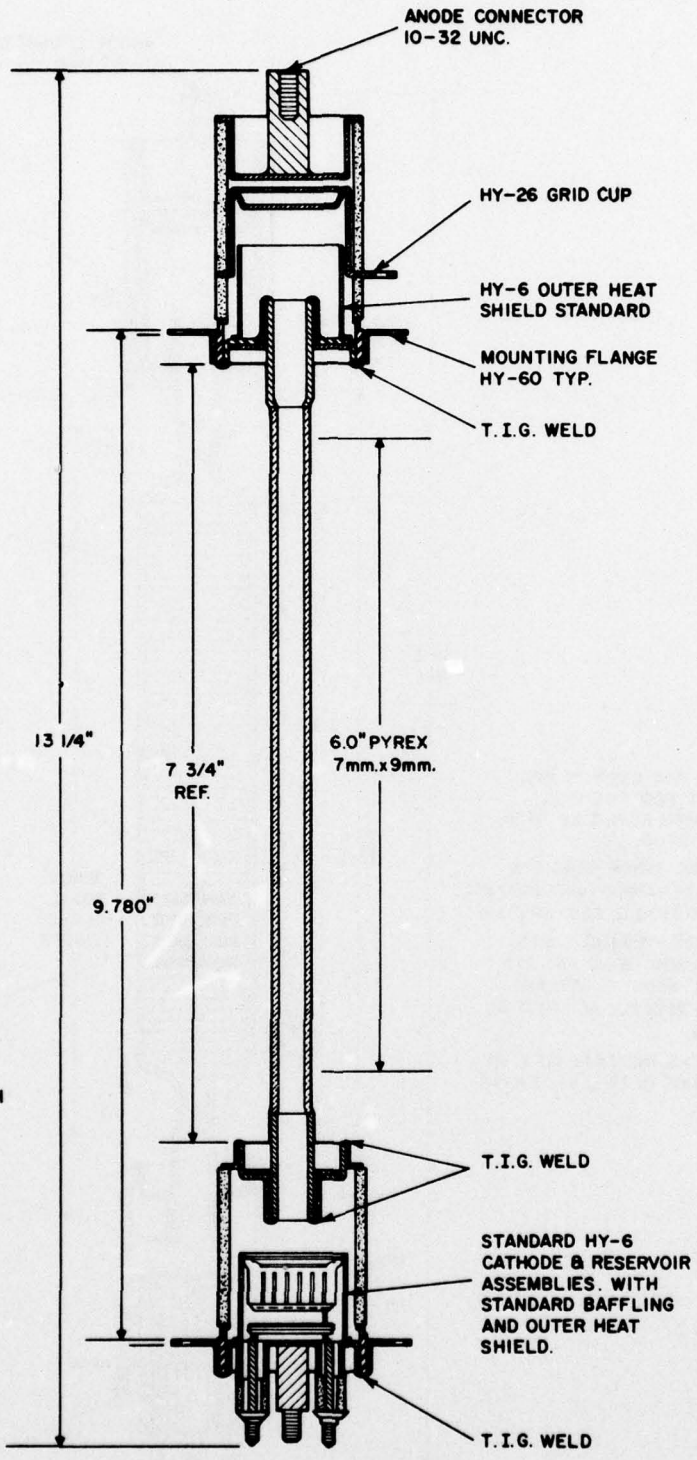

NOTES:

1. LOWER PAN ASS'Y IS STD. EXCEPT FOR THE GRID FEEDTHRU REPLACED WITH STEEL STUD.
2. RESISTANCE READINGS REF. #84216.

Figure 4. Tube RSI 004.

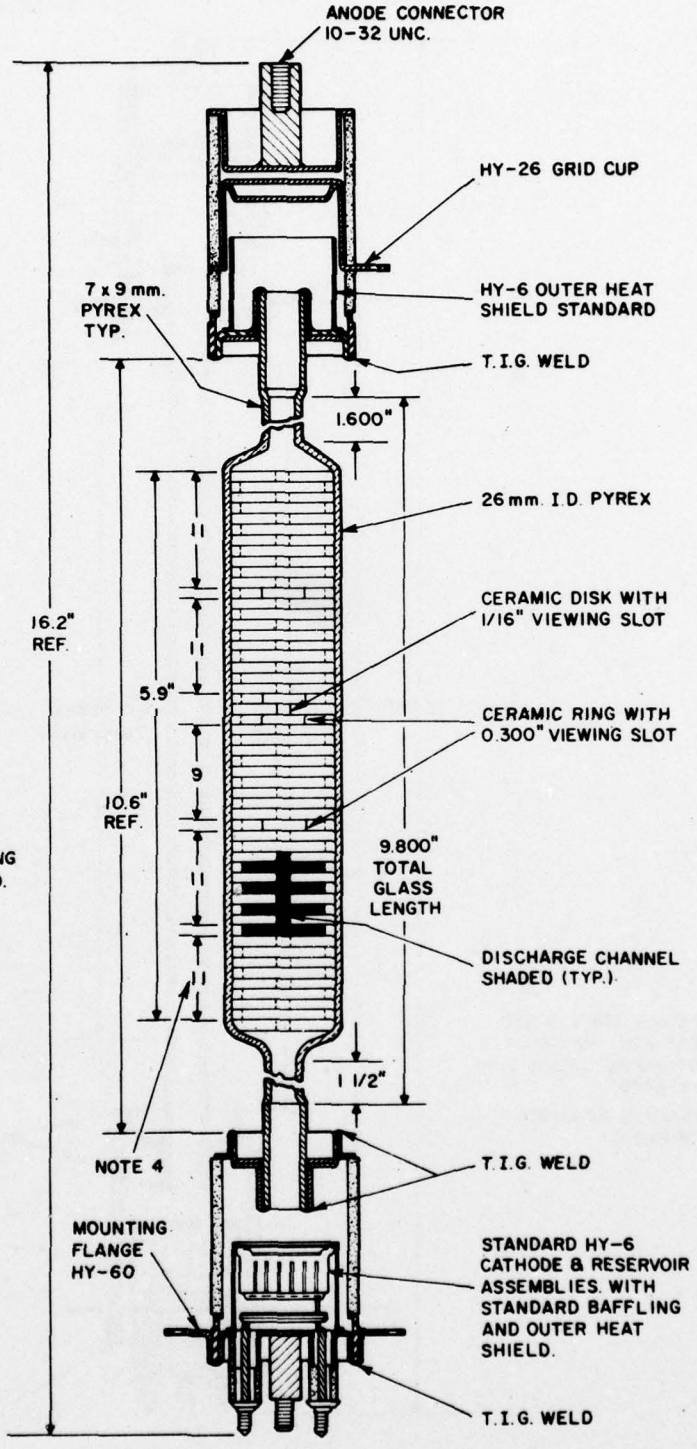

NOTES:

1. LOWER PAN ASS'Y IS STD. EXCEPT FOR THE GRID FEEDTHRU REPLACED WITH STEEL STUD.
2. CERAMIC STACK CONSISTS OF 59 CERAMICS-ALTERNATING FROM 0.130 I.D. TO 0.800" I.D.
3. NOTE (6) VIEWING SLOTS, (5) ≃0.300" WIDE AND (1) ≃ 1/16" WIDE, SLOTS ARE NOT PERFECTLY ALIGNED AS SHOWN.
4. NUMBERS INDICATE QTY. OF CERAMICS BETWEEN VIEWING SLOTS.

Figure 5. Tube RSI 005.

3.0 COURSE OF THE INVESTIGATION: EXPERIMENTAL WORK

a. RSI Design

(1) Significant Design Parameters

The most important aspects of an RSI design are the choice of the interaction channel designs, the anode-grid structure and location, and the selection of the operating pressure. Structural rigidity and strength must also be assured with appropriate transition components between the individual structures, and cathode and reservoir structures must be built to meet the required current and gas demands. The most important aspect of the tube design is the interaction channel structure.

The anode-grid holdoff structure may be placed above or below the interaction channel relative to the cathode. Location below the interaction structure provides the benefit of holding the grid near ground potential during current interruption, but adds the problem of commutation of the discharge through an additional structure, specifically an anode baffle to supply appropriate holdoff capability. Location of the holdoff structure above the interaction structure increases the initial ionization path length (for triggering or keep-alive) and requires additional circuitry to assure keep-alive discharge formation after interruption.

The important design parameters of the interaction channel are channel length, diameter, and geometry. Increased channel length decreases the magnetic field required for interruption but increases the voltage drop in the RSI. Reduced channel diameter also increases the tube drop but decreases the magnetic energy required for interruption. The geometry of the channel is of paramount importance, since it controls the shaping and structure of the plasma discharge during interruption and poses the possibility of substantially altering the physical mode of current interruption to the benefit of lowering the switching energy requirement and the corresponding voltage drop. Geometrical considerations must provide for a maximum interaction between the gas discharge and a wall surface, but must also ensure that the interrupted discharge not have the opportunity to revert to a physical mode which reduces interruptible control, such as an arc mode or a channel jumping mode.

The final significant parameter is the tube pressure. Standard thyratrons operate in a restricted pressure regime governed by the need for efficient triggering, low anode power dissipation, and reliable voltage holdoff capability. Magnetic control of a discharge column is heavily pressure dependent (see subsection 3.c(3)(e)) and best operation occurs in a low pressure regime, where current interruption is most successful, and where plasma column sustaining electric fields are low. Holdoff structure design must be dependent upon the choice of pressure level.

The phenomena which could affect RSI lifetime include the possible generation of minor amounts of O_1, O_2, OH, or H_2O by interaction of the hydrogen discharge with the alumina wall. These by-products could result in enchanced degradation of the cathode and reservoir materials, although such an effect was not seen after considerable testing of RSI 003 in spite of the fact that contamination of the gas itself was apparent from spectrographic data. Contamination effects are the only factors likely to cause any alteration of RSI cathode or reservoir designs from those of standard hydrogen thyratrons.

(2) RSI Thyratron Test Series

The RSI thyratron design has evolved to a certain degree during the course of this program, and particularly in that nonuniform interaction channels have been used. The series of thyratron test vehicles includes tubes constructed to test holdoff structure location (RSI 001 and RSI 002), parametric evaluation (RSI 003), gas discharge structure (RSI 004), wall chuting effects (RSI 005), channel geometry and electric field grading (RSI 7-2), and grid-quenching phenomena (RSI 7-3). The final tube design selected for exploratory development was solidified in the RSI 10 series of tubes.

Also available for test in this program were several tubes of similar design which were developed under the Magnetically Controlled Charging Diode (MCCD) program, useful particularly in examining parametric dependence and gas fill effects.

The principal parameters of the RSI devices are tabulated in Table 1; drawings of these thyratrons appear in Figures 1 through 11. A photograph of several of the tubes is shown in Figure 12b, and one of the unassembled chuted RSI 10 components is given in Figure 12a.

Table 1. Principal Parameters of RSI Devices

Tube No.	Interaction Channel I.D. (in.)	Number of Interaction Channel Sections	Total Effective Interaction Channel Length (in.)	Fill Gas	Fill Pressure (torr)	Interaction Region Location (cathode-grid or post-anode)
RSI 001	0.24	1	5.5	H_2	0.400	K-G
RSI 002	0.24	1	5.5	H_2	0.400	PA
RSI 003	0.375	5	31.75	H_2	0.400	K-G
RSI 004H_2	0.28	1	6	H_2	0.400	K-G*
RSI 004D_2 (repump)	0.28	1	6	D_2	[illegible]	K-G*
RSI 005	Alternating 0.13 and 0.80	1	6	H_2	0.370	K-G
RSI 7-2	0.28	1	12.0	H_2	0.400	K-G**
RSI 7-3	Inapplicable	1	Inapplicable	H_2	0.450	anode-grid***
RSI 10A	0.30 chuted	1	6	H_2	0.400	K-G
RSI 10B	0.30 chuted	1	6	H_2	0.400	K-G
RSI 10C	0.30 chuted	1	6	H_2	0.400	K-G
RSI 10D	0.15 chuted	1	6	H_2	0.400	K-G
RSI 10E	0.15 chuted	1	6	H_2	0.400	K-G
RSI 10DD	0.15 chuted	2	12	H_2	0.400	K-G
MCCD 380D-250	0.25	6	23.25	D_2	0.380	PA
MCCD 400D-250	0.25	4	24.6	D_2	0.400	PA
MCCD 425H-181	0.181	4	36.5	D_2	0.425	PA

*Glass Interaction Channel
**S-Shaped Channel
***Grid-Quenching Test

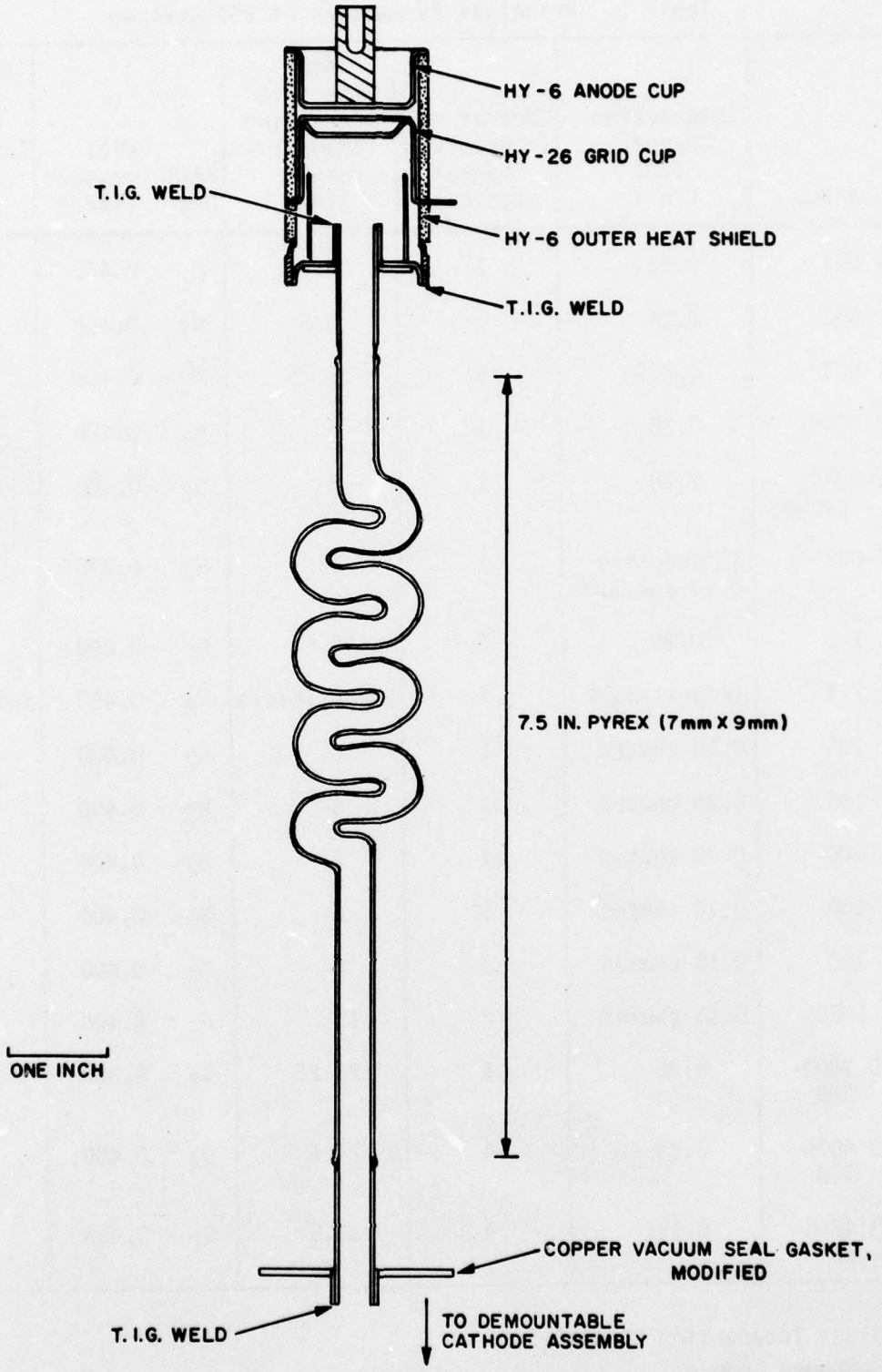

Figure 6. Tube RSI 7-2.

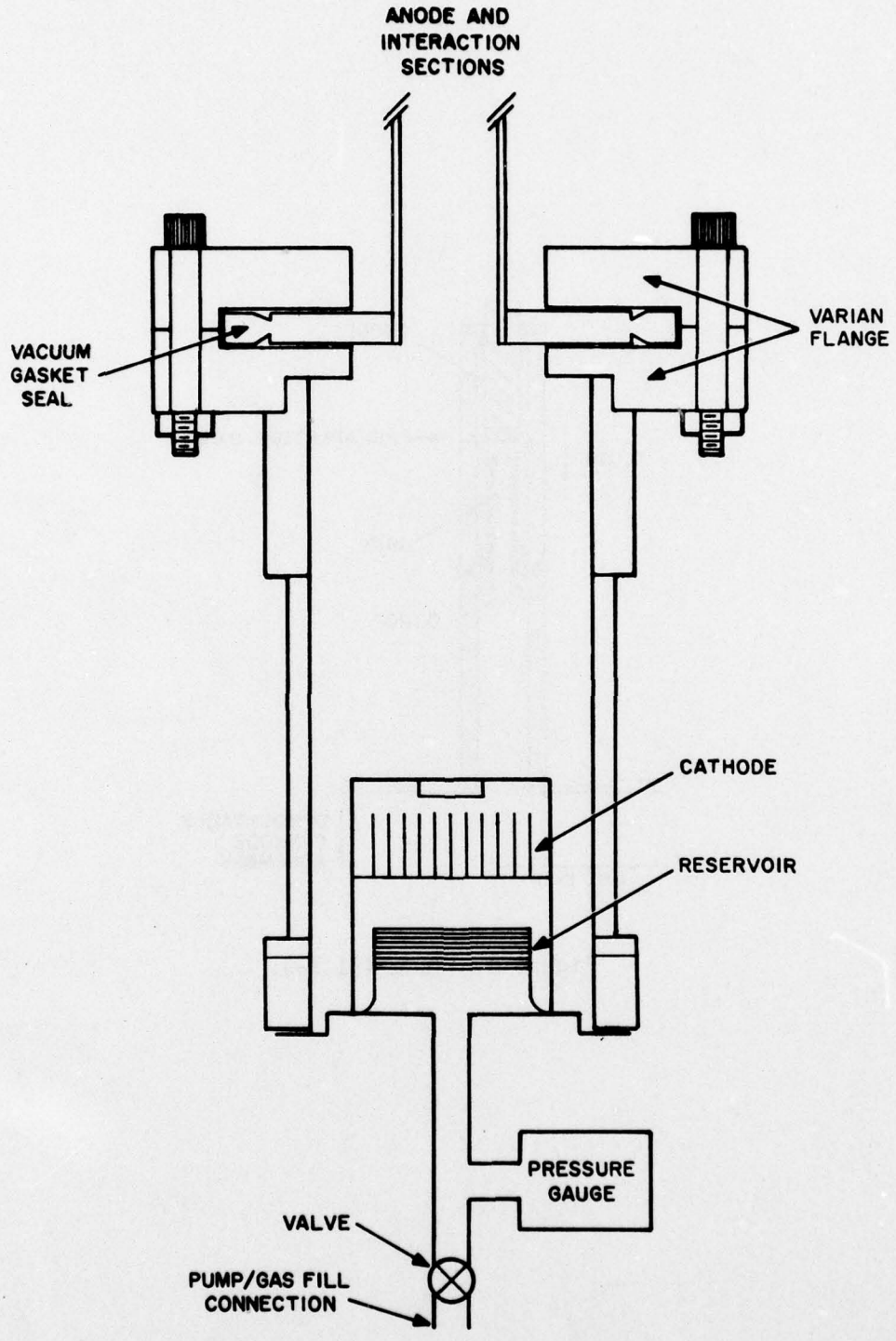

Figure 7. Interchangeable cathode for RSI tests.

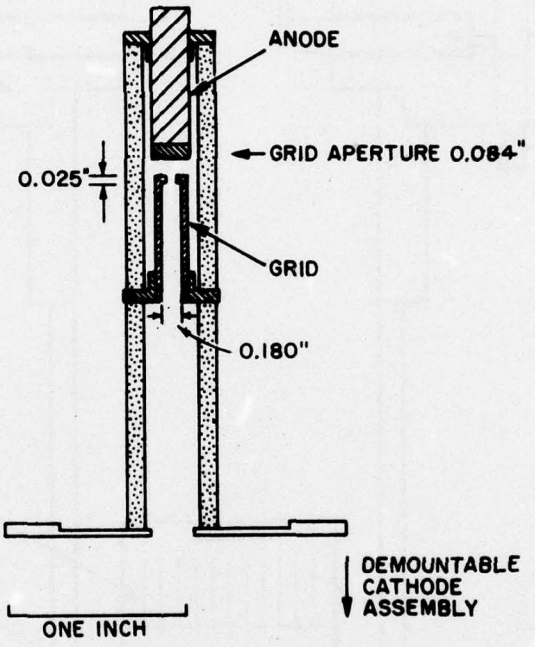

Figure 8. Tube RSI 7-3.

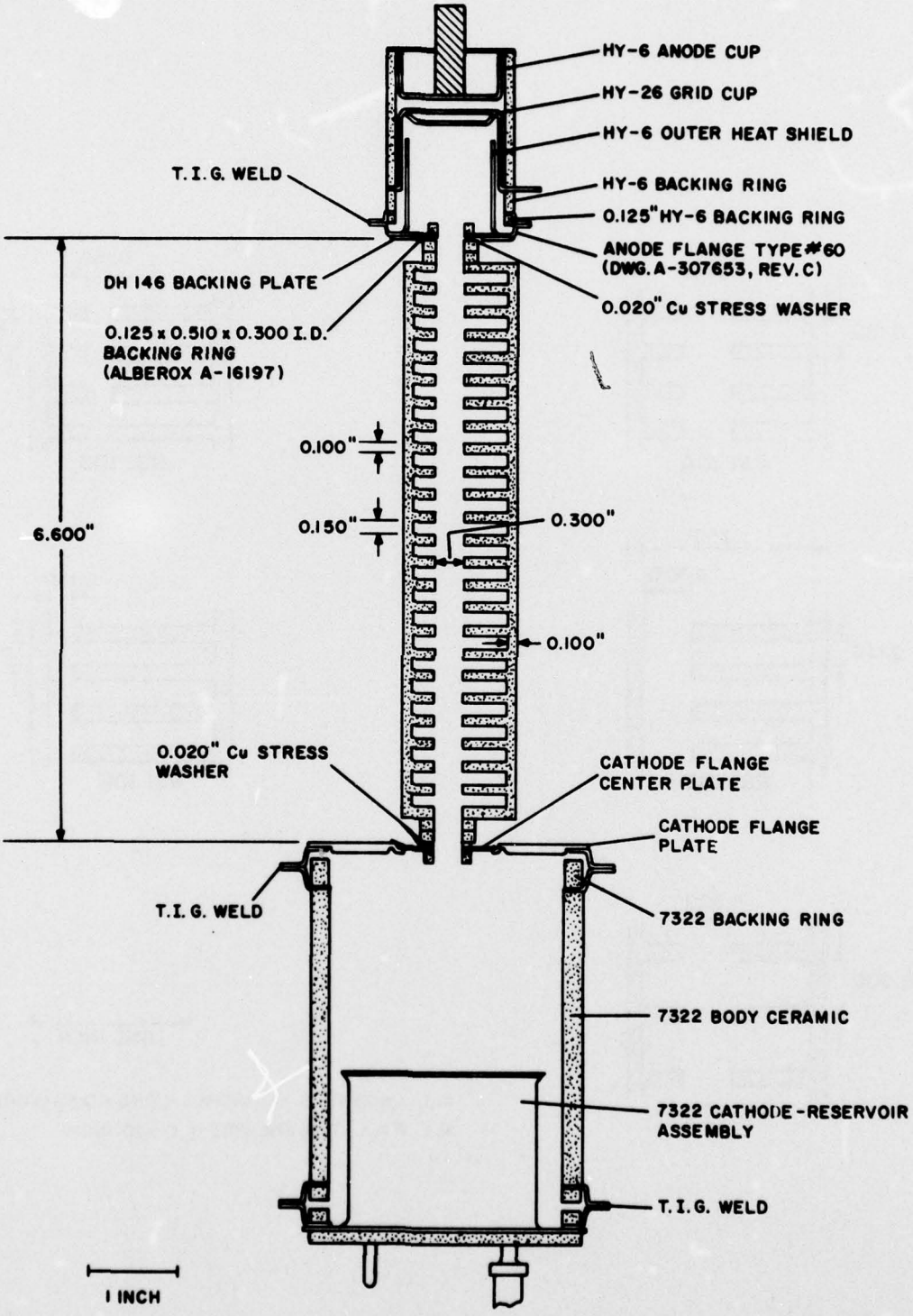

Figure 9. Tube RSI 10A.

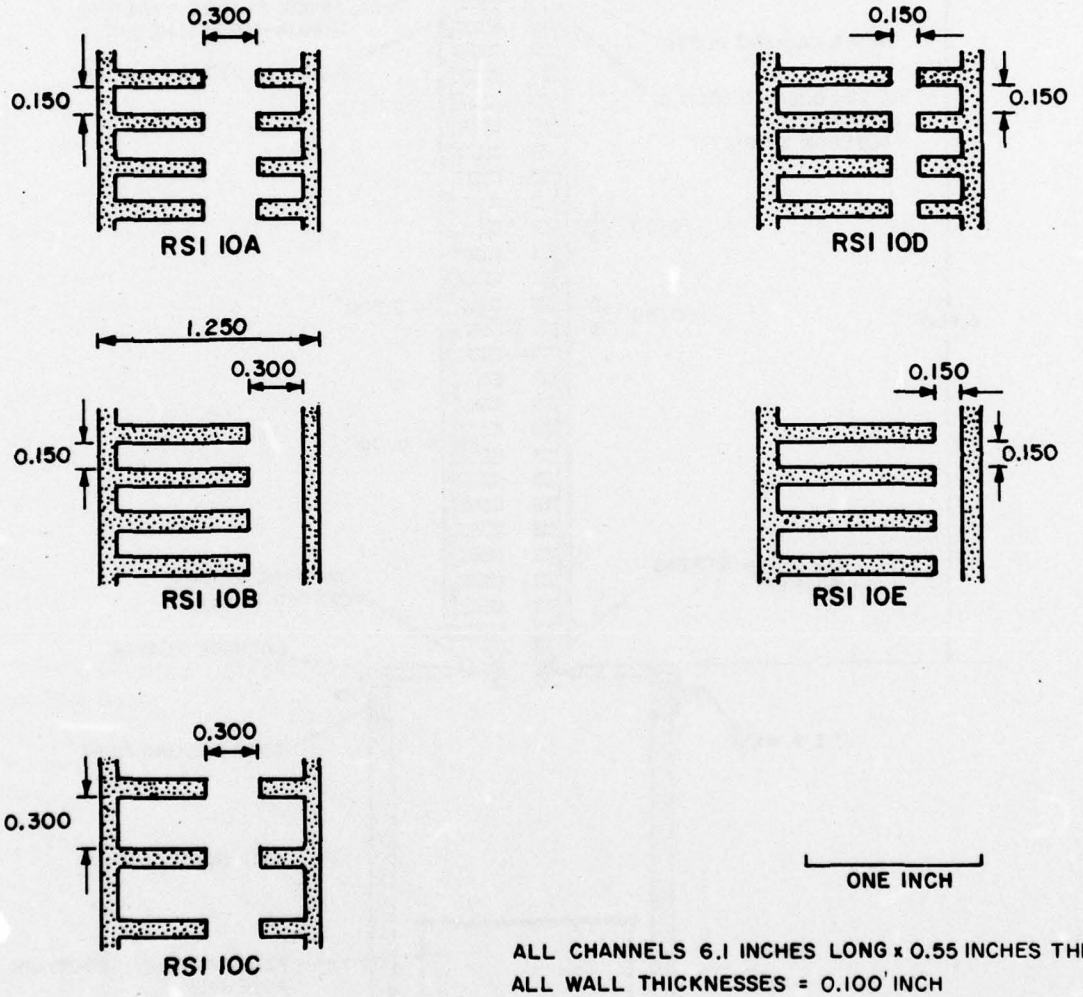

Figure 10. Tube RSI 10 interaction channels.

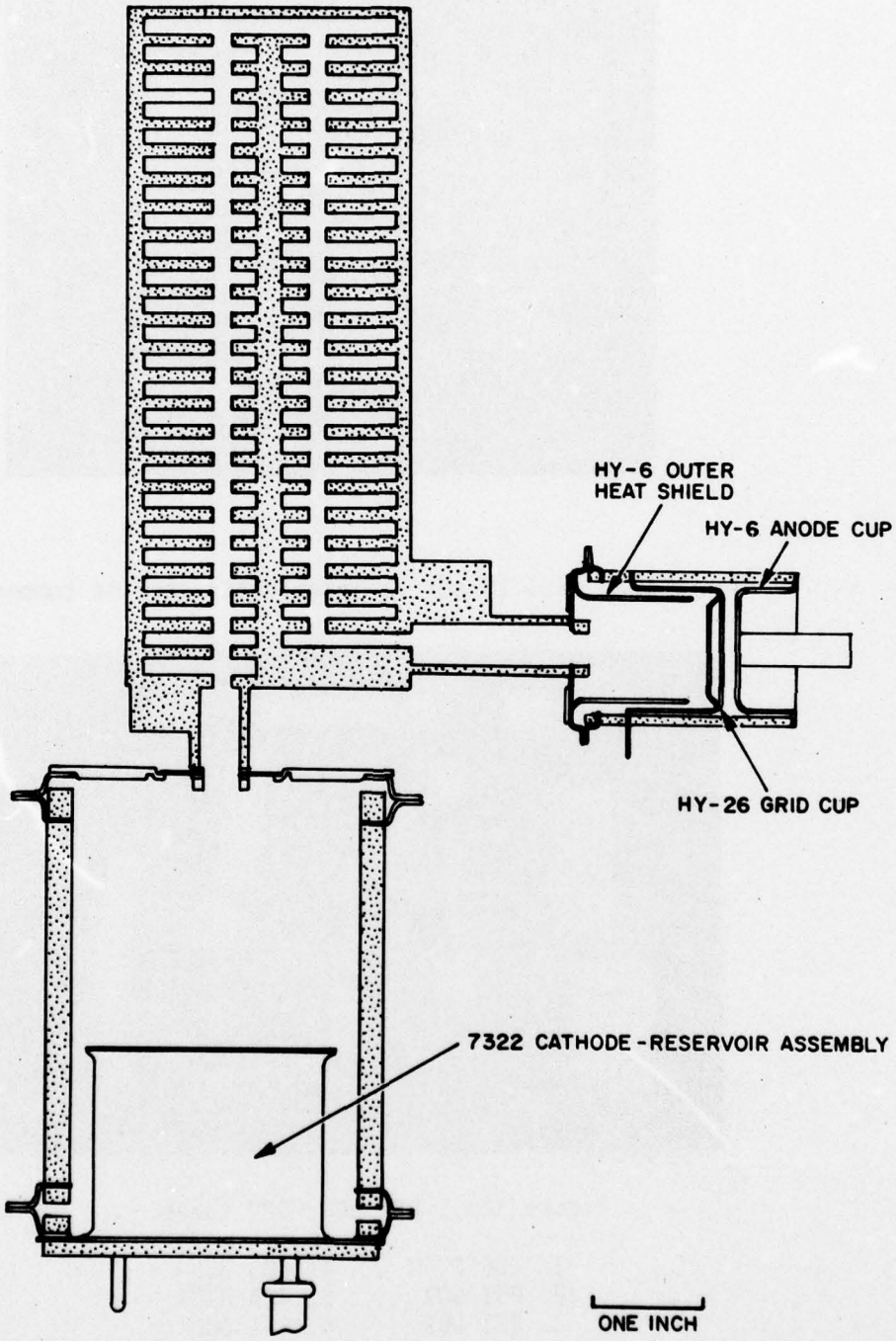

Figure 11. Tube RSI 10DD (30 kV design).

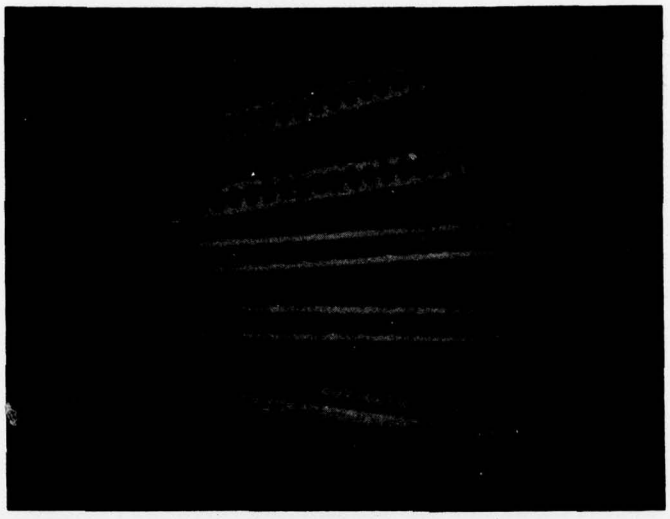

Figure 12a. RSI 10 series interaction section components.

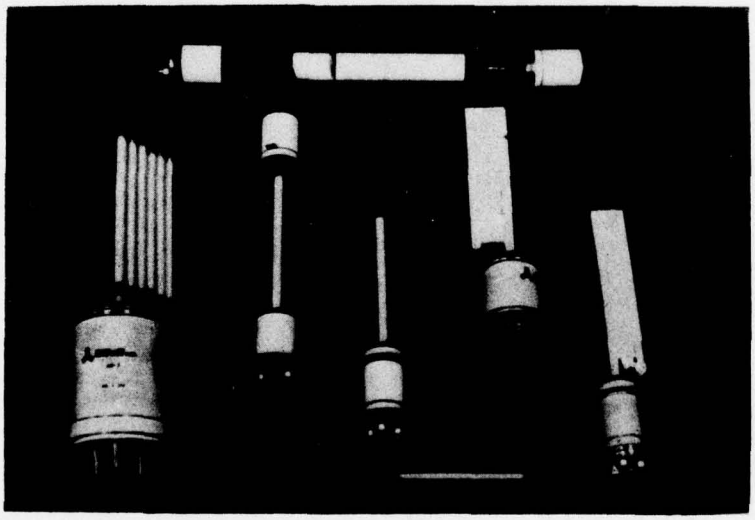

Figure 12b. RSI and MCCD tubes.

1. 380 D250
2. RSI 001
3. RSI 002
4. 400 D250
5. 425 H181
6. RSI 005

Figure 12. RSI tubes and components.

The series of test thyratrons, RSI 001 through RSI 005, were constructed with HY-6 type cathode-reservoir assemblies and anode-grid structures to comply with guideline requirements of 15 kV holdoff and 300 amperes peak fault current. HY-6 heat shields are used in the cathode structures to direct the discharge toward the grid aperture and away from the ceramic wall and grid-ceramic seal area. Holdoff structure dimensions were not altered from those used for production thyratrons.

(3) RSI 10 Design

A chuted wall interaction channel design was selected for the first phase demonstration tube series. Designs for the 15 kV and the 30 kV tubes are shown in Figures 9 and 11 respectively.

A modified 7322 cathode assembly (Ib capability = 2.2 Adc, ib = 1500 A) and modified HY-6 high voltage holdoff structure (epy = 16 kV) were used to meet the technical requirements of Ib = 0.8 Adc, i fault = 300 A, and Ebb = 15 kV. A 6-in. high alumina chuted ceramic interaction section was chosen to meet the requirements for etd (350 volt) and the switching magnetic field energy, εj (50 joules). An etd of 310 volts (210 volt channel drop, 100 volt anode-grid and cathode drop) and an εj of 25 joules were predicted for the RSI 10 series from an extrapolation of RSI 005 performance.

A variety of interaction channel cross-sections were devised for the six tube requirement. Figure 10 shows sample cross-sections for the five 15-kV tubes. The series utilizes eight differing chute wall geometries for interruption, as well as two flat interaction walls as an experimental control. Wall interaction is switched from one wall surface to the other by reversal of the magnetic field direction (resulting in a reversed $\vec{I}\times\vec{B}$ force). The 30-kV interrupter utilizes a twin, series-connected discharge column. An awkward hold-off structure location is tolerated to allow for maximum use of the magnetic field energy while retaining moderate simplicity of ceramic construction, and to serve as a model for future multiple channel, chuted wall, higher voltage interrupters.

Ceramic interaction sections for the RSI tubes are constructed from two matching halves, where the joining seams are located along the center line of the main discharge channel. The two halves are cemented with a suitable high temperature glaze material. To provide some safety for leak prevention

at these seal junctions, lateral wall thicknesses were increased to 0.125 inch minimum and the central circular bore was given an increased (extended) flat wall length at the seal region.

Butt seals with backing rings and thin copper pads are used at the junction of the interaction structure with strengthened anode and cathode flanges. The varying dimensions chosen for the interaction sections provide a means of exploring most efficient interruption geometries. In this regard, the RSI 10A, 10C, and 10D present an immediate test of the effect of differing chute depths in interruption; RSI 10B and 10E compare chuted to unchuted surfaces. Comparisons of Bq levels among different tubes are not quite as accurate as comparisons within individual tubes, due to possible pressure differences, levels of gas contamination, etc. The complete RSI 10 series will provide two four-point studies of Bq versus plasma chute depth (RSI 10A, 10B: chute depth = 0, 0.25, 0.50, 0.75 inch with a central channel of 0.300 inch diameter; RSI 10D, 10E: chute depth = 0, 0.25, 0.65, 0.90 inch with a central channel of 0.150 inch diameter). A comparison between these two groups will test the importance in interruption of the central channel dimension.

(4) RSI Construction Notes

RSI thyratrons have been built utilizing established production techniques and materials where possible. Cathode and anode components are selected from those available from production thyratrons and spark gaps in order to assure reliability and low cost. Interaction channel ceramics are made in close cooperation with ceramic vendor engineering personnel to assure optimal designs for minimum cost production.

RSI thyratrons are constructed with three major subassemblies: anode structure, cathode structure, and interaction section structure. (In the case of post-anode tube design, anode and cathode structures are incorporated in one component.) Subassemblies are joined at flange, pan, or header joints with TIG welds.

Ceramic components utilize high voltage 94% alumina material. Ceramic-metal seals use Mo-Mn or titanium hydride techniques, with expansion-matched iron-nickel alloys.

All tubes are assembled with the necessary precautions for cleanliness suitable to electron tube production. The gas-filling operation which completes tube construction utilizes a 400°C bakeout and direct gas-fill monitoring with a McLeod gauge.

b. Test Circuitry and Experimental Procedures

(1) Test Circuitry

The RSI test circuitry has varied somewhat through the course of the investigation, but the general concept has not. The principal circuitry is shown in Figure 13.

To represent pulse conditions, a 600-ohm PFN was resonantly charged through a 30-kV reactor and a solid state holdoff diode, and discharged through a load R1 of 500-600 ohms either through thyratron A and the series RSI tube (suitably connected), or directly into (and triggered by) the RSI tube under test. The former mode of operation provided information concerning interaction channel voltage drop, particularly for some MCCD tubes and for the RSI 003, where only the interaction channel length could be varied without providing voltage holdoff capability. The series ML-7845 vacuum triode and its auxiliary triggering and protective circuitry were introduced late in the investigation.

Thyratron B was used to trigger a fault discharge (time constant = 50-250 μsec) via Crc and Rrc through the RSI for interruption testing. Again, direct triggering of the RSI without the series thyratron A was also performed when possible.

The magnet circuit was fired after a short time delay (generally set to 5 μsec) via Rm and Cm. Several alternate field circuits were tested to provide long decay times for the magnetic field in the quest for permanent current interruption (see subsection 3.c(6)).

Specific TUT voltage-dividing or compensation circuitry was varied for individual tubes. Megohm resistive grading and a small capacitance (500-1000 pf) in parallel with the RSI generally provided more stable tube operation.

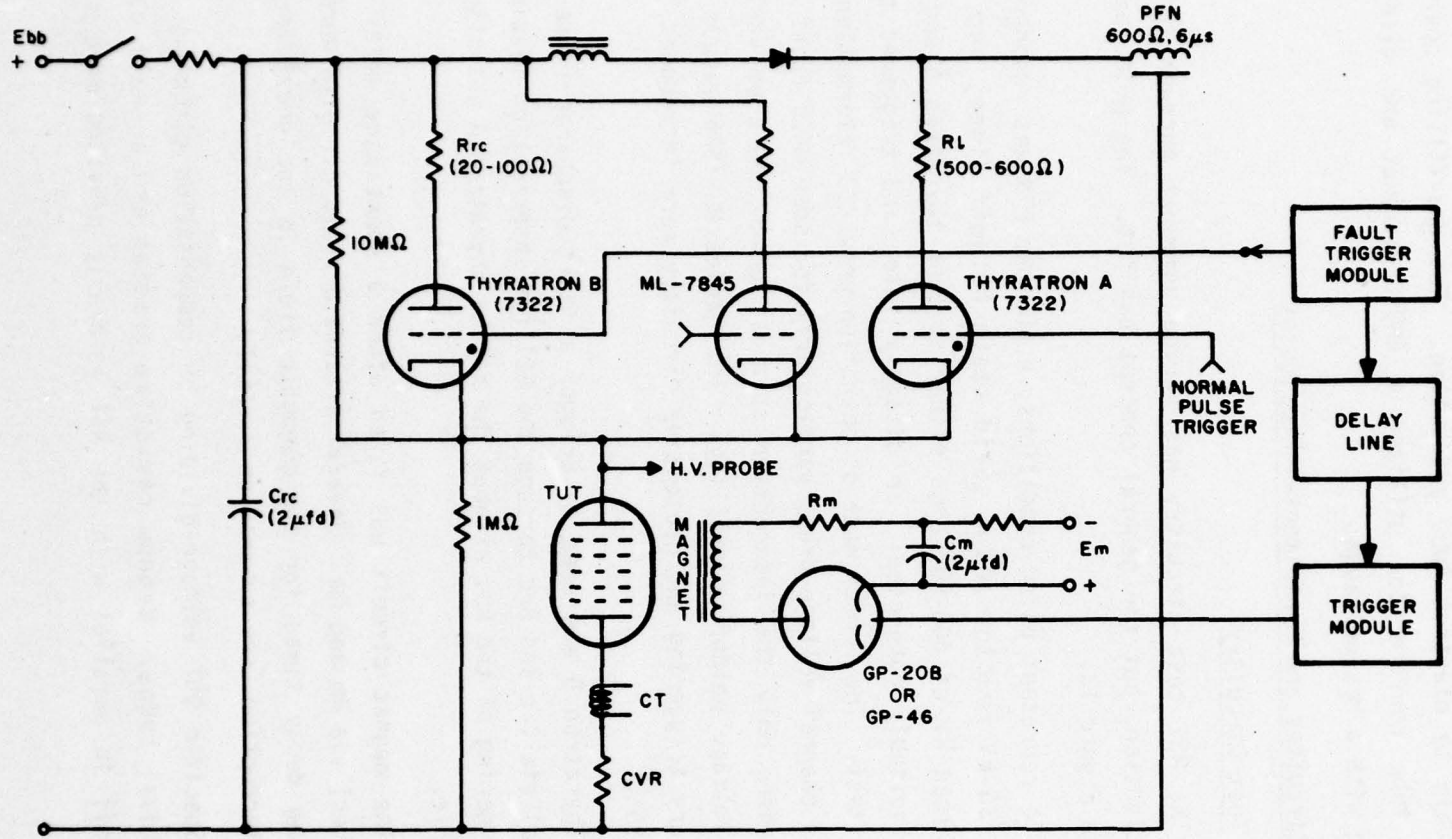

Figure 13. RSI test circuit.

(2) Experimental Equipment and Instrumentation

The experimental hardware was arranged in a tiered test structure suitably constructed to provide high voltage isolation and safety, and a relative proximity among circuit components.

Conventional high voltage circuit components were used throughout the circuit, including non-inductive Ohmite and Ward-Leonard resistors for the fault circuit and magnet circuit loads, 20 kV EDI solid state diodes for the resonant charging circuit, and Sprague and CDE high voltage capacitors.

The magnet circuit was centered at the magnet core, which was formed from the stacking of two split Arnold AH-1154 grain-oriented high silicon steel cores. A composite pole face of 6 by 2 inches was created about an air gap of one-half in. which was located between pole faces on one dimension of the core length. The RSI tubes under test were placed within the core gap, which was then clamped with a suitable spacer if possible alongside the RSI to (1) eliminate any remanent air gap on the opposite length of the core body, (2) stiffen the magnet without putting any mechanical stress on the RSI tube, and (3) allow the pole faces to be as nearly parallel as possible. Some error was introduced of necessity when using this arrangement with tube thicknesses other than one-half inch; an example of the magnetic field shape caused by 1.1 and 1.5 cm air gaps is shown in Figure 16. An additional half-inch magnet insert was constructed for placement on the opposite length of the magnet to provide a one-inch air gap for the study of the RSI 005 tube. Additional pole pieces of one-half inch were used to increase the inner dimension of the air gap from 2 inches to 2-1/2 inches to improve magnetic field uniformity for several of the multifold RSI tube experiments.

The magnet coil was constructed from two series coils, which could be connected as desired. One coil contained a single ten-turn winding, the other a ten-turn winding with taps at each turn. One to twenty turns of this coil could thereby be used to allow variation of the magnetic field risetime and duration.

Experimental diagnostics utilized high voltage Tektronix probes (6015 and 6013), calibrated with a square wave calibration system. Pearson 411 and 110 current transformers and a T & M 50 milliohm current viewing resistor provided accurate current measurement calibration. A 7633 Tektronix

storage oscilloscope and a 556 dual beam, dual trace Tektronix oscilloscope were used to examine waveforms. UVC high voltage power supplies, Datapulse and EH pulse generators, and EG&G trigger modules comprised the electronic control and power systems.

Tube pressure values were obtained through two methods. The principal method directly related tube pressure to the hydrogen reservoir heater voltage, as shown in Figure 14. The reference curves are taken from Goldberg[5], and apply to hydrogen reservoir systems in general.

To ensure that these readings were valid, particularly at the low extremes of the curves, Hastings pressure gauges were attached to several of the RSI 10 series tubes. Curves for the RSI 10A are shown in Figure 14 and are seen to relate to Eres as predicted from the reference plots.

Tube pressure levels were controlled with separate reservoir and filament heater supplies with SOLA voltage regulators at the heater power supply. Some pressure values which appear in the first phase triannual reports were based on a slightly less accurate pressure formula, and have been corrected in this report.

A magnetic field probe coil and test circuit, as shown in Figure 15a, was constructed to test magnetic field levels at the position of the RSI thyratron. The equation governing the voltage induced across the pickup coil derives from:

$$\oint \vec{E} \cdot d\vec{\ell} = -\frac{300}{c} \int_s \frac{\partial \vec{B}}{\partial t} \cdot \vec{n} dA$$

where N = number of turns in the pickup coil (ten) and r = coil radius. The magnetic field is calculated from a solution of the circuit equations to yield:

$$B = -\frac{c}{300N\pi r^2} \left\{ (L_1 + Lcoil)\, Ip + (Rchoke + Rcct) \int Ipdt \right\}$$

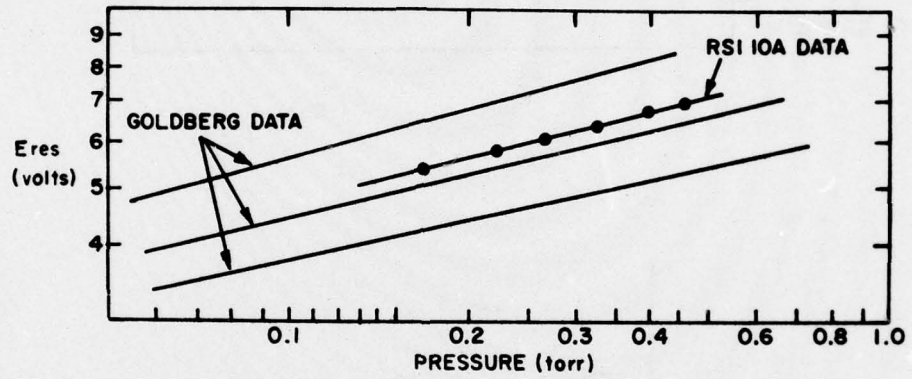

Figure 14. Pressure versus reservoir voltage.

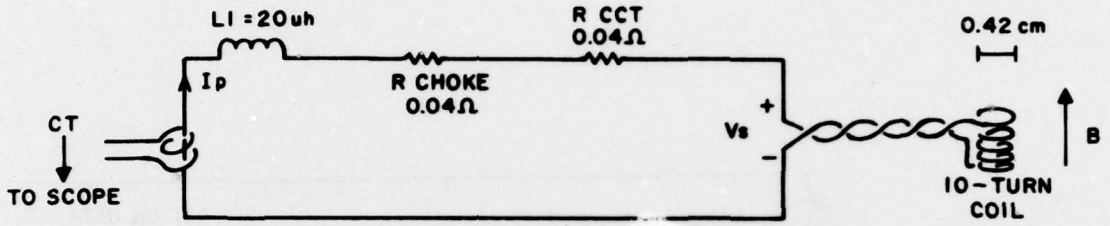

(15a)

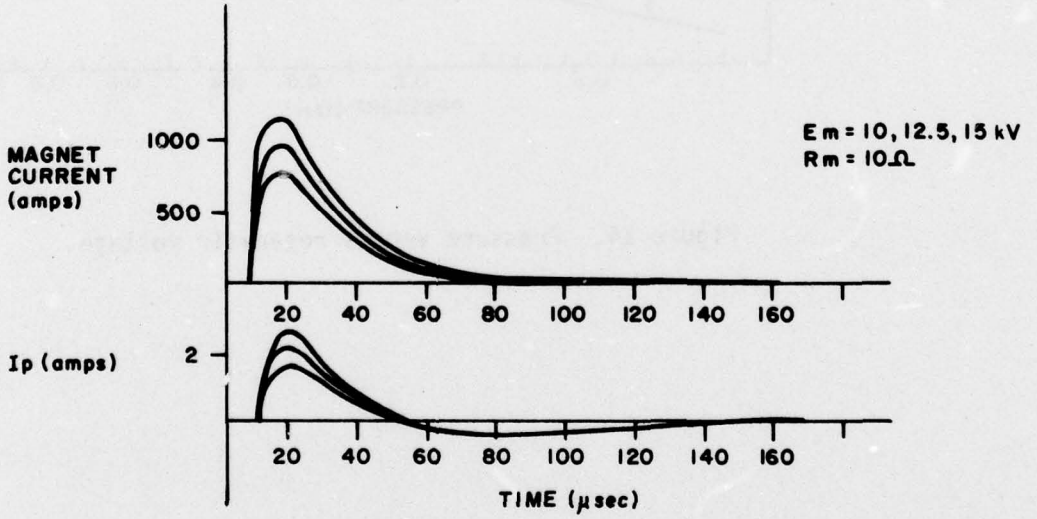

(15b)

Figure 15. Magnetic field testing circuit and output waveform.

The test circuit was designed to minimize Rcct and Rchoke to minimize the second term resistive error, for which an appropriate correction was made. Typical field probe waveforms as shown in Figure 15b demonstrate correlation of probe current with magnet current. The negative current for Ip at t > 50 μsec is a result of the resistive second term in the above equation.

A test of the magnetic field distribution within the core air gap was performed, with results as shown in Figure 16.

The expected value for the magnetic field in the gap can be calculated from:

$$\oint \vec{H} \cdot d\vec{\ell} = Ba + \frac{B\ell}{\mu}$$

where a = air gap width and ℓ = core path length. Tests with the probe circuit indicated that field levels of 77% to 83% of calculated values were obtained; the 20% loss is presumed to be due to coil leakage inductance. Magnetic field values given in the first triannual report should be multiplied by 0.8 to correct for this loss.

A test of the magnet inductance indicated a near quadratic proportionality as a function of N, varying from 2 μh at N = 2 to 100 μh at N = 10.

(3) Test Procedures

Test procedures correspond to accepted general rules of data taking, with a few provisions to simplify data handling.

Tube voltage and current measurements were performed by proxy. Measurements were taken of the circuit performance in the general circuit, and current values were related to the usual expected values through Ebb - etd divided by Rrc. Examination of actual current readings was demonstrated to agree well with the use of this formula, within the limits of experimental accuracy, and peak current figures were calculated from the calibrated values to speed data taking. The quality of the data was not reduced by this process.

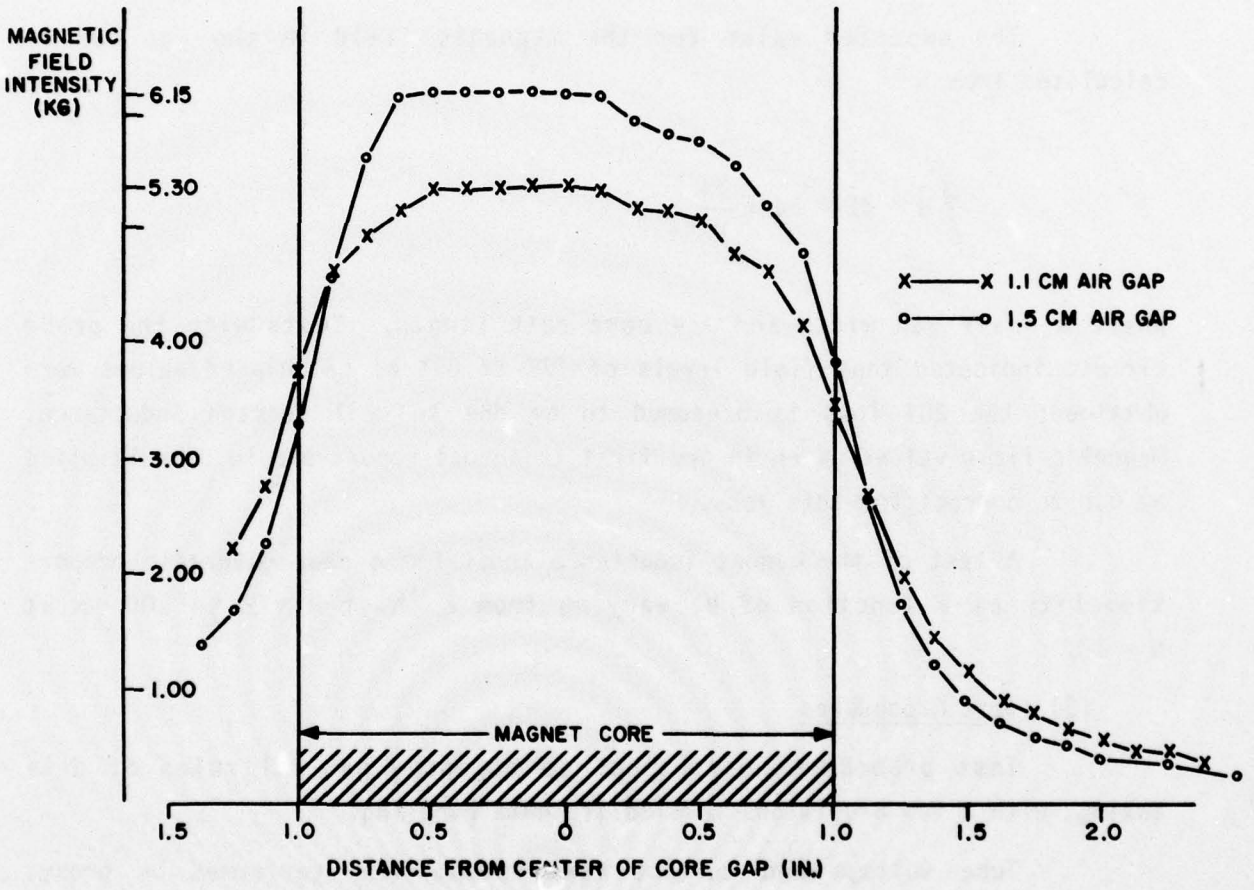

Figure 16. Magnetic field intensity versus position within the air gap.

The same type of procedure was used for obtaining magnetic field readings. With the magnet air gap set to various dimensions, magnet probe measurements were taken and related to the corresponding values of the magnet supply voltage and the current flowing through the magnet circuit. It was seen that those values were repeatable, and further field measurements were based on figures obtained for each specific magnet circuit parameter set; i.e., for each choice of N and Rm. A field probe check late in the experiment indicated that the field values were reproducible within an accuracy of 3%.

The magnet circuit parameters were chosen to provide, in general, a critically damped current pulse, as is shown in Figure 17c. In some instances, the pulse was allowed to oscillate somewhat by underdamping to provide a somewhat higher current (and hence magnetic field) level (Figure 17d).

The magnet circuit firing delay, τD, was supplied artificially with a variable delay line generally set at 5 μsec to: (1) simulate an actual worst case fault sensing delay, and (2) delay current interruption until the thyratron had a short period of time to "settle down"; i.e., to discontinue small amplitude oscillations which appear from time to time on the initial phase of the fault waveform. This procedure provided a better assurance of correlation between data from the full series of experimental tubes.

c. Test Results: Magnetically Controlled Current Interruption

(1) Bq Definition

For the purposes of this investigation, Bq is defined to be that value of the peak magnetic field (in kilogauss) for which the current in the RSI tube under test will fall to zero with a probability of 50%. This definition was chosen to save time and simplify data taking by providing a readily obtainable reference point. There exists a range of magnetic field for which the tube interrupts with varying degrees of reliability and the 50% value is often readily apparent.

A comparison of relative probabilities of current interruption is shown in Figure 38, as well as in Figures 26 and 41. Figure 38 illustrates that an increase in interrupting probability from 50% to 90% is achieved with a 15-20% increase in the magnetic field level.

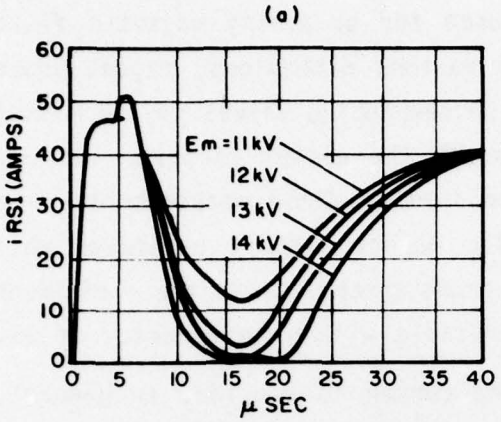

Eres = 5.6
POINT B
Ebb = 4 kV

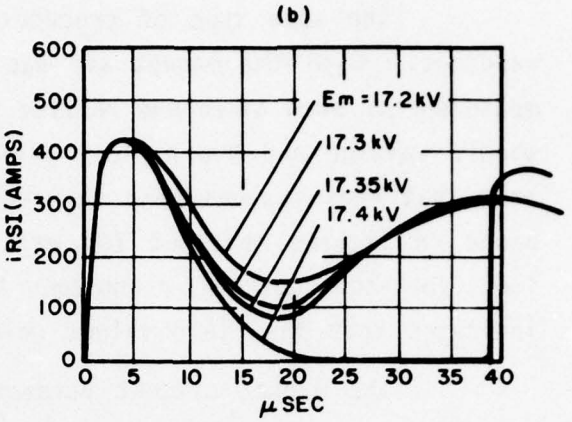

Eres = 5.6
POINT B
Ebb = 14 kV

(c)

Im 500 amp/div
5μsec/div

N = 5
Rm = 10
Em = 8, 10, 12, 14, 16, 18 kV

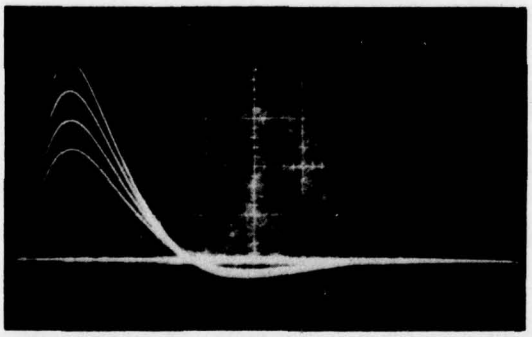

(d)

Im 500 amp/div

N = 5
Rm = 5
Em = 10, 12.5, 15, 17.5 kV

Figure 17. Magnetic current and tube current waveforms.

(2) Current and Voltage Waveforms During Interruption

Studies indicate that there are several different but related modes of current interruption. These differences appear on the current and voltage waveforms and can affect the interruption capability of the tube under test. No specific explanation has been proposed for all of these mechanisms.

The usual relationship of tube current and voltage under the influence of the applied magnetic field is shown in Figure 17. Traces shown in Figures 18 and 19 show that the relationship of increased voltage drop in the interaction column (and therefore decreased current through the tube) is nearly linear with respect to the strength of the applied magnetic field. The tube current and voltage waveform, therefore, often reflect what appears to be an image of the magnetic field pulse as shown.

What differs between waveforms, however, is the final portion of the pulse before the tube current falls to zero. In some cases the attack is gradual, as in Figure 17a. In rarer cases, it comes with more difficulty, as shown in Figure 17b. In a third mode, it comes somewhat abruptly, as shown in Figure 19a. The latter mode of current extinction appears to be connected with instability, oscillation, or noise, and is most apparent in the thin diameter, chuted RSI 10 tubes where it actually appears to be the direct cause of the current interruption. Except for this phenomenon, however, the magnetic field interrupting levels do not differ markedly between the former two modes of current extinction.

(3) Bq Dependence on the Principal Interaction Channel Parameters

(a) Parametric Equations

Parametric studies were undertaken to determine the effects of the tube pressure, interaction channel length, voltage, and current on the requirement for the interrupting magnetic field. Empirical values for the parameters β, γ, and m for the equation $Bq \alpha Ebb^{\beta}\ ib^{\gamma}\ L^{-m}$ were investigated, and for average Bq values these were determined to be:

$$\text{RSI 003} \qquad Bq = 0.97\ L^{-(0.78\pm0.10)}\ Ebb^{(1.26\pm0.10)}\ ib^{(0.24\pm0.10)}$$

normalized to Ebb = 15kV, ib = 300 amps, p = 0.25 torr

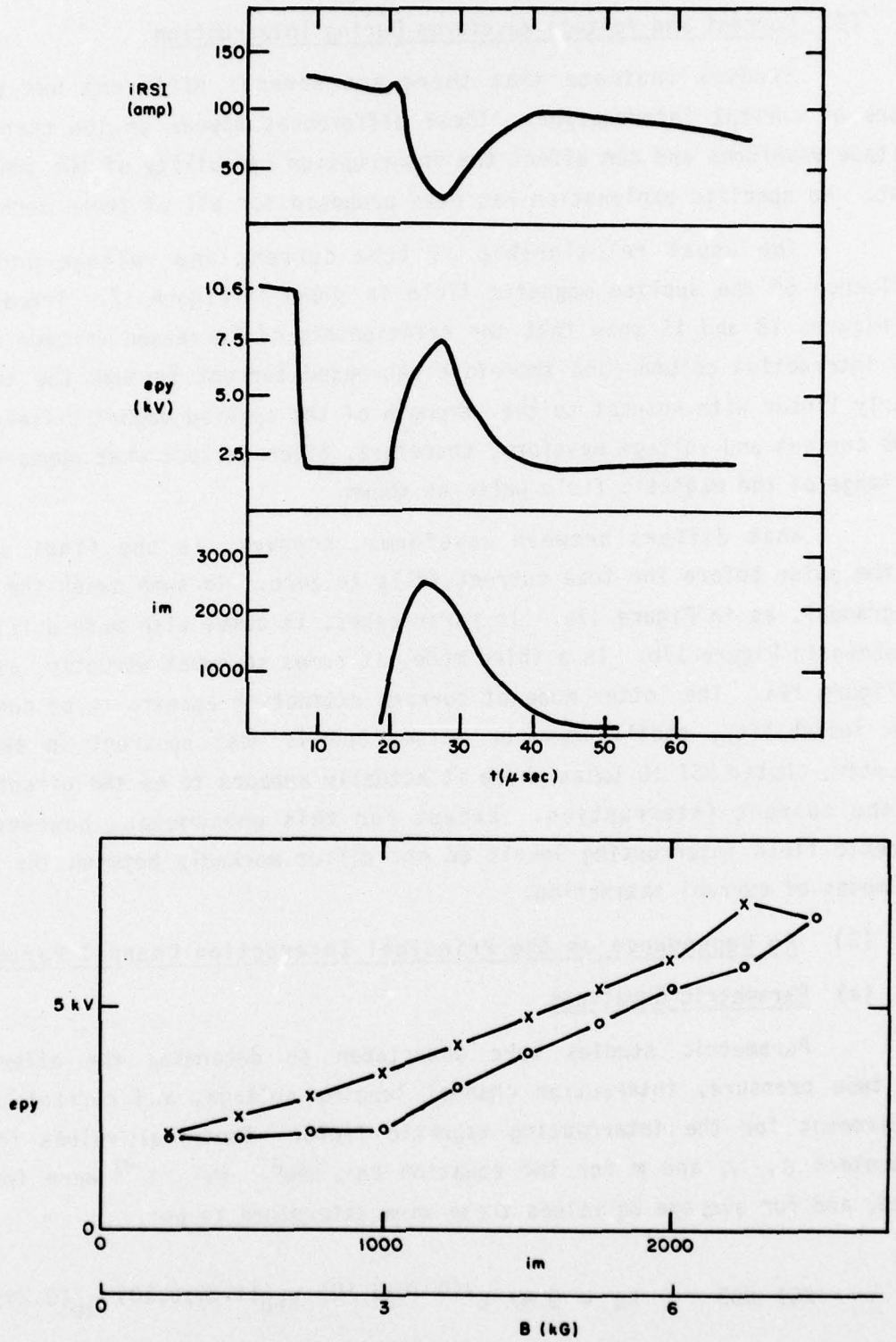

Figure 18. Tube waveforms during interruption.

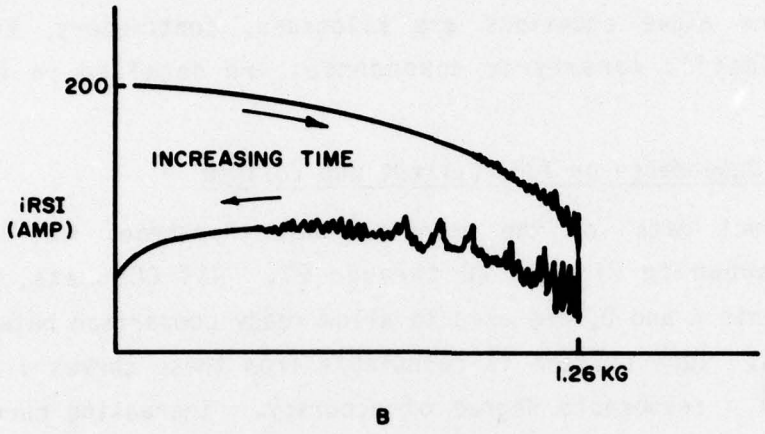

(a) RSI 10A current versus magnetic field: uninterrupted fault pulse.

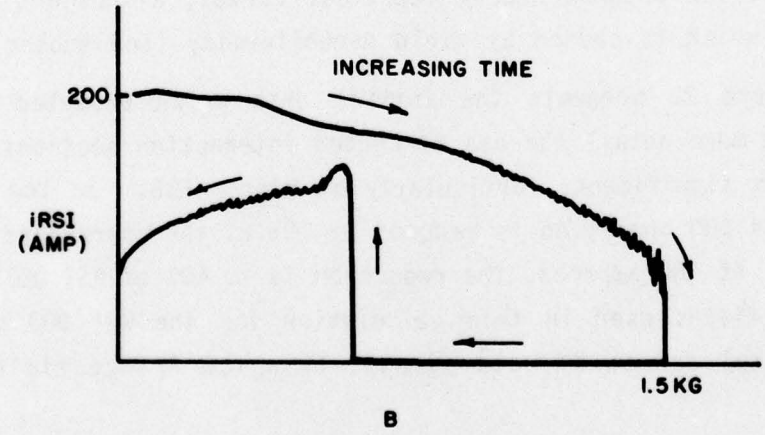

(b) RSI 10A current versus magnetic field: interrupted fault pulse.

Figure 19. RSI current versus magnetic field in RSI 10A.

RSI 7-2 $Bq = 0.79\ (L = 36\ cm)^{-0.78}\ Ebb^{1.5}\ ib^{0.27}$

normalized to Ebb = 9kV, ib = 200 amps, p = 0.3 torr

Units for the above equations are kilogauss, centimeters, kilovolts, and amperes. Specific parametric dependences are detailed in the following sections.

(b) Bq Dependence on Tube Current and Voltage

Direct data for the principal RSI thyratrons for Bq versus Ebb and Rrc is shown in Figures 20 through 27. RSI 003 data, specifically for anode points A and D, are used to allow ready comparison between curves in these figures. Tube current is calculable from these curves via ib = (Ebb - etd)/Rrc with a reasonable degree of accuracy. Increasing current at lower Rrc values is seen to consistently require higher Bq levels for interruption.

The RSI 003 data were taken to determine the effect of interaction channel length on tube interruption requirements. A, B, and D refer to the anode electrode used; point C data has been omitted for clarity, but falls neatly between those sets of curves for B and D. Data taken with the field direction reversed present nearly identical curves, although a shift to the right occurs which is caused by field nonuniformity (see subsection 3.c(5)).

Figure 22 presents the initial data which prompted the decision to examine in more detail the use of chuted interaction sections. The reduction in Bq is significant, particularly at higher Ebb. In low current discharges (Rrc = 100 ohms), Bq is reduced to 25% of the corresponding value for the RSI 003. At 300 amperes, the reduction is to 40% of RSI 003 values. The interrupting fields used in this calculation for the RSI 003 represent the best of several series of data points, in which fringe fields have been eliminated.

Figure 24 demonstrates interruption requirements for the S-shaped RSI 7-2. It is apparent that Bq values have not shifted markedly from those for the RSI 003.

Testing of two of the MCCD tubes gave the results shown in Figure 23. The MCCD 400 D 250 results in Bq versus Ebb, ib curves which are quite similar to those of the RSI 003, despite the change in fill gas to deuterium. The

increased magnitude of Bq for these curves is presumed to be due to the deuterium fill (see subsection 3.e(2)). A curve for the MCCD 425 H 181 is included in this figure (see subsection 3.c(3)(d)).

Results from the first RSI 10 series thyratrons are shown in Figures 25, 26, and 27. These tests indicate that the reduced dependence on Ebb and ib continues to hold at higher voltage and current levels, although some nonlinearities begin to appear which shift the curves from the previously obtained form.

Specifically, high current data for the RSI 10A indicate what appears to be a transition toward the higher Bq levels which were seen in the uniform channel tubes. This could be the result of discharge formation which "hops" from chute to chute along the central channel bore, supported by high velocity electrons, as conceived for the RSI 7-2 (see subsection 3.c(9)). In addition, data for the RSI 10E1 indicate a transition to an interrupting form of lower Bq at low fault current. This phenomenon can be ascribed at least in part to a current dependent instability occurring early in the interruption process rather than at the time of peak magnetic field, and is believed to result from thin-channel quenching or ion/gas starvation.

An analysis of the data for the RSI 003 was undertaken in an attempt to separate the effects of voltage and current upon Bq. The exponents of the equation $Bq \propto Ebb^{\beta}\ ib^{\gamma}$ were calculated from log-log plots of the data (Figure 28); values for these exponents are given in Tables 2 and 3. It is noted that the data are somewhat erratic.

A plot of Bq versus Ebb for constant Rrc for the RSI 003 is shown in Figure 29. Note that the linearity of this plot is better than that for the analyzed data according to the equation $Bq \propto Ebb^{1.75}$ where no allowance has been made for the increased current at higher Ebb. This unusual linearity cannot be directly attributable to a functional dependence on either Ebb or power switched, as is seen by examining Bq versus Rrc.

Similar analysis was done for the RSI 7-2; values for β and γ are given in Tables 4 and 5. These values are similar to those obtained for the RSI 003.

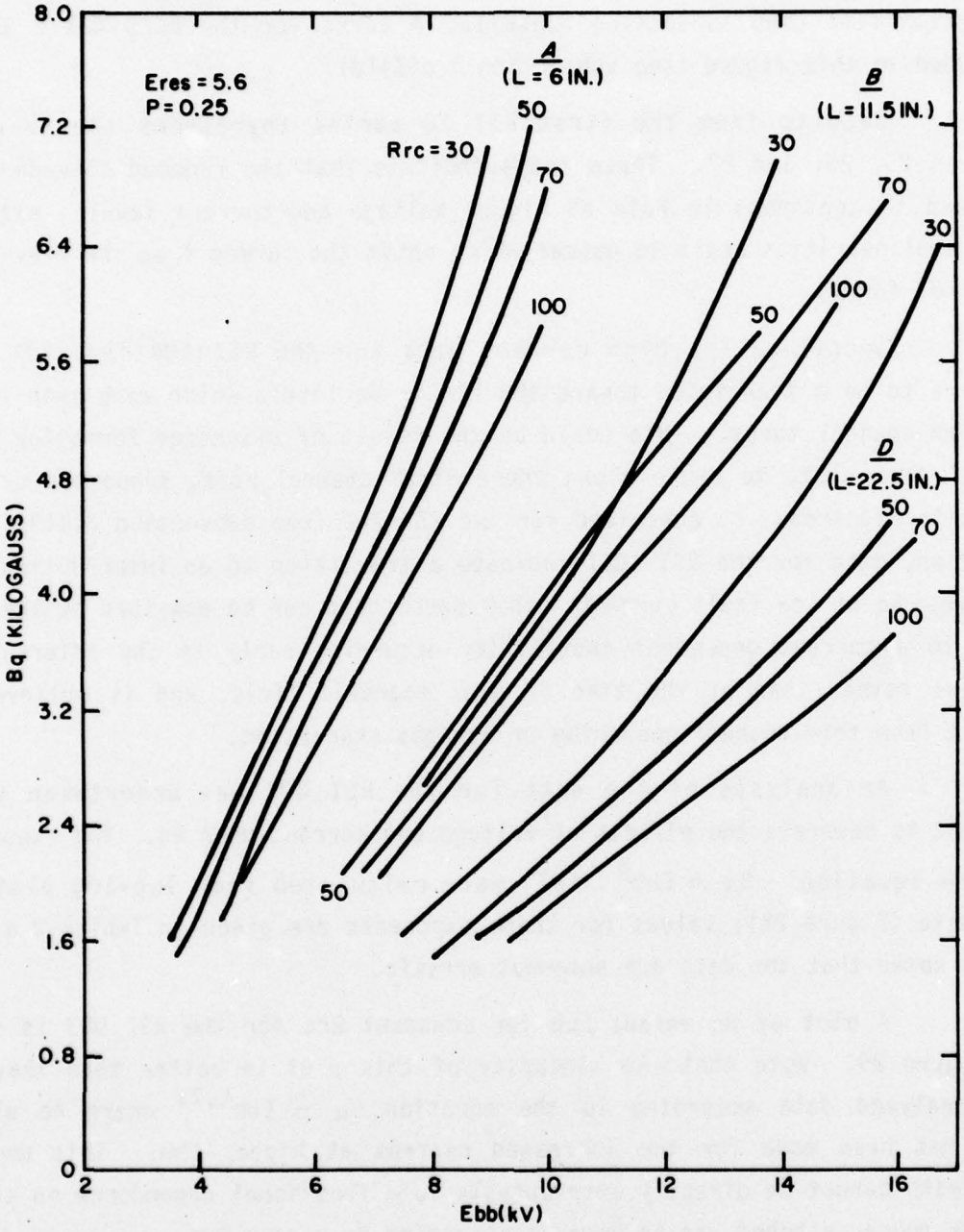

Figure 20. Quenching magnetic field versus RSI supply voltage (Ebb), length of interaction tube (L), and the fault network load resistance (Rrc) for the RSI 003.

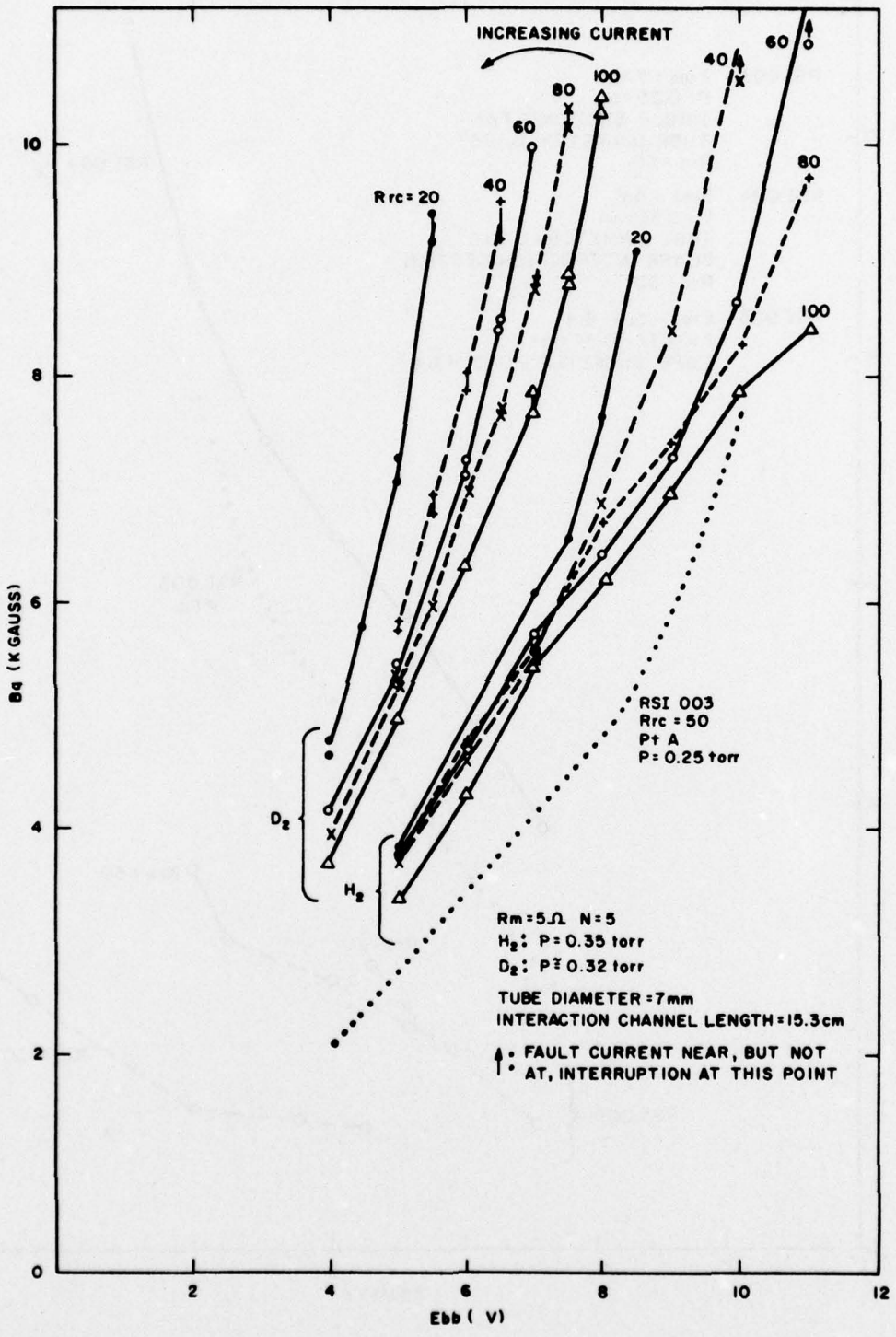

Figure 21. Bq versus Ebb, Rrc for RSI 004: D_2 versus H_2.

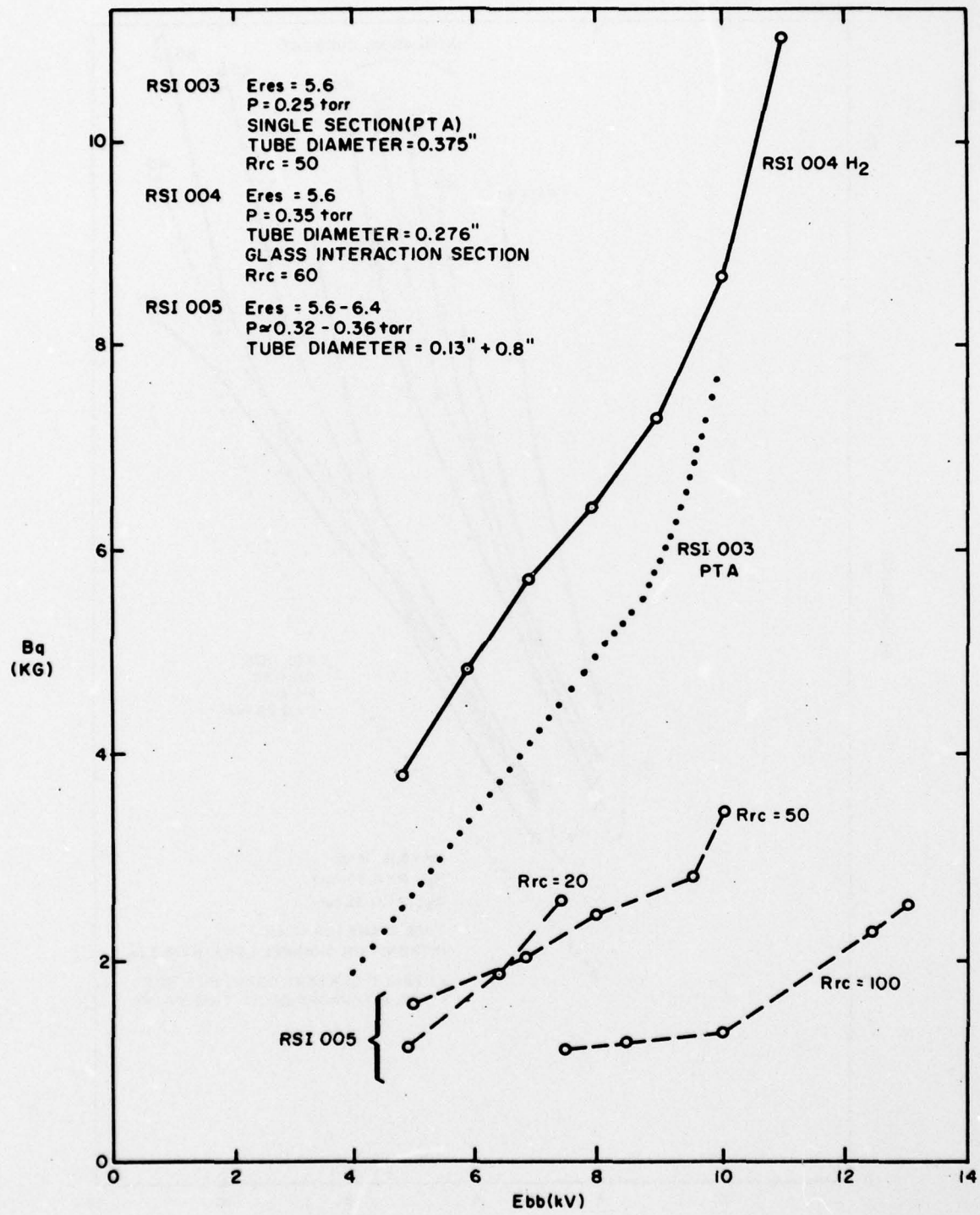

Figure 22. Bq versus Ebb for several tubes.

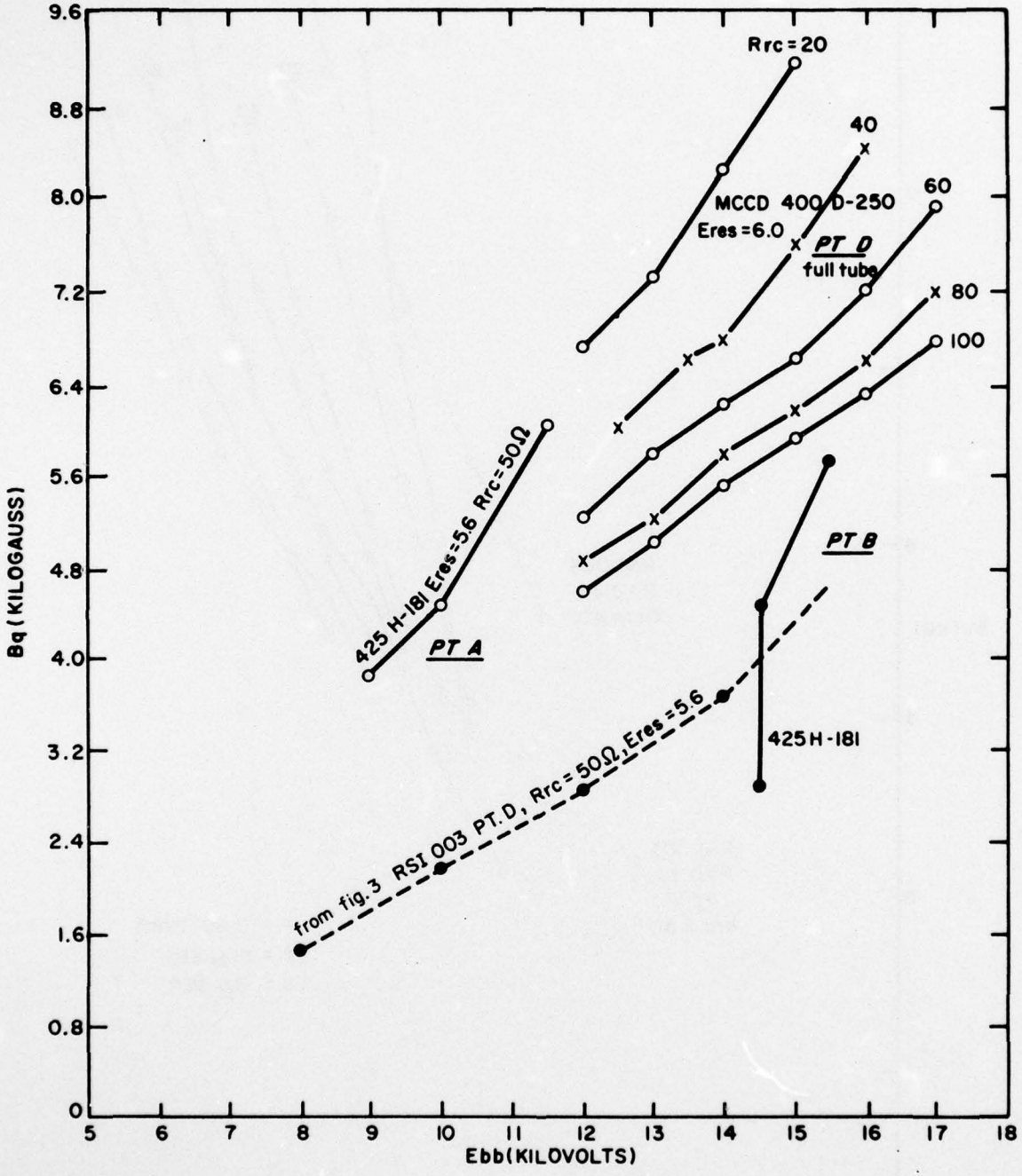

Figure 23. Quenching field versus main supply voltage (Ebb) for several tubes.

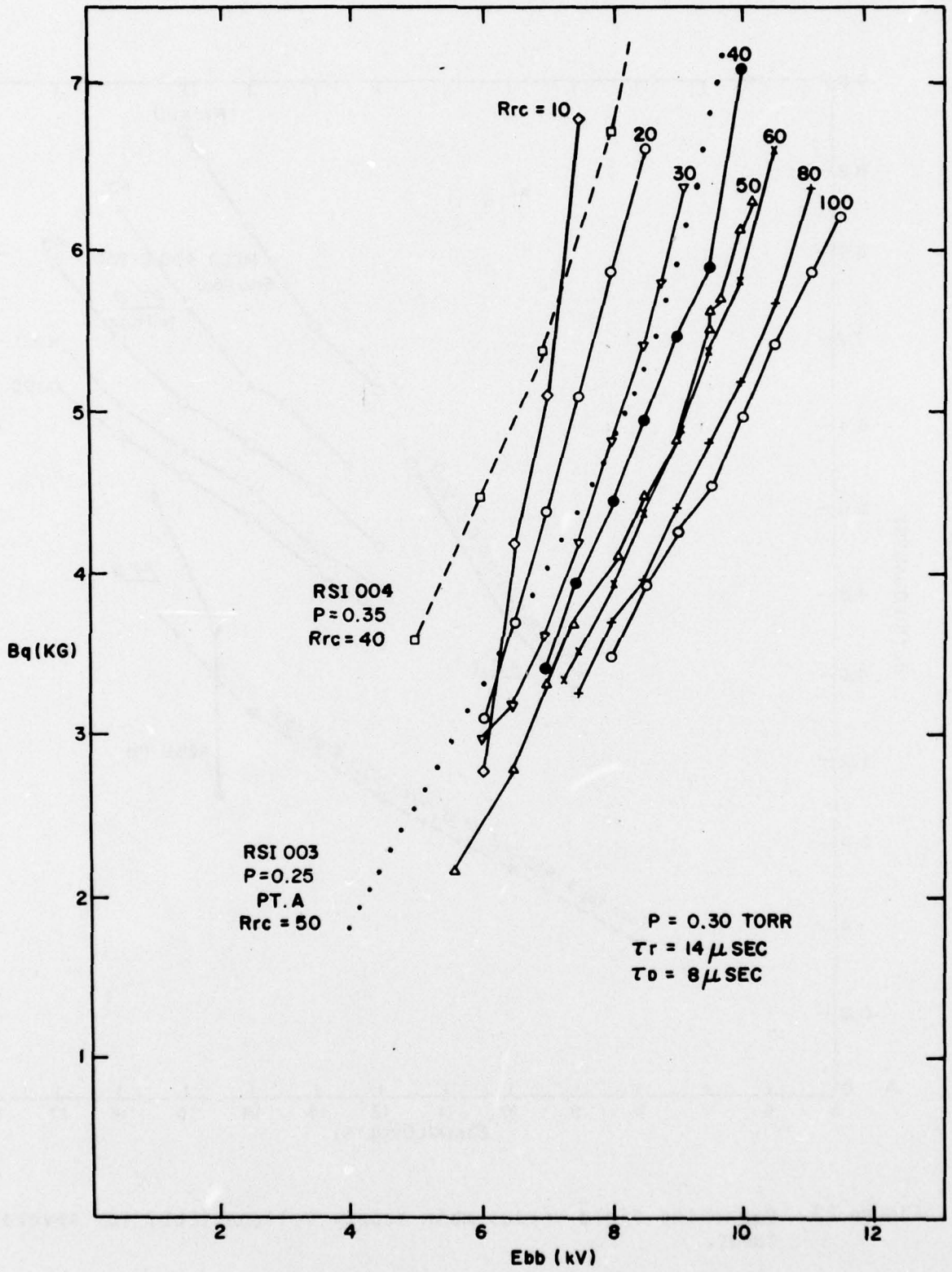

Figure 24. Bq versus Ebb, Rrc for RSI 7-2.

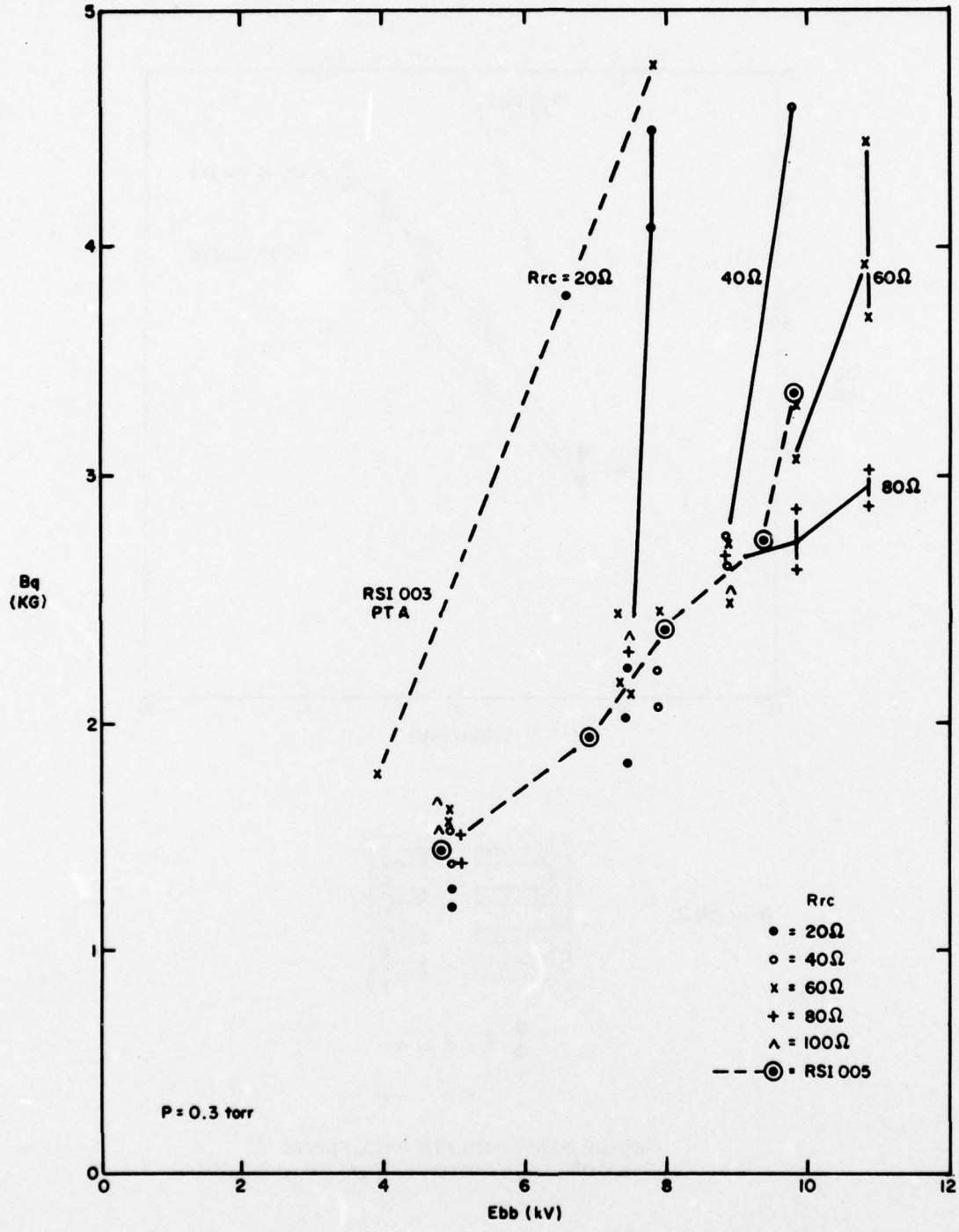

Figure 25. Bq versus Ebb for RSI 10A.

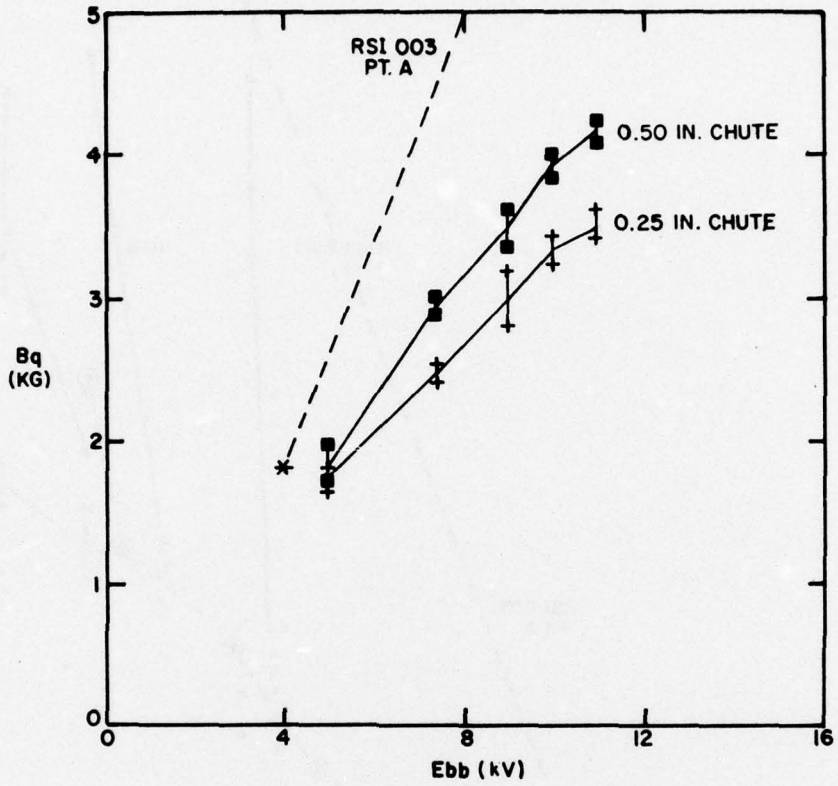

Rrc = 80Ω

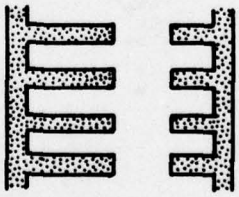

$\vec{I} \times \vec{B}$: ←

$\vec{I} \times \vec{B}$: →

"ERROR BARS" INDICATE DATA POINTS
FOR 50%, 90% INTERRUPTION PROBABILITY

Figure 26. Bq versus Ebb, chute depth for RSI 10A.

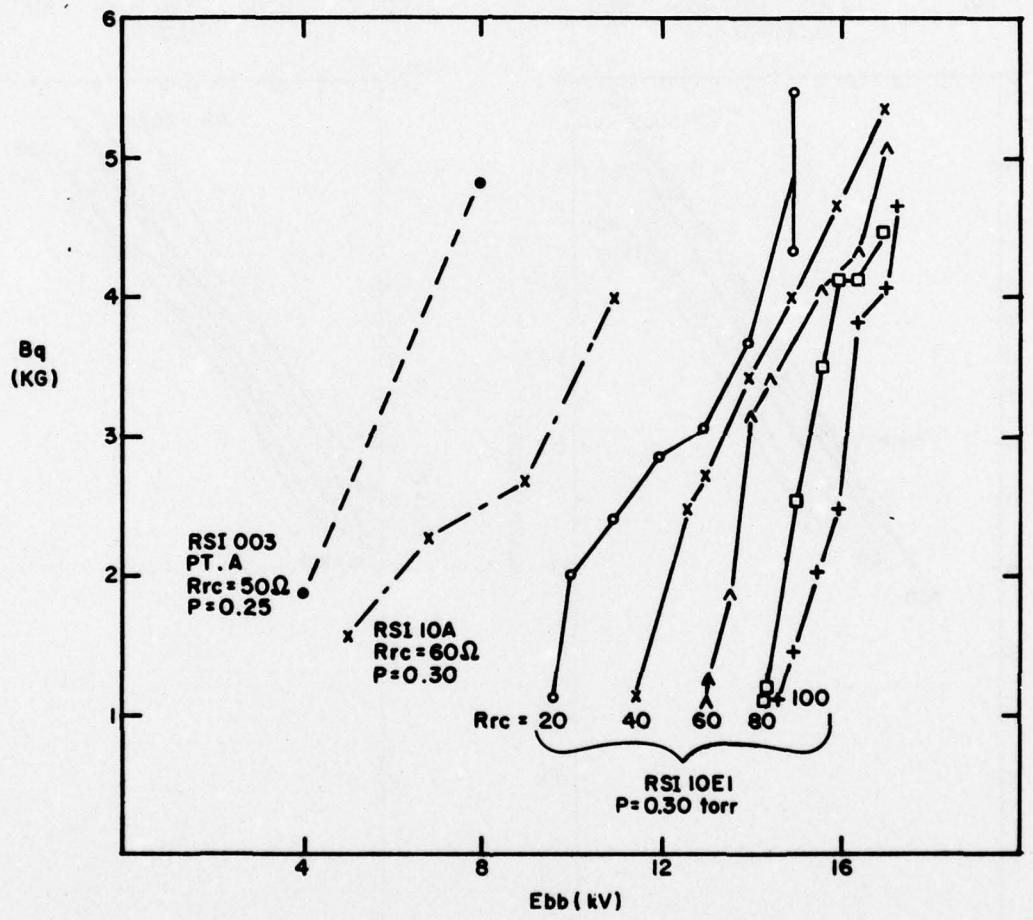

Figure 27. Bq versus Ebb, Rrc for RSI 10E1.

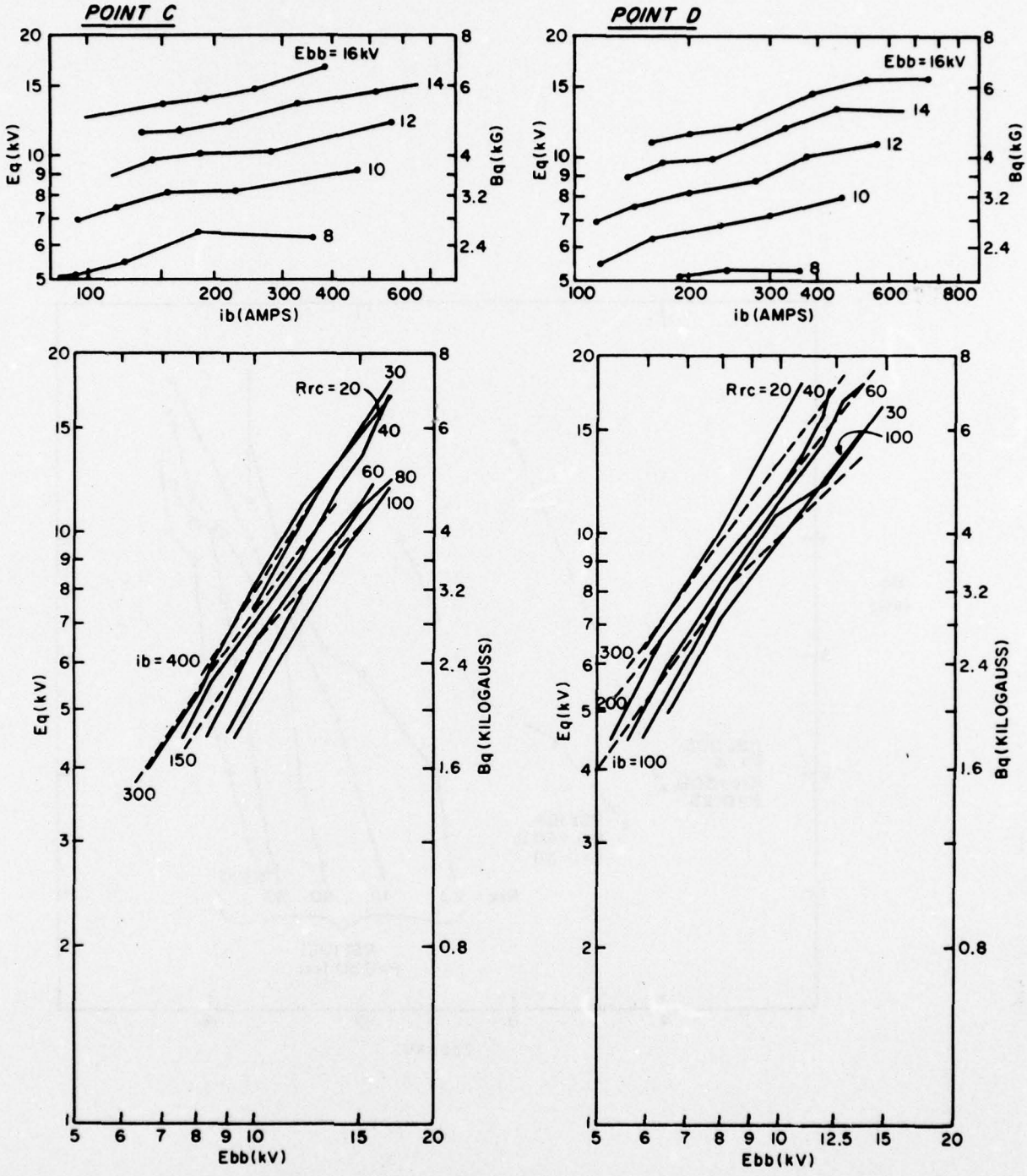

Figure 28. Quenching magnetic field (Bq) versus peak RSI-current (ib) and voltage (Ebb): Separation of parameters in the RSI 003.(Eres = 5.6).

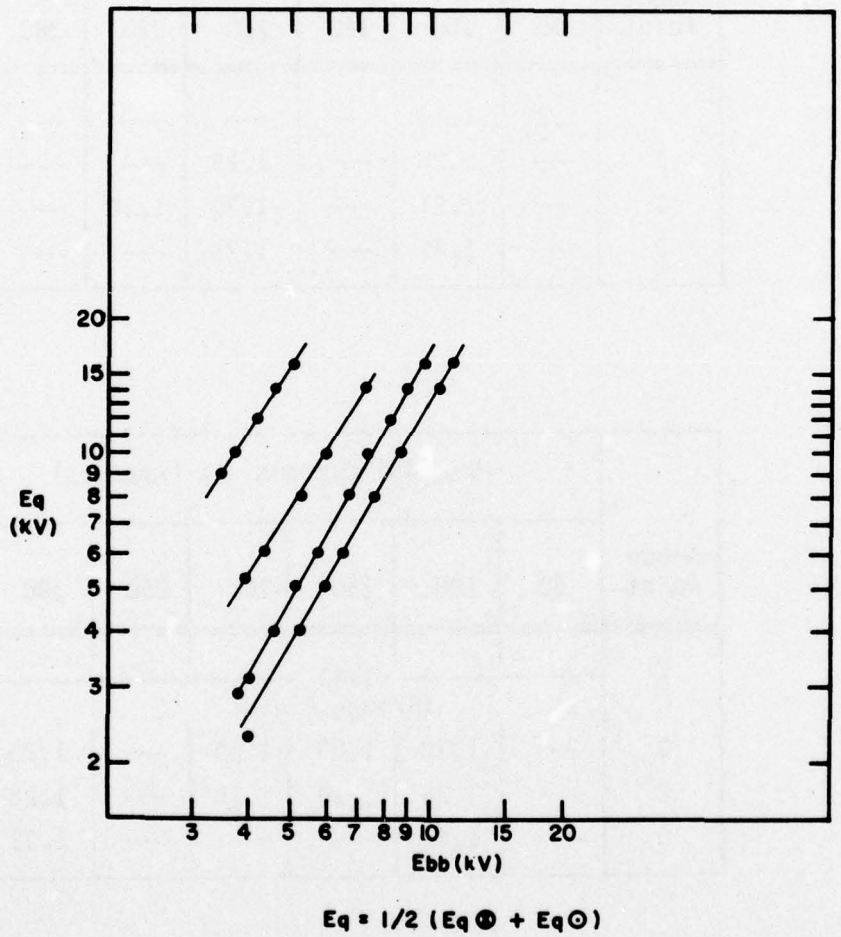

Figure 29. Eq versus Ebb for RSI 003.

Table 2. Experimental Values of β for the Equation Bq α $(Ebb)^{\beta}$. RSI 003 Eres = 5.6, p = 0.25 torr.

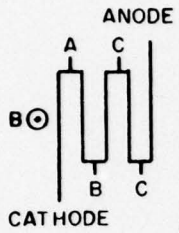

FIELD DIRECTION

Anode Point	Peak RSI Current, ib (Amperes)						
	50	100	150	200	250	300	400
A	1.22	1.16	—	—	—	—	—
B	—	1.25	—	1.25	—	—	—
C	—	1.21	—	1.30	1.32	—	—
D	—	1.41	—	1.21	—	—	—

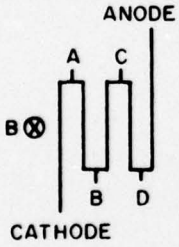

FIELD DIRECTION

Anode Point	Peak RSI Current, ib (Amperes)						
	50	100	150	200	250	300	400
A	← 1.41 (Fringe Field) →						
B	—	1.28	1.05	1.19	—	1.25	—
C	—	1.26	1.10	1.15	—	1.28	1.32
D	—	1.47	—	—	—	1.32	1.43

Table 3. Experimental Values for δ for the Equation $Bq \alpha (ib)^{\delta}$. RSI 003 Eres = 5.6, p = 0.25 torr.

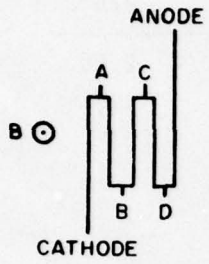

Anode Point	Main Supply Voltage, Ebb (Kilovolts)								
	5	6	7	8	10	12	14	15	16
A	—	0.18	—	0.43	0.57	—	—	—	—
B	—	—	—	0.24	0.06	0.19	—	0.17	—
C	—	—	—	0.42	0.21	0.25	—	0.31	—
D	—	—	—	0.47	0.44	0.30	—	0.34	—

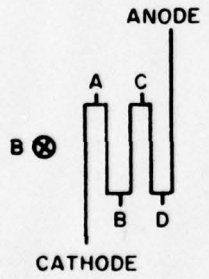

Anode Point	Main Supply Voltage, Ebb (Kilovolts)								
	5	6	7	8	10	12	14	15	16
A	0.04	0.02	0.04	0.07	—	—	—	—	—
B	—	—	—	0.17	0.22	0.30	0.30	—	—
C	—	—	—	0.14	0.14	0.14	0.18	—	0.19
D	—	—	—	0.06	0.28	0.31	0.32	—	0.31

Table 4. Experimental Values of β for Bq α $(Ebb)^{\beta}$
For the RSI 7-2 (p = 0.3 torr).

ib (amp)	100	125	175	225	275
β	1.46	1.45	1.26	1.72	1.65

Table 5. Experimental Values of δ for Bq α $(ib)^{\delta}$
For the RSI 7-2 (p = 0.3 torr).

Ebb (kV)	7	7.5	8	8.5	9	9.5	10	10.5	11
δ	0.21	0.29	0.29	0.30	0.29	0.32	0.37	0.29	0.41

An alternate method of data presentation is shown in Figure 30, where ib and Ebb are related through constant Bq for the RSI 7-2 and the RSI 003.

(c) Bq Dependence on the Length of the Interaction Channel

An expectation that the interrupting magnetic field level will be inversely proportional to the length of the interaction channel is based on the observation that the enhanced voltage drop induced in the plasma column by the application of the magnetic field is nearly proportional to the magnetic field, as is demonstrated in subsection 3.c(2). Since the total enhanced voltage drop in the interaction column is equal to the sum of the multiple lengths in series of the interaction column, the expectation is that the total enhanced drop should be proportional to the length of the column, and that therefore the interrupting field should act in the same manner. Previous experimentation based on limited data (Thomas et al.[13], p. 100) concluded that this relationship is nearly linear.

Results from parametric studies of the RSI 003, the MCCD 425 H 181, and the MCCD 400D 250 (Figures 31 and 32), however, indicate that the dependence is less than linear: average exponential dependences for the three tubes are $Bq \alpha L^{-0.78}$, $Bq \alpha L^{-0.71}$, and $Bq \alpha L^{-0.87}$, respectively. Furthermore, studies with the RSI 003 (Tables 6 and 7) indicate that the exponent decreases at higher power.

The nonlinear relationship is caused by: (1) the folding of the discharge channel, and (2) the nonuniformity of magnetic field within the air gap (Figure 16). At the point of a fold in the discharge channel, the plasma column apparently shortens its path length to follow the electric field lines, thereby decreasing the total path length somewhat from that of the channel center. A 10% decrease in column length can be derived in this manner.

The magnetic field level decreases by as much as 25% at the outside edges of the air gap. An average 15% decrease in field strength toward the air gap extremities results in a completion of the correction factor to explain the nonlinearity of Bq versus L.

In the consideration for selection of design length for the interaction channel, however, these corrections must be taken into consideration.

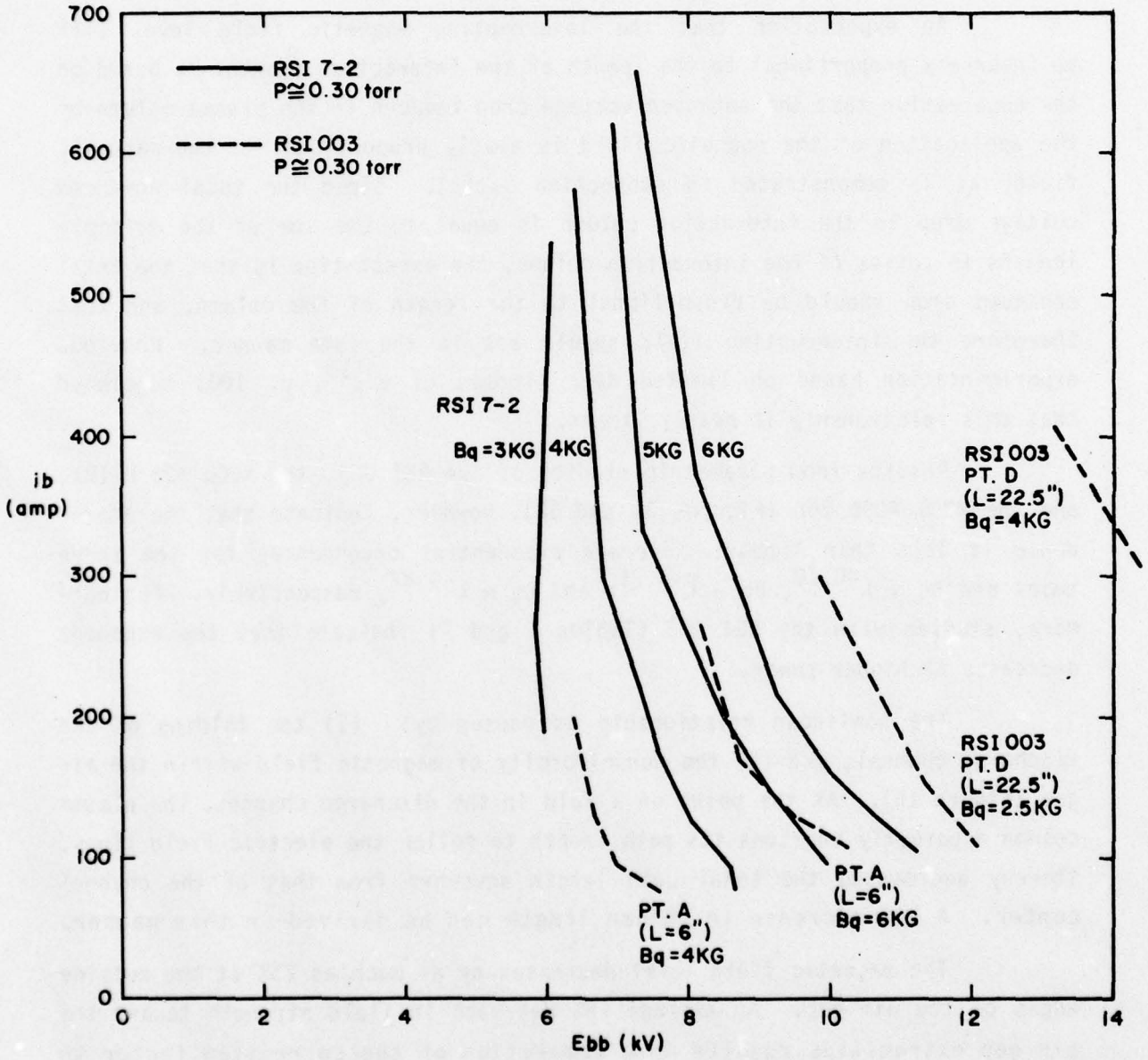

Figure 30. Interrupting magnetic field versus tube voltage and current for RSI 7-2.

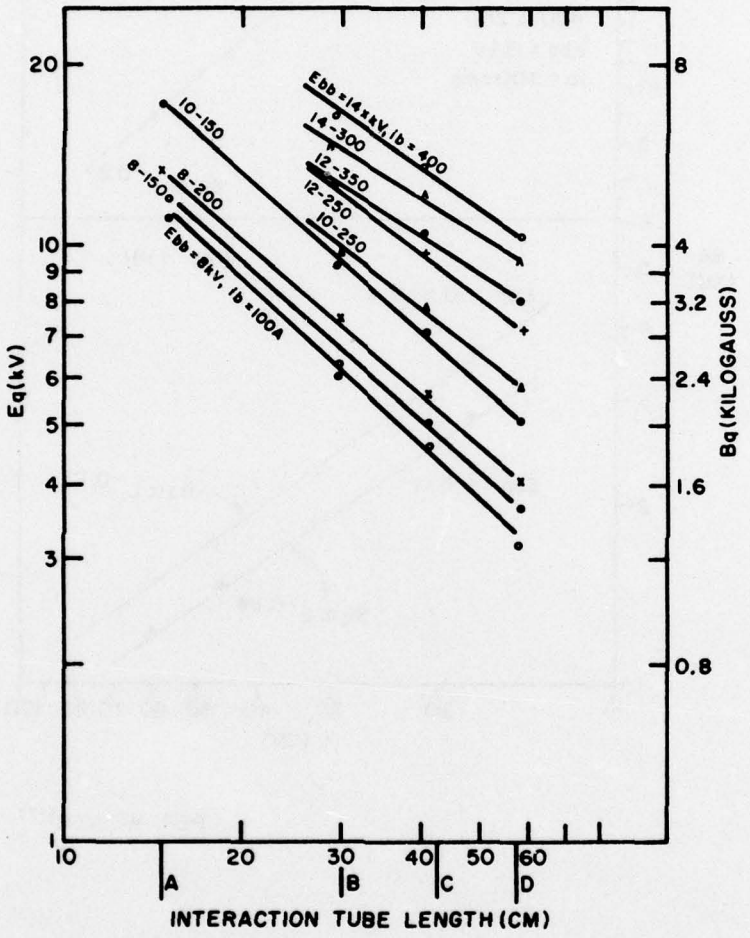

Figure 31. Quenching magnetic field versus tube length, main supply voltage (Ebb), and peak-RSI-carried current (ib) for the RSI 003.

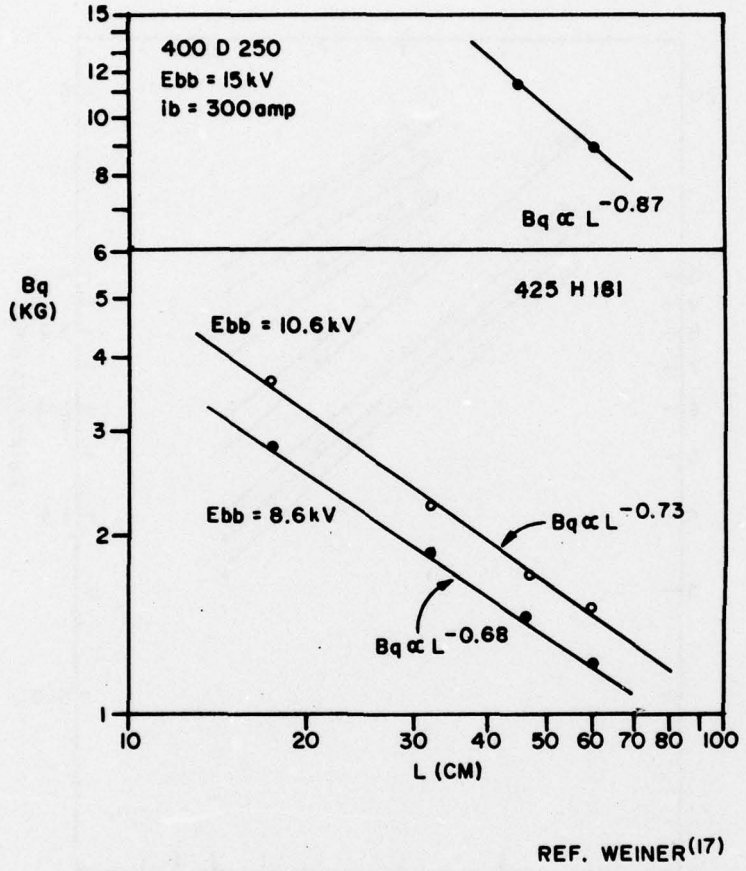

Figure 32. Bq versus L for tubes 425H181 and 400D250

Table 6. Values of m for $Bq \alpha L^{-m}$ for RSI 003.

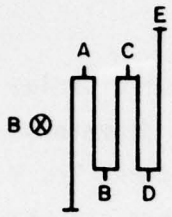

FIELD DIRECTION

ib (amperes)	Ebb (kilovolts) → 8	10	12	14	16
100	0.90	0.92	0.74	—	—
150	0.83	0.74	0.69	0.59	—
200	0.73	0.65	0.73	0.70	—
250	0.76	0.77	0.77	0.74	—
300	0.76	0.68	0.81	—	—
400	0.76	0.83	—	—	—

Table 7. Values of m for $Bq \alpha L^{-m}$ for RSI 003.

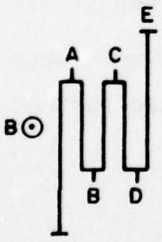

FIELD DIRECTION

ib (amperes)	Ebb (kilovolts) → 8	10	12	14	16
100	0.93	0.89	0.88	0.87	—
150	0.91	0.89	—	0.87	—
200	0.87	—	0.90	—	0.68
250	—	0.76	0.76	0.87	—
300	0.83	0.68	0.77	0.62	—
350	—	—	0.63	—	—
400	—	—	—	0.71	—

A final design must use a folded discharge channel and a "real world" air gap in order to minimize magnetic field fringe losses. In this regard, the use of a value for m = +0.75 is required.

(d) Bq Dependence on Interaction Channel Diameter

Figure 33 illustrates the relative requirements for Bq for a series of tubes of approximately 6-inch length with differing internal diameters. Test conditions for the series of tubes are nearly equal (p = 0.3 torr, Rrc = 50Ω) with the exceptions that the RSI 003 tube was tested at 0.25 torr and the RSI 004 H_2 at approximately 0.35 torr and Rrc = 60Ω. These effects can be eliminated by a shift of the RSI 003 curve by +15% and of the RSI 004 curve by -10%.

When these corrections are made, there is little difference between the Bq values for the RSI 003 and the RSI 004 H_2, but there is a reduction in Bq of 50% in changing from 0.25-inch or 0.375-inch channel bore to a 0.19-inch bore. The cause for this behavior is uncertain; theoretical arguments suggest that the constructed plasma column sustaining voltage is independent of tube diameter (see section 4.b). A contributing factor to explain this phenomenon may be the added instability caused by a gas starvation mechanism similar to grid-quenching seen at somewhat higher current densities.

It is apparent from Figure 33 that the nonuniform channel tubes effectively reduce the requirement for Bq. This feature is discussed further in subsection 3.c(10).

(e) Bq Dependence on Tube Pressure

Tube pressure has a substantial effect upon the Bq requirement, particularly at low values, as is demonstrated in Figures 34 through 39. Figures 34 and 35 illustrate the fact that this dependence is more pronounced at higher Ebb.

Figures 36 and 38 reveal two forms of dependence upon pressure. At higher pressure levels, a gradual and constant slope occurs over a fairly wide range of pressure. At lower pressure, a sudden decline occurs as the thyratron apparently runs out of gas and becomes considerably easier to interrupt. The pressure at which this occurs is considerably higher for the chuted RSI 10 series tubes.

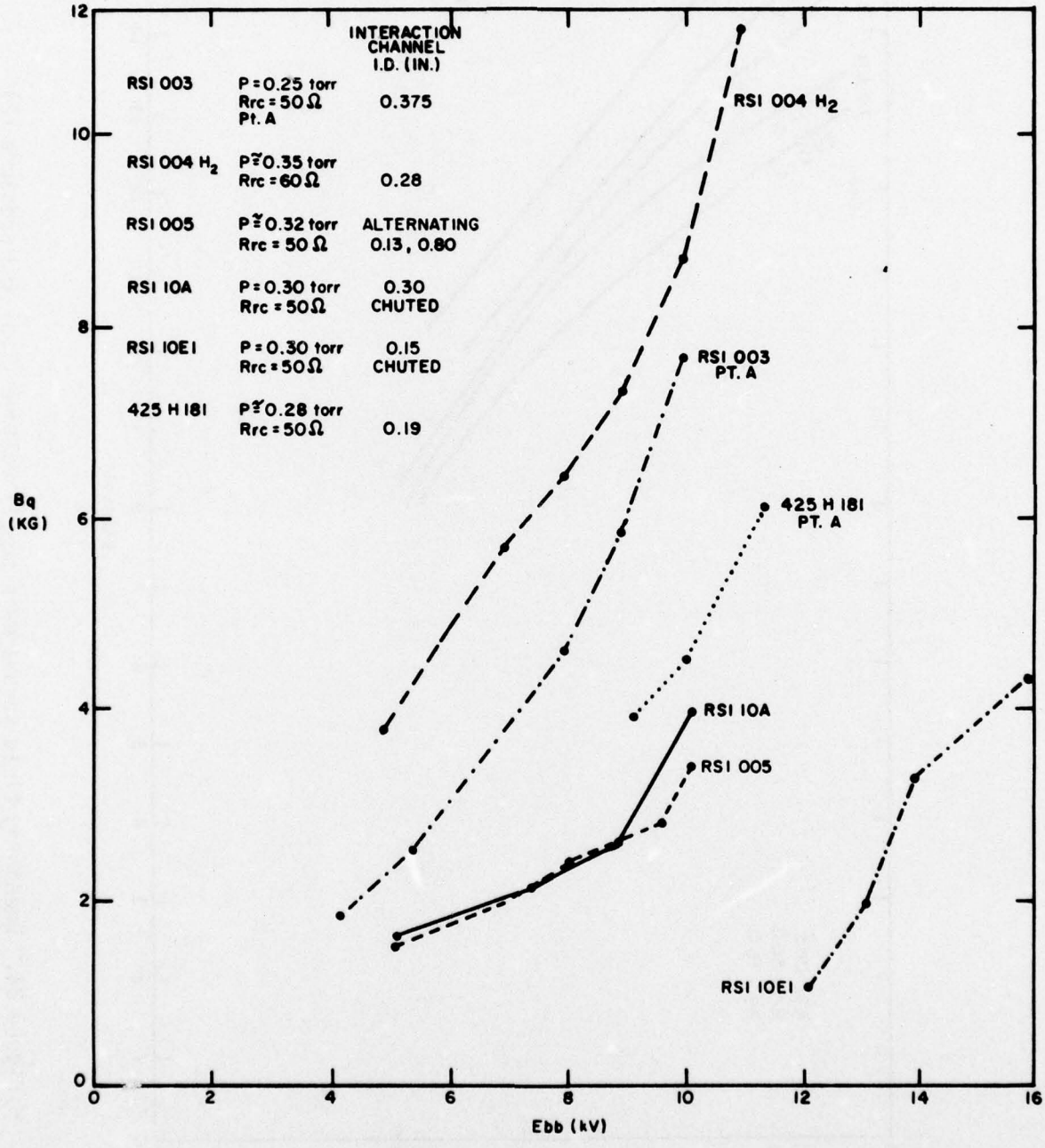

Figure 33. Bq versus Ebb for 6-inch interaction channels of varying I.D.

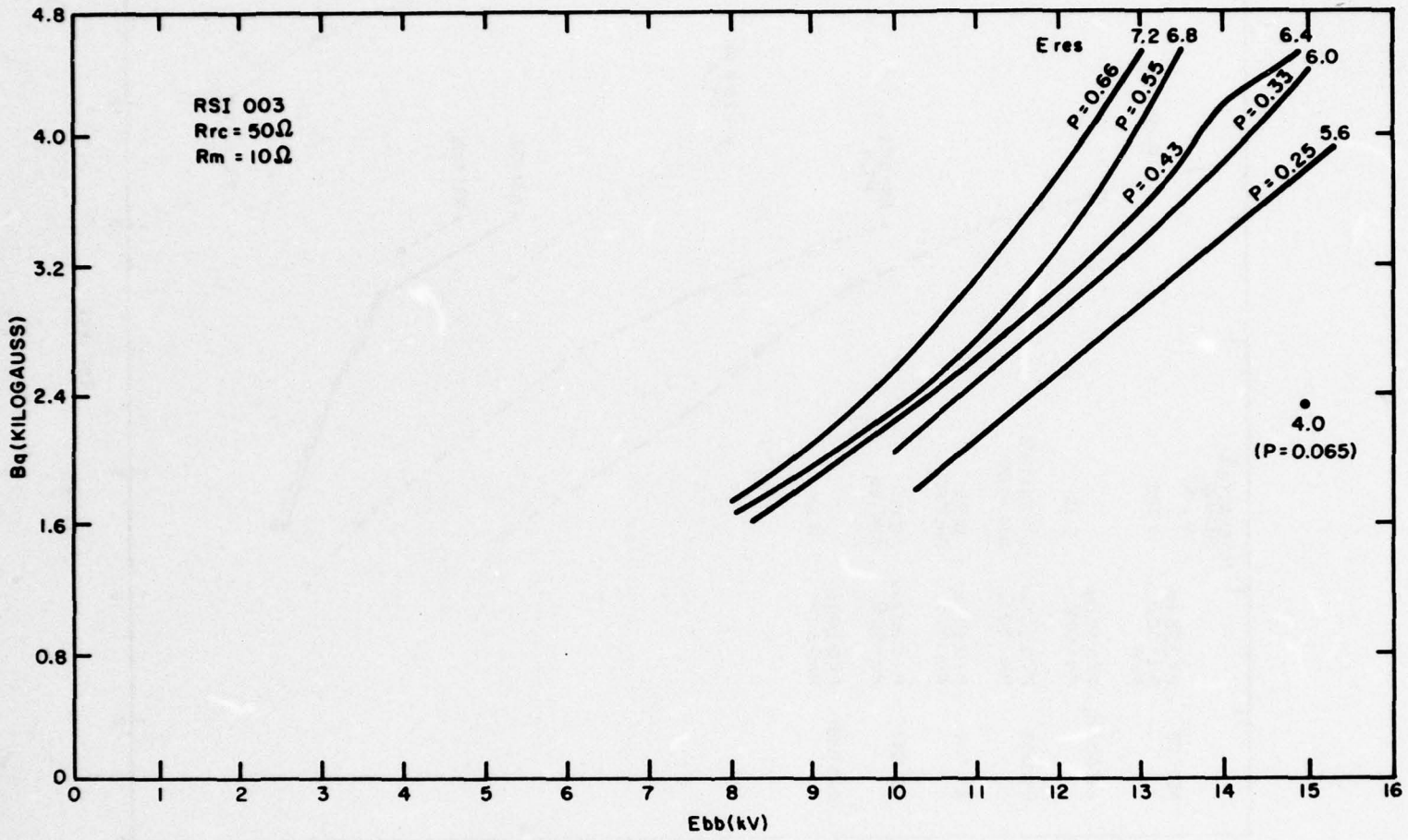

Figure 34. Quenching field versus main supply voltage (Ebb) and pressure (P) for the RSI 003.

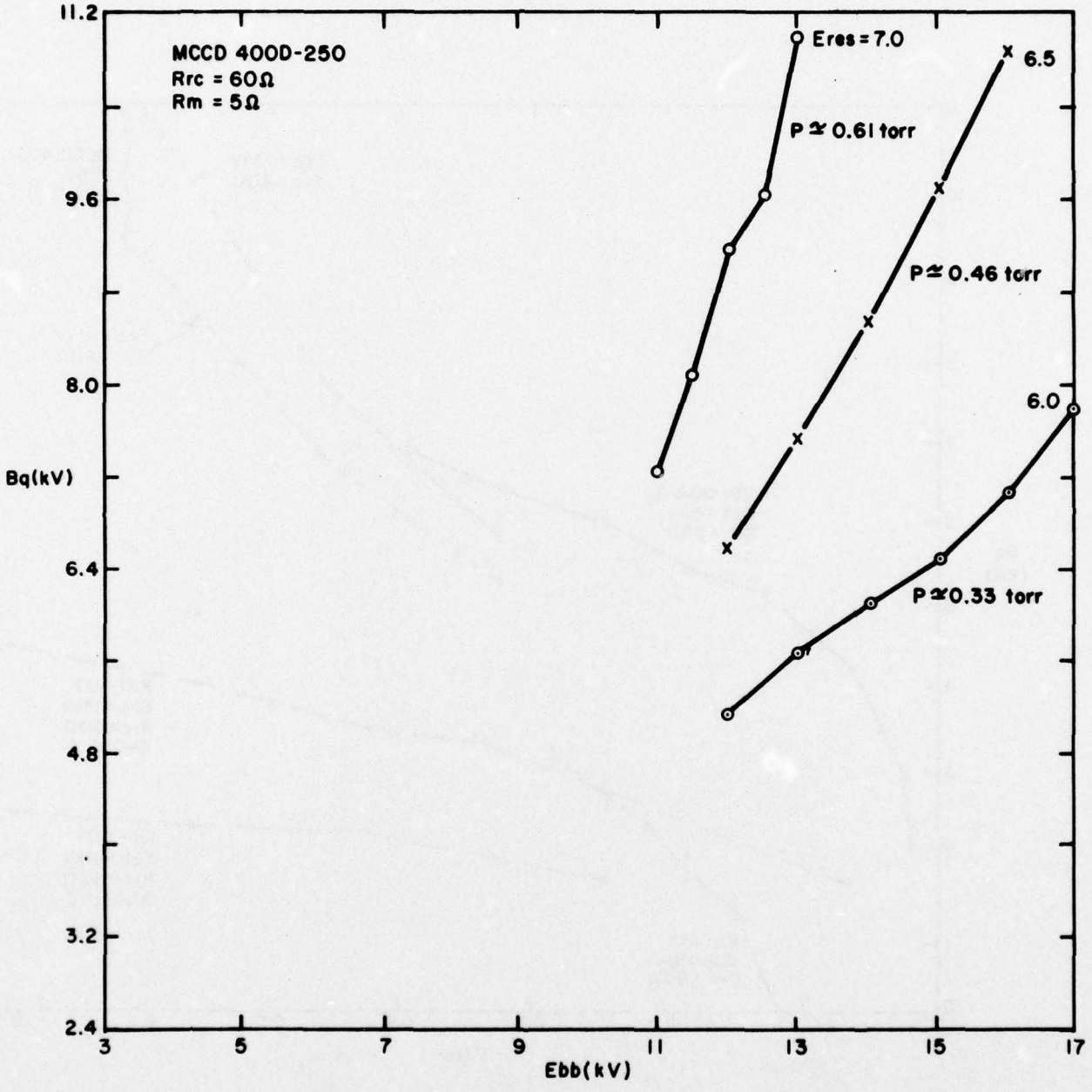

Figure 35. Quenching field versus main supply voltage (Ebb) for the MCCD 400D-250.

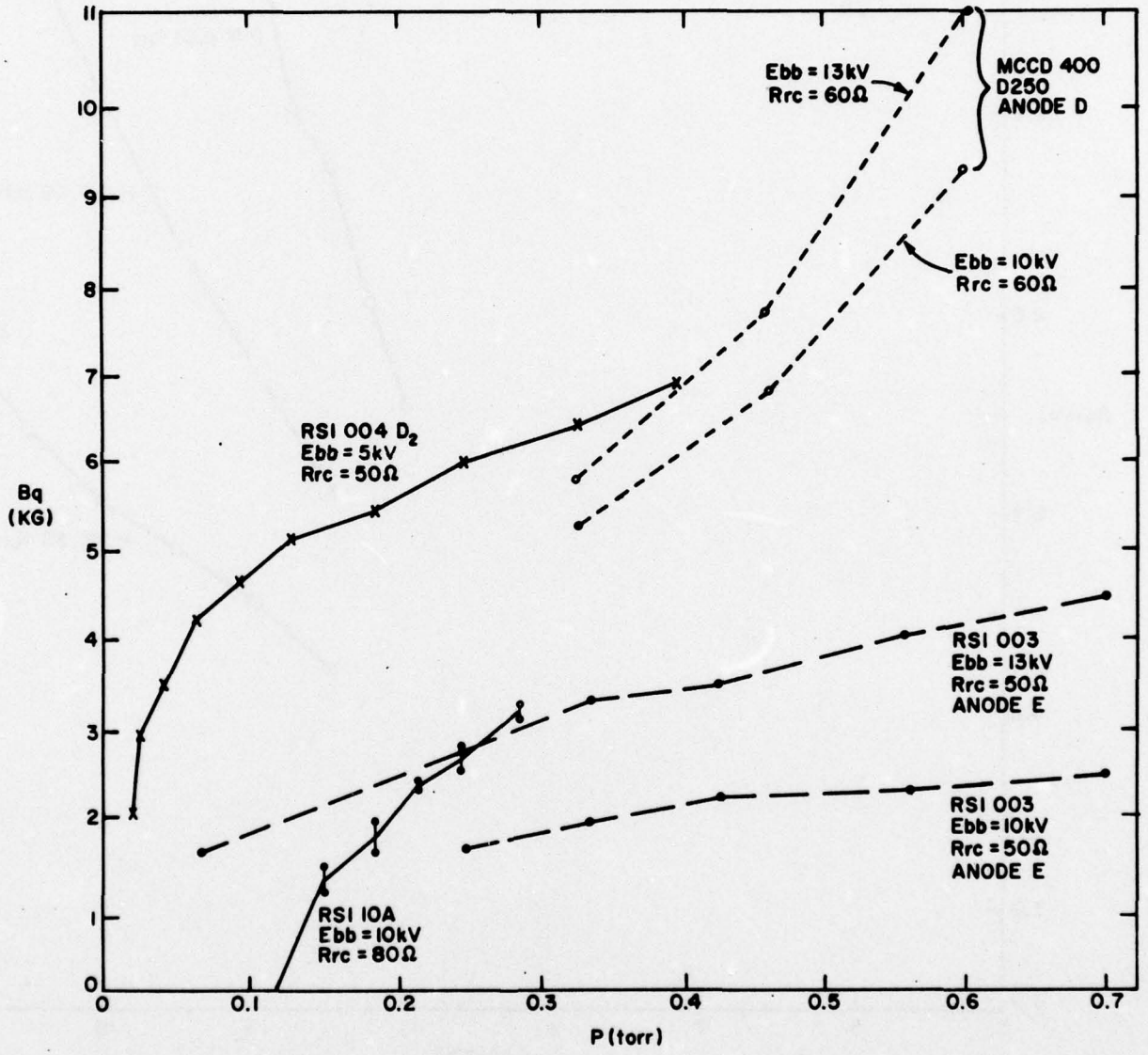

Figure 36. Bq versus tube pressure for several tubes.

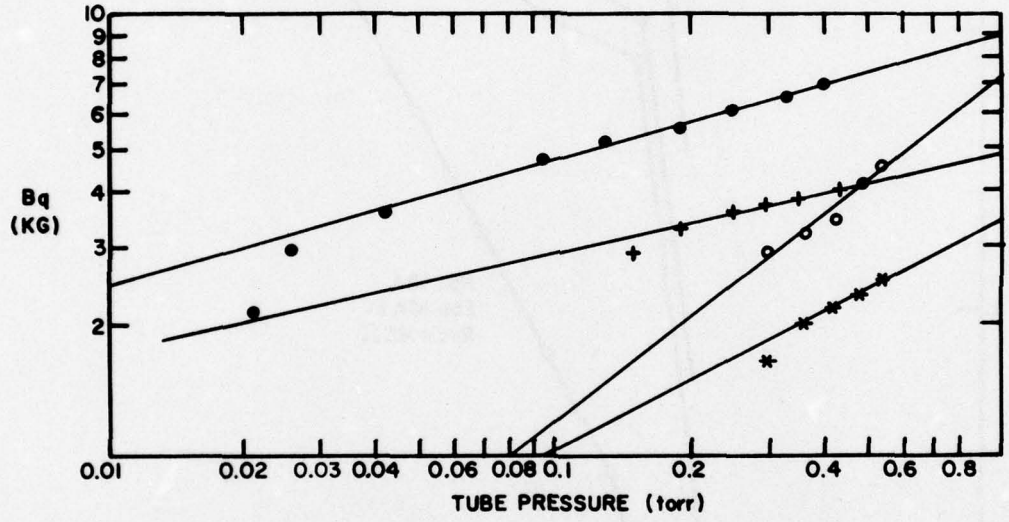

Figure 37. Interrupting magnetic field versus tube pressure for RSI 003, RSI 004 D_2, RSI 10E1.

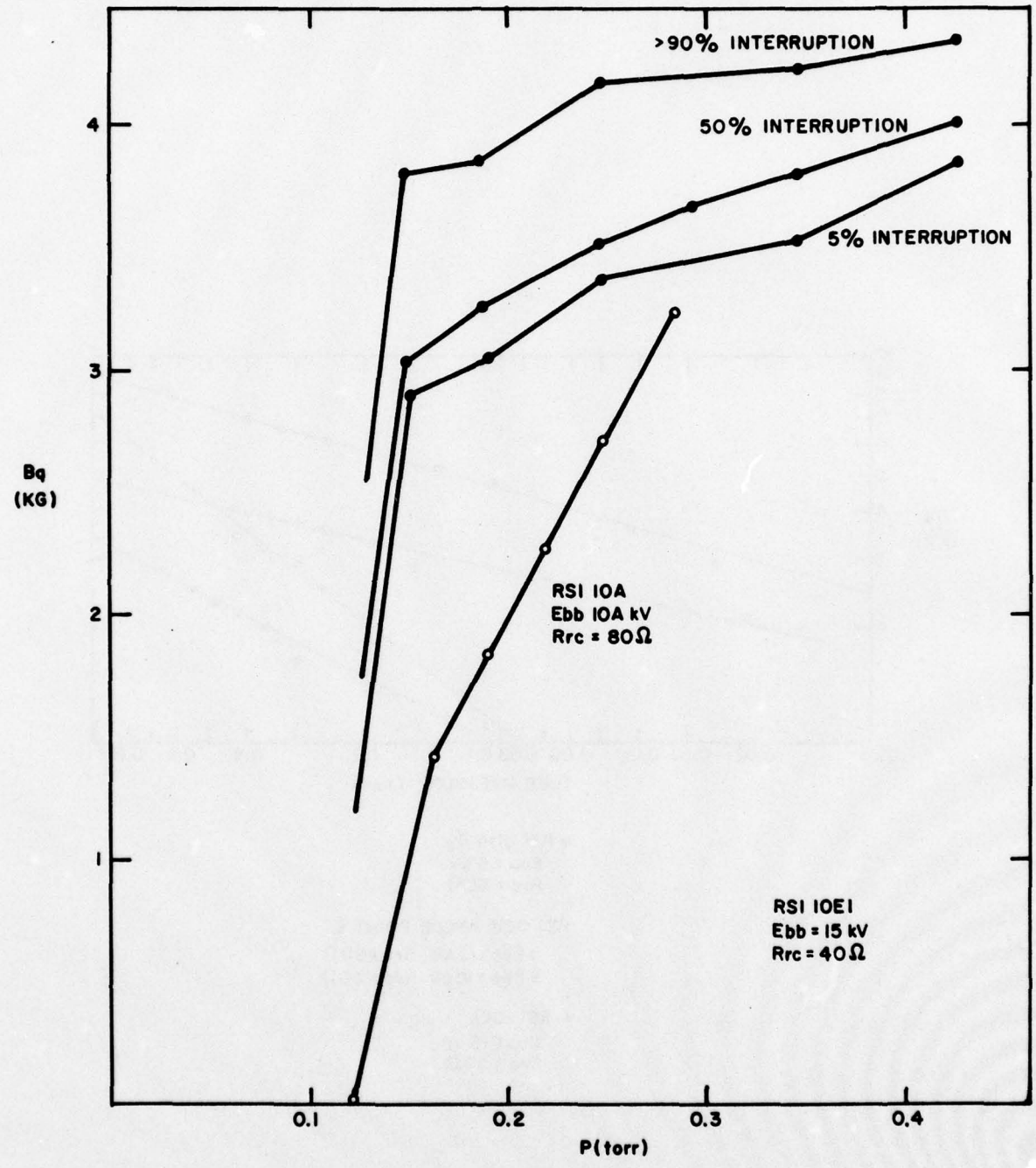

Figure 38. Interrupting magnetic field versus pressure for RSI 10E1.

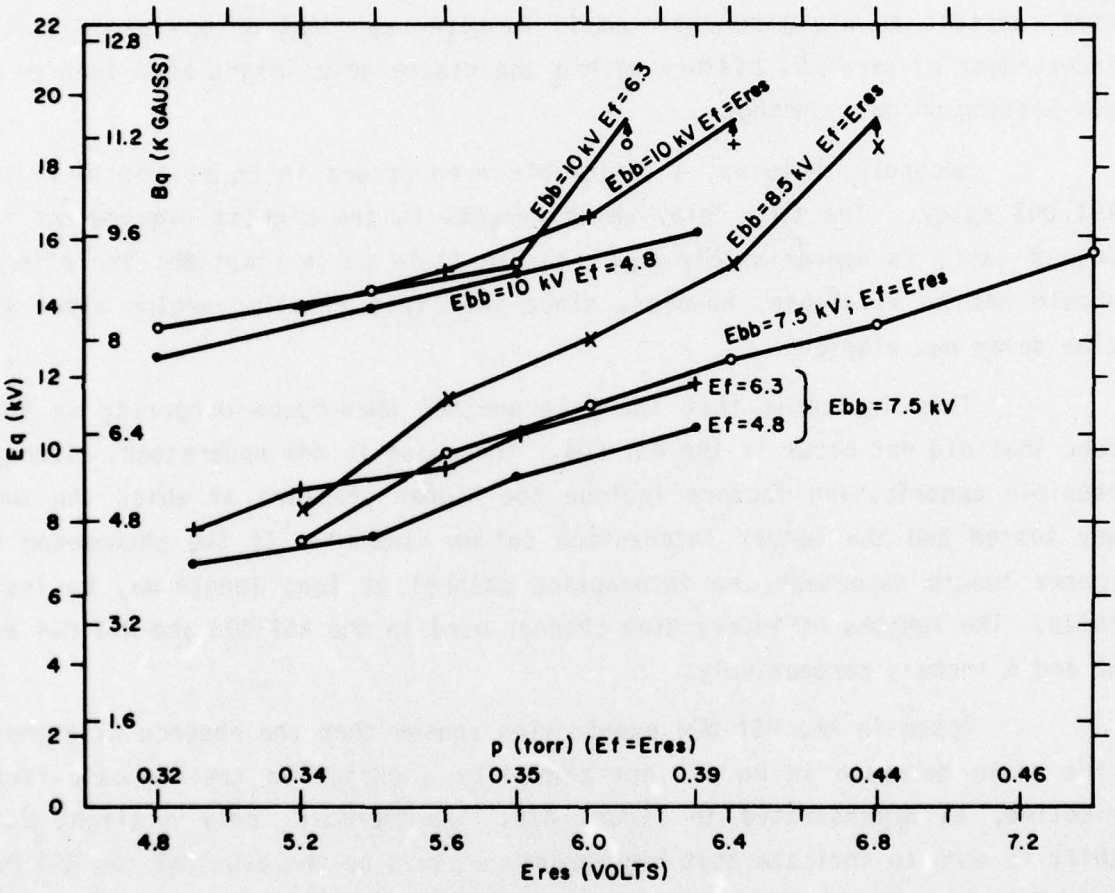

Figure 39. Interrupting magnetic field versus tube pressure for RSI 004.

(4) Bq Dependence on Magnetic Field Pulse Delay and Risetime

Two examinations were made to determine the effect of the magnetic field pulse delay (τD, the interval between the firing of the fault discharge and the triggering of the magnet circuit discharge) on Bq; results of the two tests are shown in Figures 40 and 41. These results reveal two differing dependencies. First, both demonstrate that after an initial portion of time for stabilization of the discharge, the magnetic field required for interruption is proportional to the fault voltage waveform, dropping with the same RC time constant as would be expected if Bq were dependent on epy alone (i.e., independent of previous history within the discharge as might be evidenced in gas heating or gas pumping).

Secondly, however, a noticeable drop occurs in Bq at low τD in the RSI 003 study. The time delay which results in the highest requirement for Bq, 12 μsec, is approximately equal to the field pulse risetime; the effects should not be relatable, however, since the field risetime begins after the time delay has elapsed.

This indicates that there is another phenomenon occurring in this tube that did not occur in the RSI 004. The cause is not understood, although possible contributing factors include the higher pressure at which the tube was tested and the longer interaction column studied. If the phenomenon is indeed length dependent, an interaction channel of long length may be indicated. The lengths of interaction channel used in the RSI 003 and RSI 004 are 32 and 6 inches, respectively.

Tests in the RSI 004 examination showed that the absence of a short time scale decrease in Bq was not caused by a change in the magnetic field risetime, as demonstrated in Figure 41b. Furthermore, only a slight data shift is seen to indicate that high pressure could be the cause of the RSI 003 type low time delay Bq drop, and that data point is inside the limits of experimental error ("error bars" shown in Figure 41a represent the points of 50% and 90% interrupting probability). The shifts within the Figure 41a curves versus Ef are believed to be caused by parasitic heating of the reservoir from the cathode heating element.

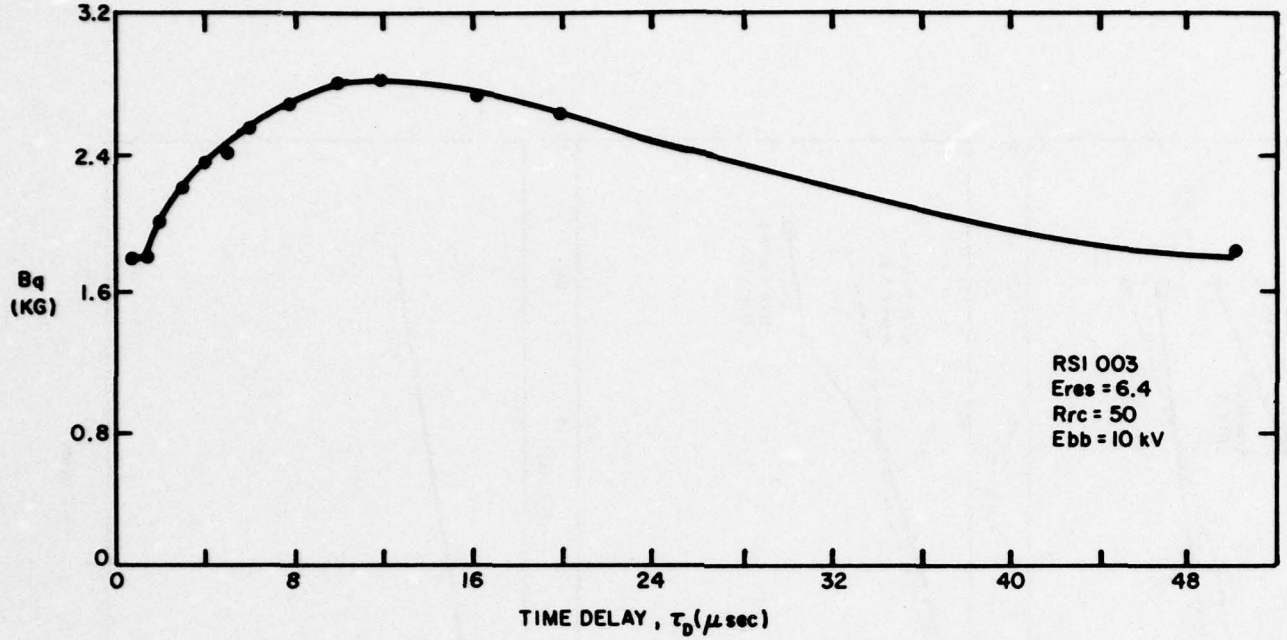

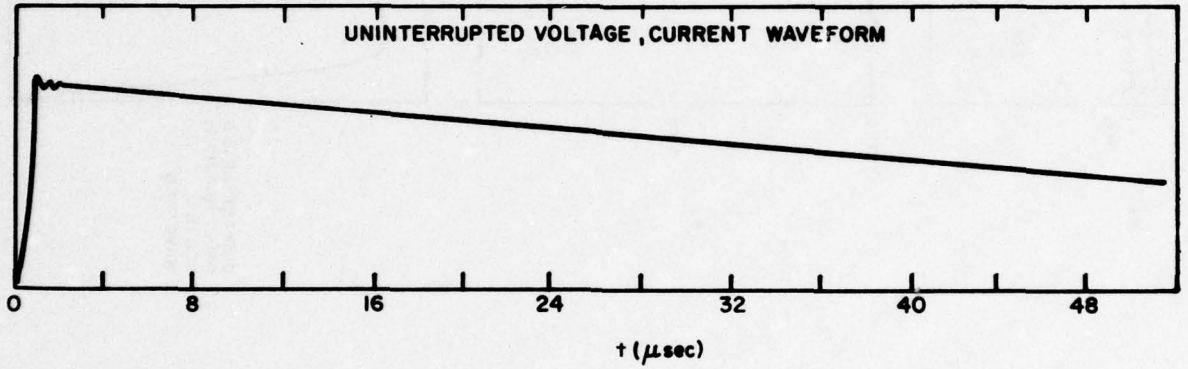

Figure 40. Bq versus magnetic circuit firing delay for RSI 003.

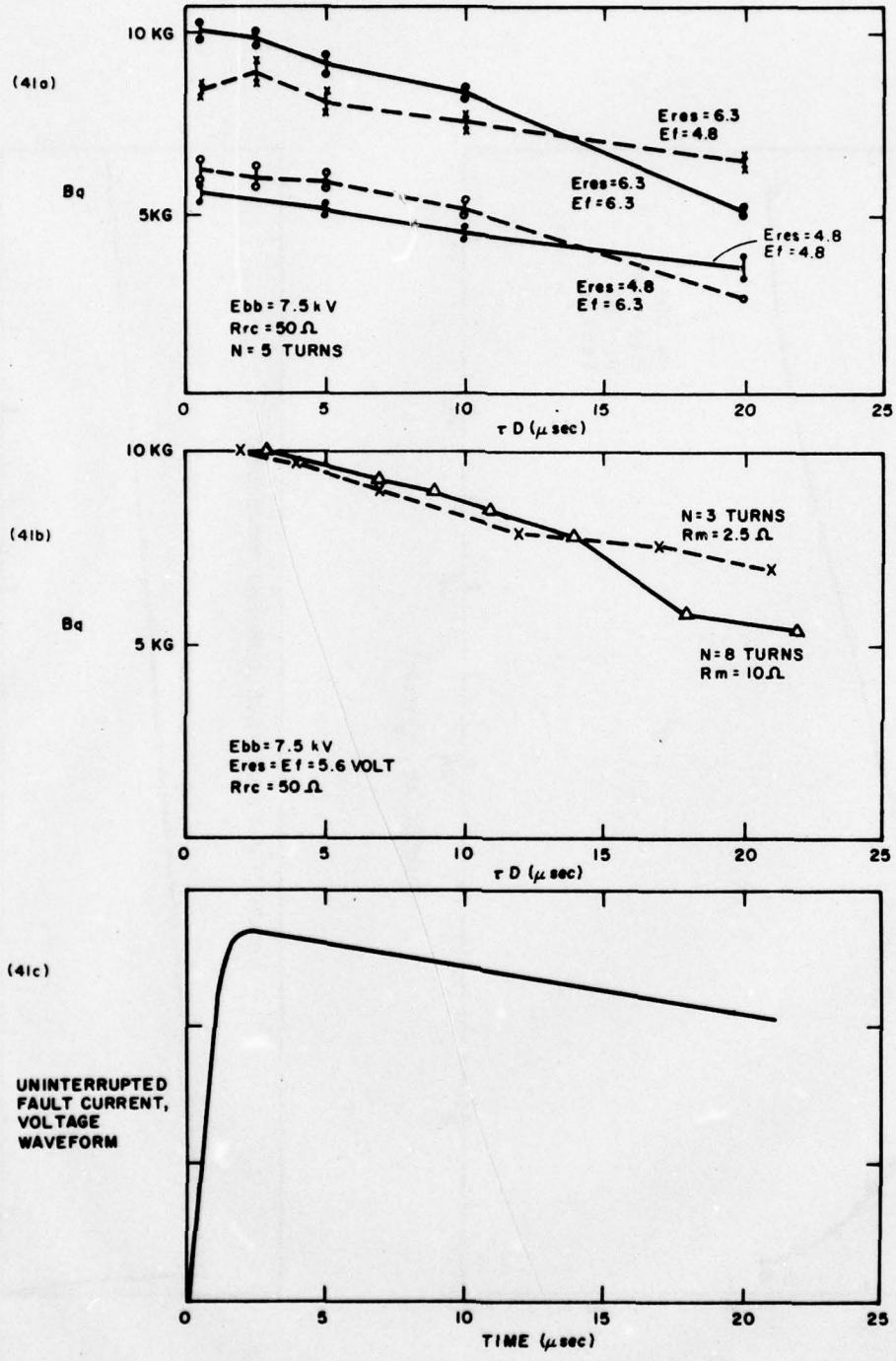

Figure 41. Interrupting field versus magnet firing delay time for RSI 004.

The effect of the magnetic field risetime on the required interrupting magnetic field was observed. The magnet circuit shown in Figure 42a was used, where N and Rm were varied to produce a series of near critically damped magnet current pulses, with varying risetimes. Results are shown in Figure 42b, and they seem to indicate an optimum risetime of 10 μsec. These data should be reviewed with a degree of caution, however, since: (1) inductances elsewhere in the circuit become comparable to the magnet inductance at low values of N, so that stray magnetic fields become an important factor; and (2) each data point represents a slightly different waveshape corresponding to a slightly different degree of overdamping.

A study reported by Thomas et al.[13] indicated that at low power, Bq was independent of the magnetic field risetime. An increase in Bq was seen at τ_D near 1 μsec, but was attributed to nonuniformities in the magnetic field distribution.

(5) Effects of Magnetic Field Direction and Nonuniformity

Early experiments suggested that there might be a preferred field direction for fault quenching. A study of this effect demonstrated that the probable cause for observed discrepancies was due to fringe-field quenching rather than field direction.

No specific work was performed regarding field shape except for a study of the effects of fringe fields at the borders of the core gap. Figure 12 of the Second Triannual Report (Simon and Turnquist[12]) shows the effect of shifting the RSI away from the fringe fields at the interaction regions nearest the cathode. As would be expected, the discharge becomes easier to quench when all or part of the plasma column is farther within the full-field region of the magnet gap. An unexpected result obtained from a different experimental run indicated that a plasma column subjected entirely to a fringe field could be quenched with an equal but high field, independent of tube current (for the same tube voltage) (Figure 43).

(6) Restrike Occurrence

Prevention of restriking of the fault discharge after current interruption is extremely important to the success of the RSI program. One proposal for restrike prevention is to shape the magnetic field pulse to

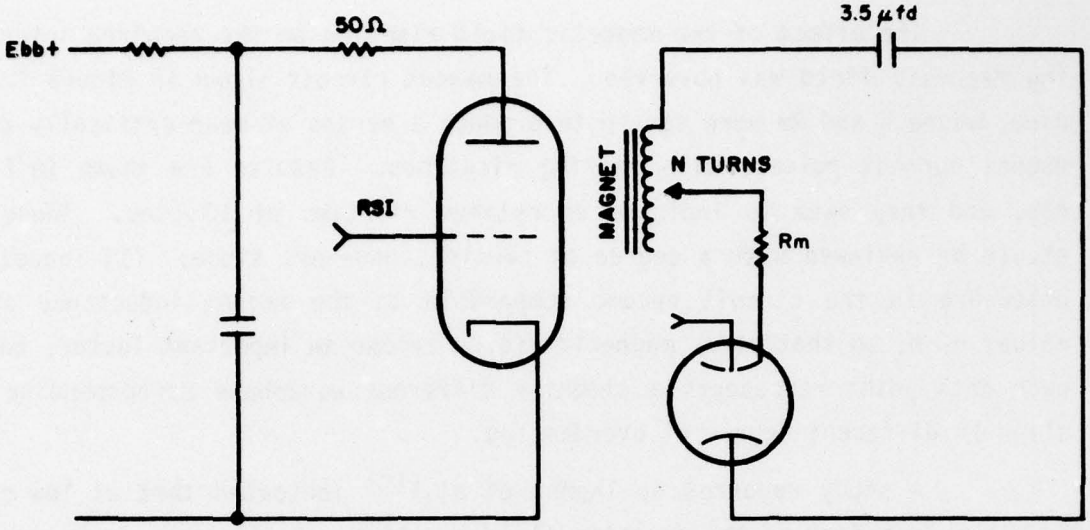

(42a)

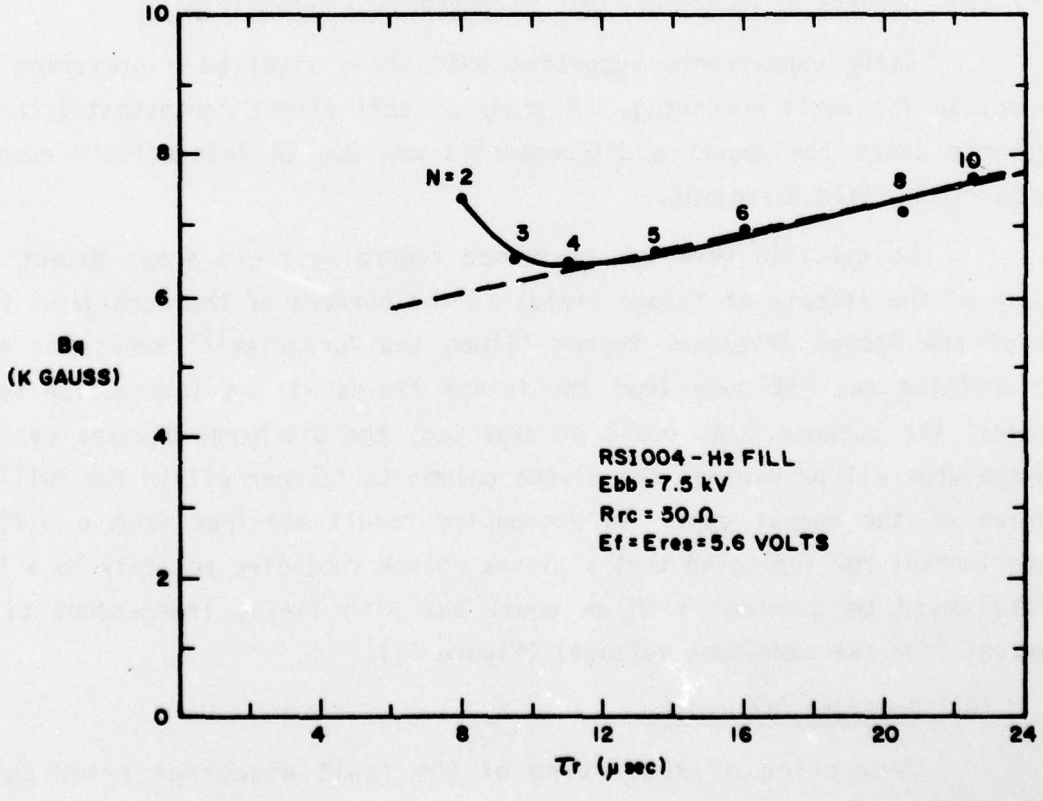

(42b)

Figure 42. Interrupting magnetic field versus magnet pulse risetime.

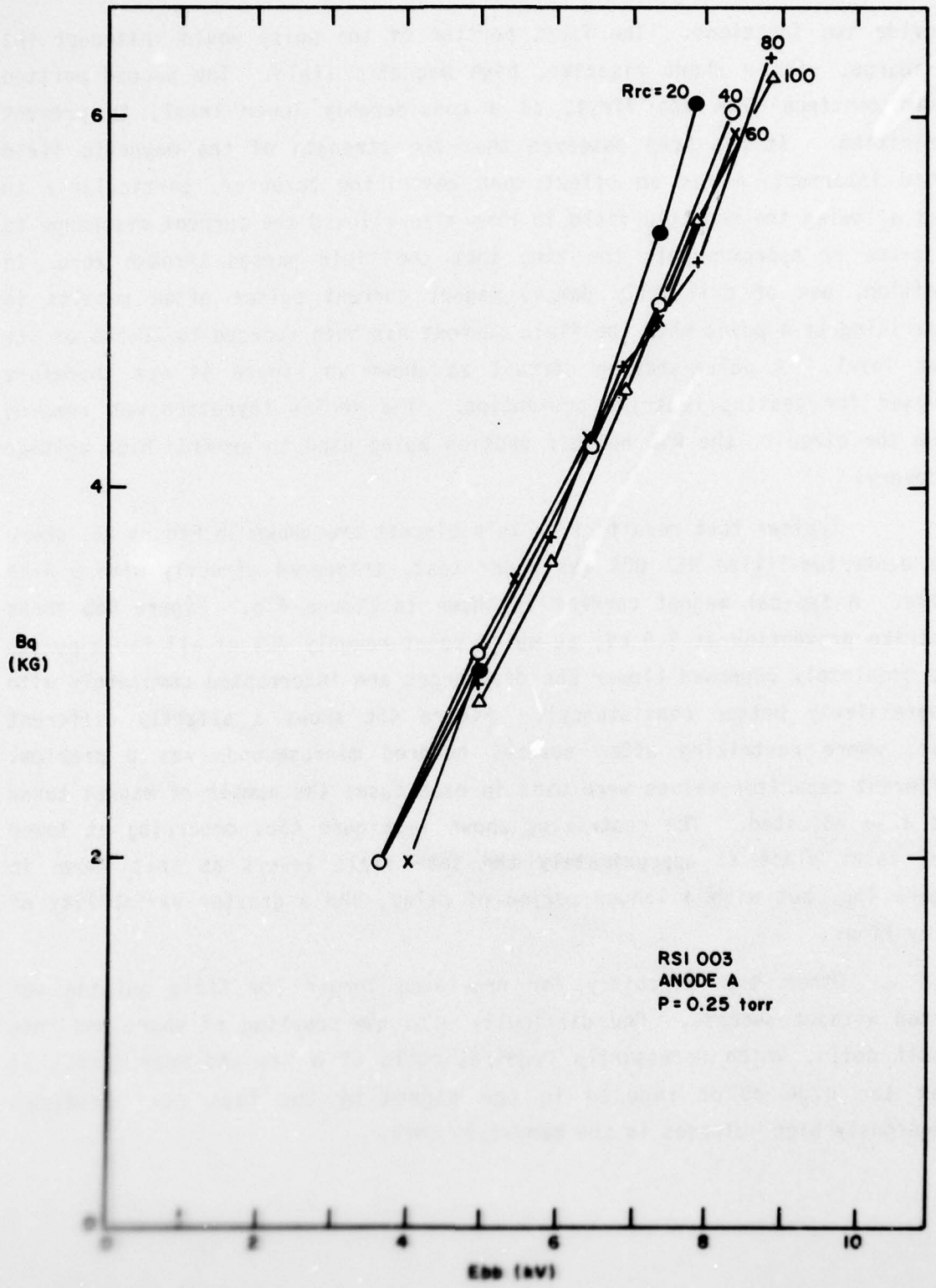

Figure 43. Bq versus Ebb, Rrc for RSI 003 subject to magnet fringe field.

provide two functions. The first portion of the pulse would interrupt the discharge, with a short risetime, high magnetic field. The second portion would continue from the first, at a considerably lower level, to prevent restriking. It has been observed that the strength of the magnetic field after interruption has an effect upon restriking behavior, particularly in that allowing the magnetic field to ring also allowed the current discharge to restrike at approximately the time that the field passed through zero. In addition, use of critically damped magnet current pulses often results in restriking at a point when the field current has been reduced to 10-50% of its peak level. A pulse-shaping circuit as shown in Figure 44 was therefore devised for testing restrike prevention. The series thyratron was removed from the circuit, the RSI holdoff section being used to provide high voltage recovery.

Typical test results from this circuit are shown in Figure 45, where the deuterium-filled RSI 004 was under test, triggered directly with a 4-kV pulse. A typical magnet current is shown in Figure 45a. Figure 45b shows restrike prevention at 5.9 kV, at which point roughly 70% of all fault pulses are completely quenched (lower Ebb discharges are interrupted completely with progressively better consistency). Figure 45c shows a slightly different case, where restriking after several hundred microseconds was a problem. Different capacitor values were used in each case; the number of magnet turns was also adjusted. The restriking shown in Figure 45b, occurring at lower Ebb, takes place at approximately the same field levels as that shown in Figure 45c, but with a longer period of delay, and a greater variability of delay time.

Other test circuitry for providing longer low field pulsing was tested without success. One difficulty with the coupling of short and long magnet coils, which necessarily requires coils of a few and many turns, is that the high dB/dt induced in the magnet by the fast coil produces dangerously high voltages in the many-turn coil.

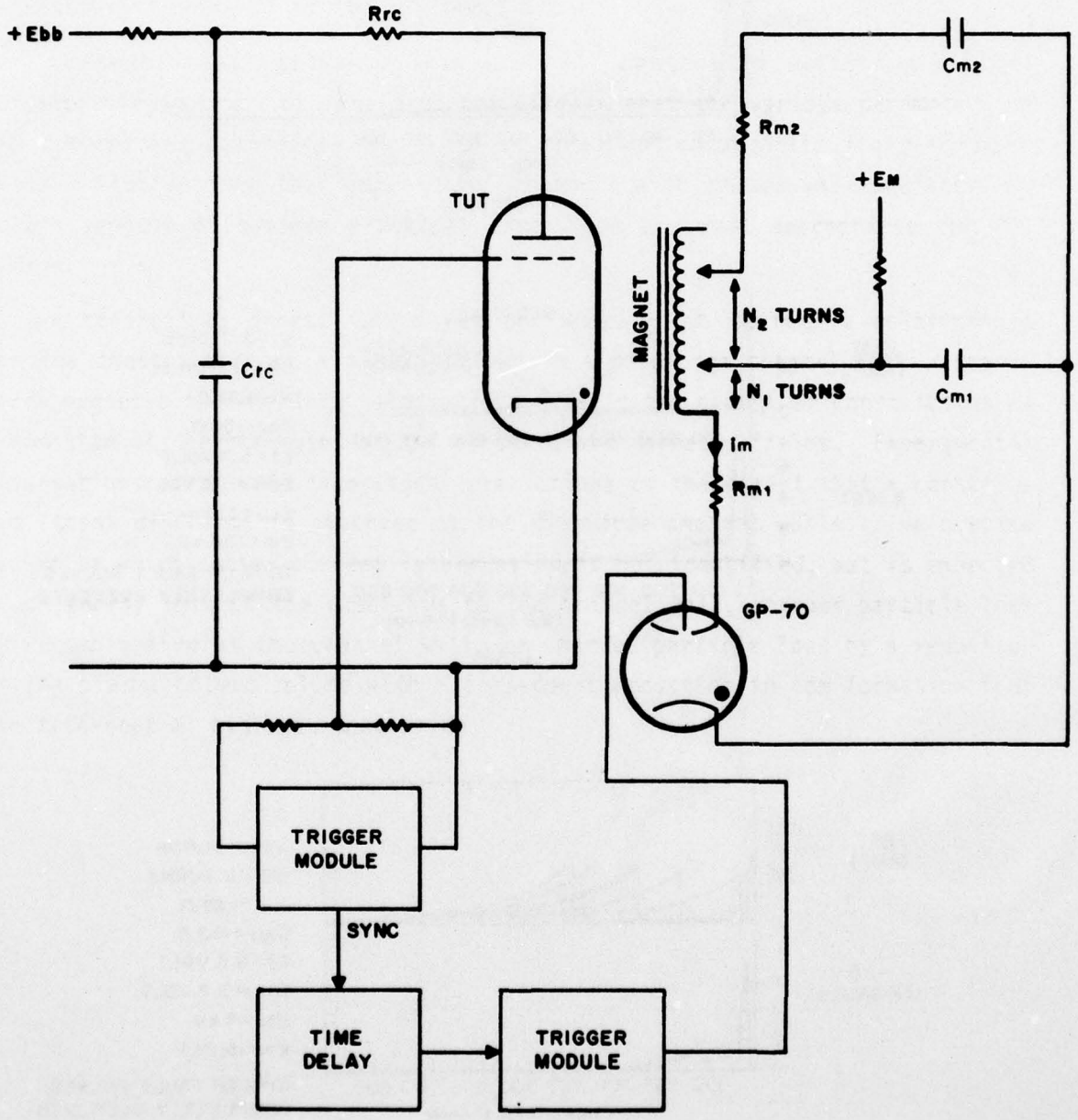

Figure 44. Magnetic field shaping test circuit.

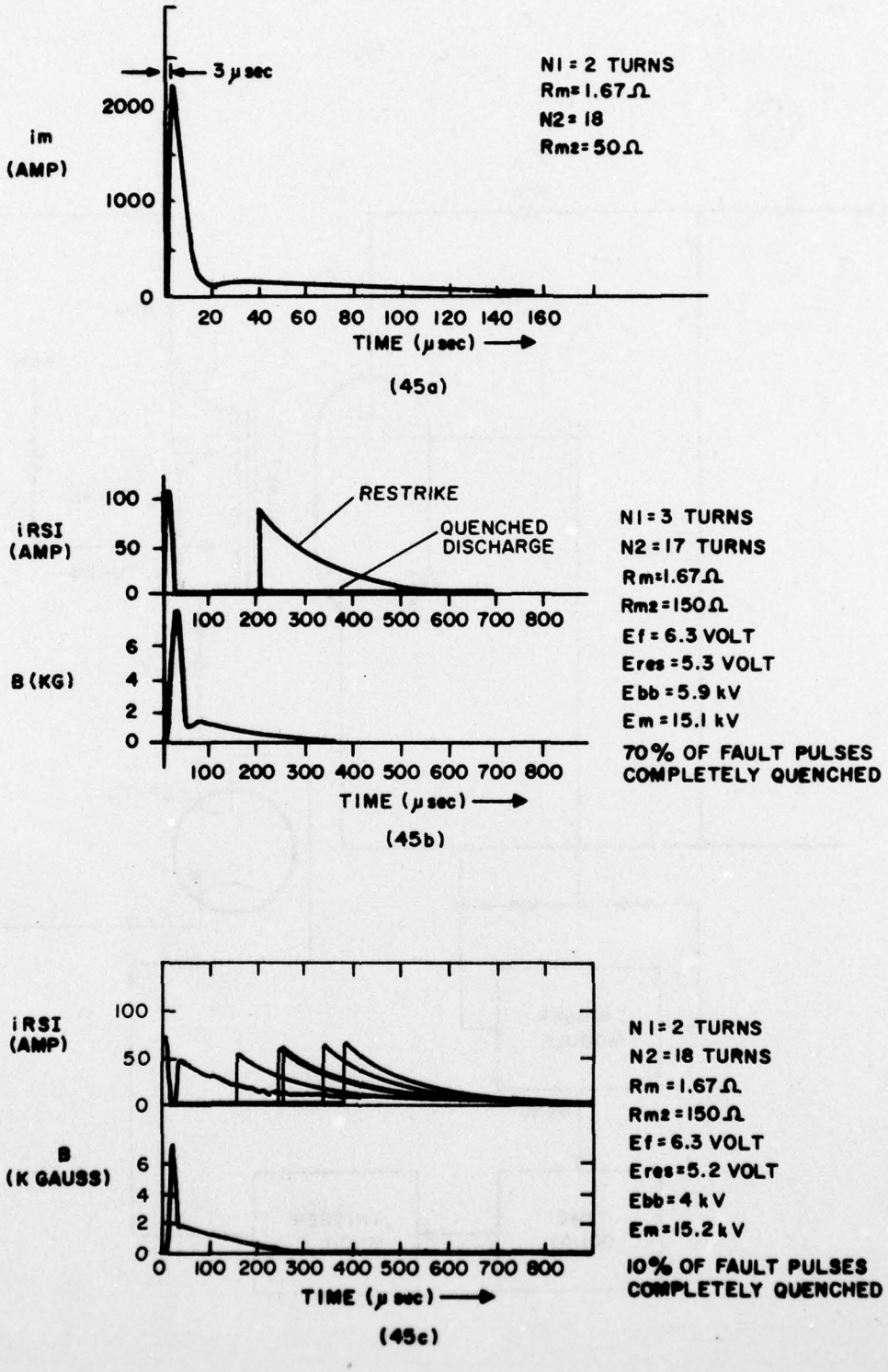

Figure 45. Fault discharge restriking in D_2-filled RSI 004.

Alternate methods of eliminating restrike behavior which were tested with the RSI 7-2 were: (1) the use of grid bias circuitry, and (2) the addition of an auxiliary magnetic field applied to the anode-grid section of the RSI. Both studies showed inconsistent improvement in restrike reduction and complete restrike elimination at high Ebb was not achieved. A study which was intended to test the use of reverse electric field grading in the RSI 7-2 to prevent restriking was not done due to the fracture of the tube. The S-shaped discharge channel had been intended to provide a more effective means of field reversal (with capacitive coupling at the folds of the discharge column).

The grid bias test made use of the circuit shown in Figure 46. Due to the high voltage developed across the interaction section during interruption, the grid could not be biased relative to cathode ground, but rather to an alternate point below grid potential but above the high interaction section potential. Use was made of the upper Kovar glass sealing sleeve assembly to provide a low reference point for grid biasing. Values of L_b = 2.5 mh and C_b = 1 μf provided best results for restrike elimination without loading down the required 3 kV trigger pulse. (Use of a lower impedance high voltage trigger system might allow the use of lower L_b, and perhaps reduce grid bias requirements.)

Results from these tests were mixed; test runs provided the data shown in Figures 47 and 48, where restrike occurrence was noted to be a function of tube pressure and grid bias. Deviation from these results was seen, however, particularly if the grid bias circuitry was changed. Elimination of the grid bias voltage without elimination of the series L, C, for instance, reduced critical restrike pressure to 0.25 torr. At other times, restriking would be eliminated at a particular test condition, only to reappear shortly afterward. Tests indicated that it is more likely for a restrike to occur following an initial restrike than following a completely interrupted discharge.

An auxiliary magnet with a 2-inch gap was used to provide a weak transverse field across the anode-grid holdoff structure, and was connected in series with the principal magnet coil winding. A field of approximately 300 gauss was obtained at the center of the gap.

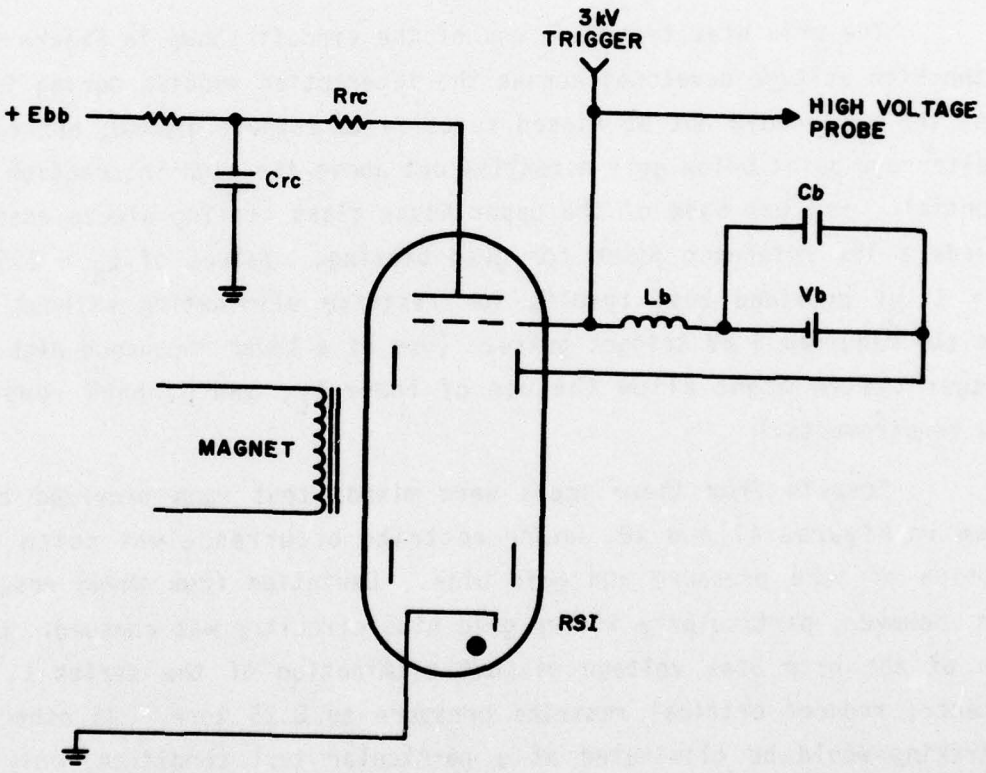

Figure 46. RSI 7-2 grid bias circuitry.

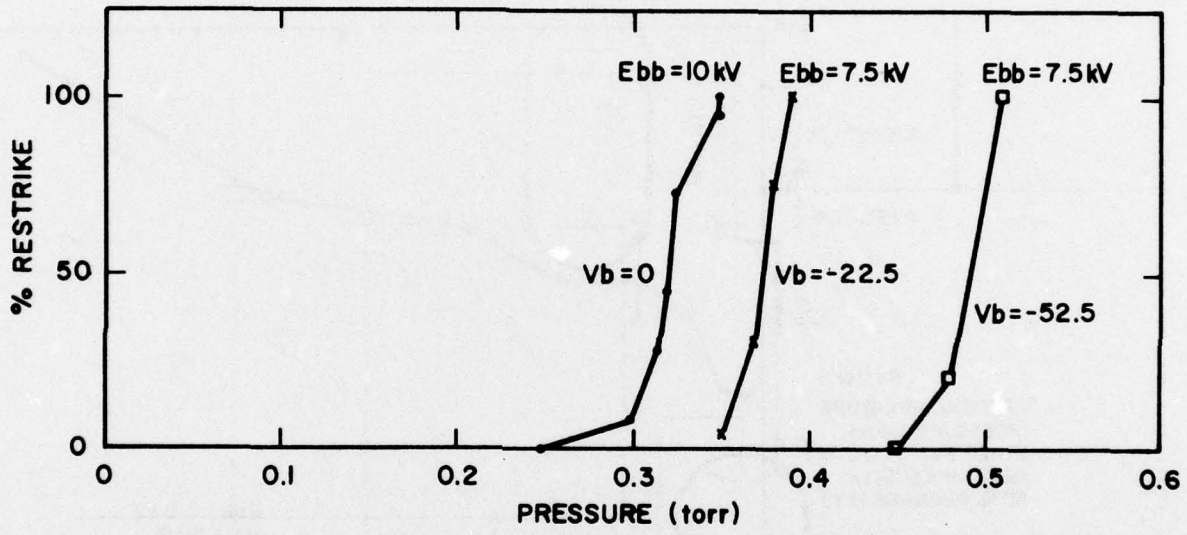

Figure 47. Percent restrike of fault pulses versus pressure, grid bias for RSI 7-2.

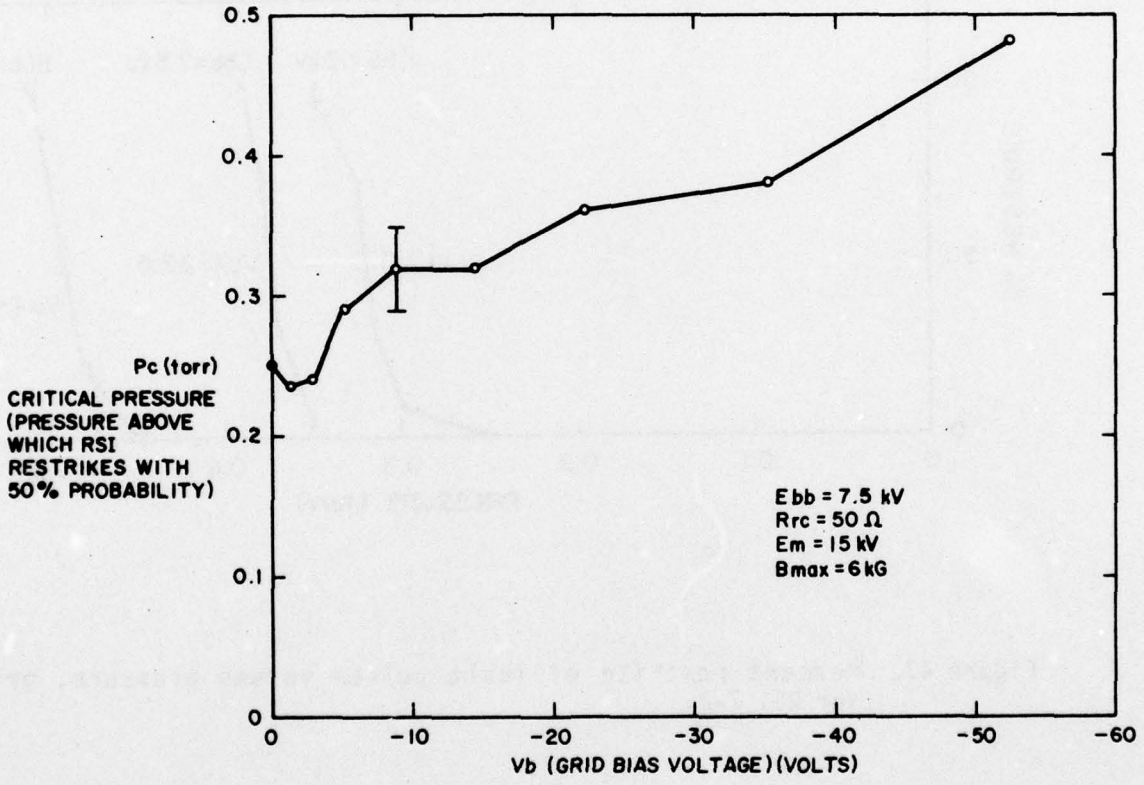

Figure 48. Restrike pressure versus grid bias for RSI 7-2.

Various results were obtained, including the complete but unreproducible elimination of restrikes up to 0.43 torr at Ebb = 7.5 kV. Generally, restriking was reduced in frequency to 5-50%, with restriking occurring least frequently at low pressure, low Ebb, and low B, independently. Increasing p, Ebb, or B independently of the other two variables causes a sudden increase in restriking.

The overall conclusion taken from these tests is that two (or more) different mechanisms are responsible for the production of restrike activity. The first is related to grid noise, the second to a failure of high voltage transfer from the interaction region to the holdoff region, and a third to spurious causes, perhaps due to unseen grid noise.

Grid noise does appear in the present experimental arrangement, and if present at a level above approximately 1 kV, will restrike the tube. One mode of restrike represents a drop of egy to a 1-2 kV decaying oscillation above ground. Restriking occurs as the oscillation swings upward, and may repeat itself up to 10 or more times every 2-3 μsec, in a voltage chopping pattern. This chopping occurs while a high magnetic field is still present across the interaction region, so that a full restrike does not occur (i.e., epy stays at its interrupted potential). However, if the chopping continues until the magnetic field is considerably reduced, as it often does, a full restrike occurs.

Grid noise caused by the magnetic field circuit also causes restriking after a period of 20-60 μsec or more. This noise has been eliminated only with a low impedance circuit from grid to cathode ground which also loads down the trigger pulse and prevents tube firing. This noise may be due to dB/dt induced voltages or magnet circuit spark gap noise.

Alternately, the grid potential can rise to epy after interruption but fail to fall to ground (i.e., transfer high voltage to the anode-grid gap) for 50 μsec or more. The magnetic field level has by this time fallen considerably, and the tube may restrike. It has been observed in some pulses that the grid voltage rises to epy to provide interruption, but begins to fall toward ground after a pause of 1-2 μsec, while the anode remains at epy. An implication is that this short time period is sufficient to deionize the anode-grid gap, but that grid to cathode capacitance in the tightly coupled

tube-magnet system holds the grid at epy. This requires that the interaction section deionize before the anode-grid region, preventing a discharge of the capacitive voltage through the discharge channel. An explanation of this nature would concur with observations of the variable frequency of occurrence of long to short time period duration of high grid potential, since occurrence of the two effects would depend upon which of the two regions deionized first. Difficult to explain, however, is the lack of decay of egy after even 50 μsec. Furthermore, introduction of additional capacitance between grid and cathode increases the rate of fall of grid potential, while the opposite would be expected for RC decay.

Further circuitry must be tested to bring the grid potential to ground 20-30 μsec after interruption without causing grid voltage oscillations. Use of the RSI in a free-running mode must also be looked at more carefully, as this operational method eliminates all triggering requirement, particularly the isolation of the grid trigger for the full Ebb voltage off ground.

(7) Series Tube Power Dissipation

The purpose of the RSI tube is to prevent damage from occurring in the traveling wave tube which will operate in series with the RSI. To minimize damage in the TWT, power dissipation should be kept to a minimum. This power dissipation, during the fault conduction period, can effectively be taken as equal to $\int V_{TWT} I dt$ for the period in which the fault current is being carried. This value is essentially equal to $\int V_{TWT} I dt = VQ$, where Q equals the total charge transferred during this interval. This assumes that an arc occurs in the traveling wave tube, with an arc voltage between 10 and 100 volts. To keep the total dissipation under 1 joule, Q should be less than 0.01 coulomb. Q may be regarded as a useful figure of merit for the RSI, since this parameter is proportional to the amount of energy dissipated in the microwave tube.

Our present tubes are capable of switching off in a period of roughly 10 μsec. The $\int I dt$ is somewhat less than 1/2 $ib\Delta t$, which for a peak current of 300 amps yields Q = 0.0015 coulomb, which would indicate an energy dissipation of 0.15 joule in the faulted TWT. This assumes that the RSI

magnet is switched on immediately (less than 1 μsec) after the fault current begins. Even if an extreme delay of 5 μsec is assumed for firing the RSI, the total Q switched would only double, so that series tube power dissipation ould still be only 0.3 joule.

It is also possible to reduce these numbers still further by decreasing the magnetic field risetime. A 5-μsec field risetime is possible; combined with a realistic 3-μsec firing delay, the total charge transferred, Q, would equal 0.00165 coulomb. The problem that develops here is that high voltages are induced in the long pulse magnet by the fast risetime of the interrupting field. These can be overcome at the expense of high capacitor storage energy discharged through a magnet coil with a moderate number of turns.

(8) Thin Channel Quenching

The RSI 7-3 tube (Figure 8) was built to test possible fault interruption by grid quenching. This tube utilized a long grid with a restrictive grid aperture of 0.084-inch diameter. Thyratron grid-quenching phenomena are observed at grid current densities of 10,000 amp/square inch; this corresponds to an expected 55-amp quenching level for an aperture of the size used.

The RSI 7-3 did not undergo quenching at any normal operating condition. Quenching was observed only at very low E_f, presumably due to cathode current limitation. In addition, the tube proved difficult to trigger, had a high grid voltage drop, and operated in a variety of modes, including the normal glow discharge, an arc discharge from the tip of the grid structure, and both arc and glow discharges from the base envelope seal of the grid structure.

A strong (8 kilogauss) magnetic field was applied across the anode-grid gap as a test for fault interruption. The application of a transverse field across a triple grid holdoff structure has been used by Wheldon[18] as an opening switch. Utilization of a thin channel anode-grid design allows the testing of such a design in opening switch applications where the total switching magnetic field energy has been minimized by volume reduction.

This test was not successful. The application of a field as high as 10 kilogauss provided fault interruption at only very low voltages (Ebb = 2 kV). It appears that a redesign would be necessary to add additional grids,

as Wheldon did. These cannot readily be stacked adjacent to each other in a thin channel tube in a reentrant design, but require a design providing either (1) feed-through through the insulator wall (which could result in a tendency to arc from the metal-dielectric junction), or (2) stacking of a complete RSI 7-3 type anode grid assembly, which would result in a long thin central channel and a correspondingly high tube voltage drop.

(9) Interaction Channel Geometry Modification

The geometry of the interaction channel has been altered in this investigation in two ways: (1) by transformation from a straight linear channel to a folded channel, with channels traveling either parallel to the tube axis (RSI 003, MCCD tubes) or perpendicular to it (RSI 7-2); or (2) by the addition to the I.D. of the channel of chuted walls, either in a circular cross-section as in the RSI 005 or along one or two wall surfaces as in the RSI 10 series.

The effect of folding the discharge column causes the gas discharge to shift toward the shortest path through the channel during interaction with the transverse magnetic field; i.e., at the folds of the discharge channel, the constructed plasma column does not follow the wall contour against which it is being propelled by the $\vec{I}\vec{X}\vec{B}$ force, but shifts from that wall surface along the direction of the electric field lines around the fold. This conclusion is inferred from an examination of the wall erosion caused in the interaction channel, and from the observation that an inclusion of this wall jumping effect improved the linearity of the relationship of Bq with channel length. The cause of this wall jumping is that under the conditions of high electric field along the discharge column during magnetic interruption, magnetic and electric forces upon the plasma column are of comparable magnitude. (At 5 kilogauss, $E/(v_H XB) \approx 1.$)

The chuted wall RSI thyratrons have demonstrated the capability of interrupting fault discharges at magnetic field levels of from 20-60% of those required for uniform channel interrupters. The RSI 005 first demonstrated this capability, although it had difficulty in preventing arc formation between what were somewhat loosely stacked ceramic washers and the enclosing glass envelope. It should be noted that although this tube interrupted at low

Bq, transitions of the customary glow discharge to an arc mode were seen, and were apparently caused by the interaction of the principal discharge with members of the ceramic stack. The phenomenon of arc spot generation on the ceramic washer material was noted, but was seen as a mode traveling between washers toward the envelope and not through the main discharge path in the center of the chuted channel.

The RSI 10 series thyratrons have achieved results equal to or better than those of the RSI 005 as regards Bq reduction (see Figure 33, subsection 3.c(3)(d)). The principal mechanisms for this reduction in Bq are presumably the same as those for the RSI 005, as evidenced by the close correspondence of RSI 10A data to that of the RSI 005. Physical processes which can be considered the source of this switching improvement are, in particular: the increased plasma energy loss by interaction of a greater portion of the plasma column with the wall surface; the increased surface area of the wall itself; and the increased loss of ionized particles to recombination at the channel wall.

An argument has previously been given (Simon and Turnquist[12]) that the reduction of Bq in the chuted channels was due to the increased path length along the surface of the wall, via:

$$\frac{\text{Bq (folded or chuted wall)}}{\text{Bq (straight wall)}} \propto \left\{ (L_{\text{folded wall}}) / (L_{\text{straight wall}}) \right\}^{-0.75}$$

For the RSI 005, this ratio equalled 0.36, which corresponds to the approximate advantage achieved with Bq reduction in the RSI 005 versus the RSI 003 interrupters. However, this theory loses a major part of its substance when consideration is given to the effect of increased Bq reduction in the RSI 10A interrupter along the wall containing the relatively shorter chute depths.

A more applicable process for consideration of these chuted wall effects is probably that of plasma starvation by a loss of electrons and ions to a limited portion of the chute surface. This basis is supported by the analysis of the RSI 005 ceramic erosion (see subsection 3.g(2)).

Under RSI conditions, the electron cyclotron radius and the electron mean free path are of approximately the same order of magnitude as the chute or washer-to-washer gap.

d. Test Results: Pulse Testing

(1) Circuitry Note

The RSI thyratrons were tested at various points in the investigation, both with or without a series thyratron, most data having been taken, where feasible, for operation of the RSI as a single switching element. This operation provides cleaner experimental characterization of the RSI tube, and, in particular, the interaction channel. Tubes with multiple section interaction channels were of necessity tested with a series thyratron to provide voltage holdoff and trigger capability for parametric studies.

(2) RSI Voltage Drop

The design objective of the RSI development was to limit the total tube voltage drop to 350 volts. The principal means of attaining this result was expected to be efficient design of the interaction channel structure toward minimal length for the required magnetic switching efficiency. Cathode and anode section voltage drops were considered necessarily additive upon the interaction channel drop; little possible improvement was expected over conventional anode and cathode structural designs.

Interaction channel voltage is expected to be linearly proportional to the length of the channel. Measurements in the RSI 003 and 400 D 250 (Figure 49) show this relation to hold within experimental error.

Dependence of voltage drop on discharge channel diameter is expected to vary by the ratio $E \alpha r^{-0.5}$ over the range of pressure and diameter applicable to the RSI (see section 4.a). Voltage drop data for several tubes are plotted in Figure 50. Considerable scatter is apparent, due in part to inaccuracies in assessment of the voltage drop division between the interaction section and the cathode structure.

AD-A055 253 EG AND G INC SALEM MASS F/G 9/1
REPETITIVE SERIES INTERRUPTER I:.(U)
APR 78 D V TURNQUIST, R SIMON
UNCLASSIFIED ECOM-76-1301-6 DAAB07-76-C-1301
NL

2 OF 2
AD
A055253

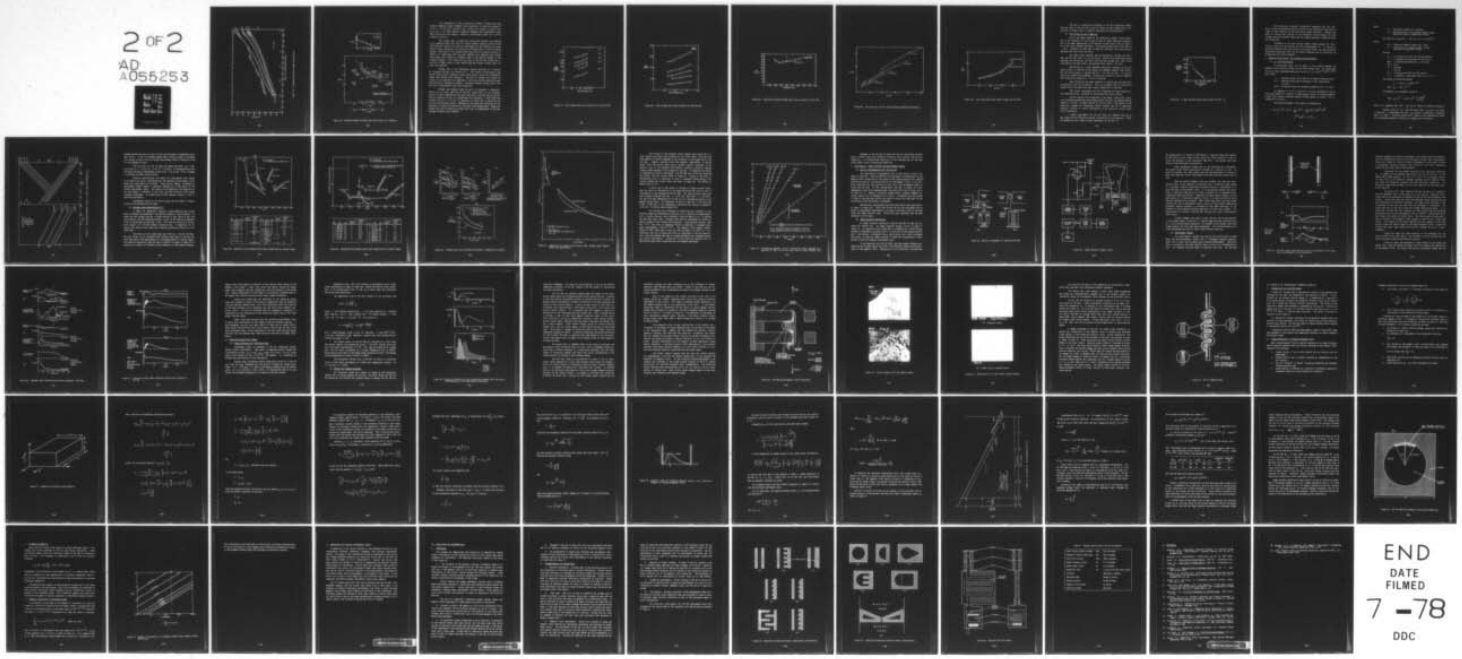

END
DATE
FILMED
7 -78
DDC

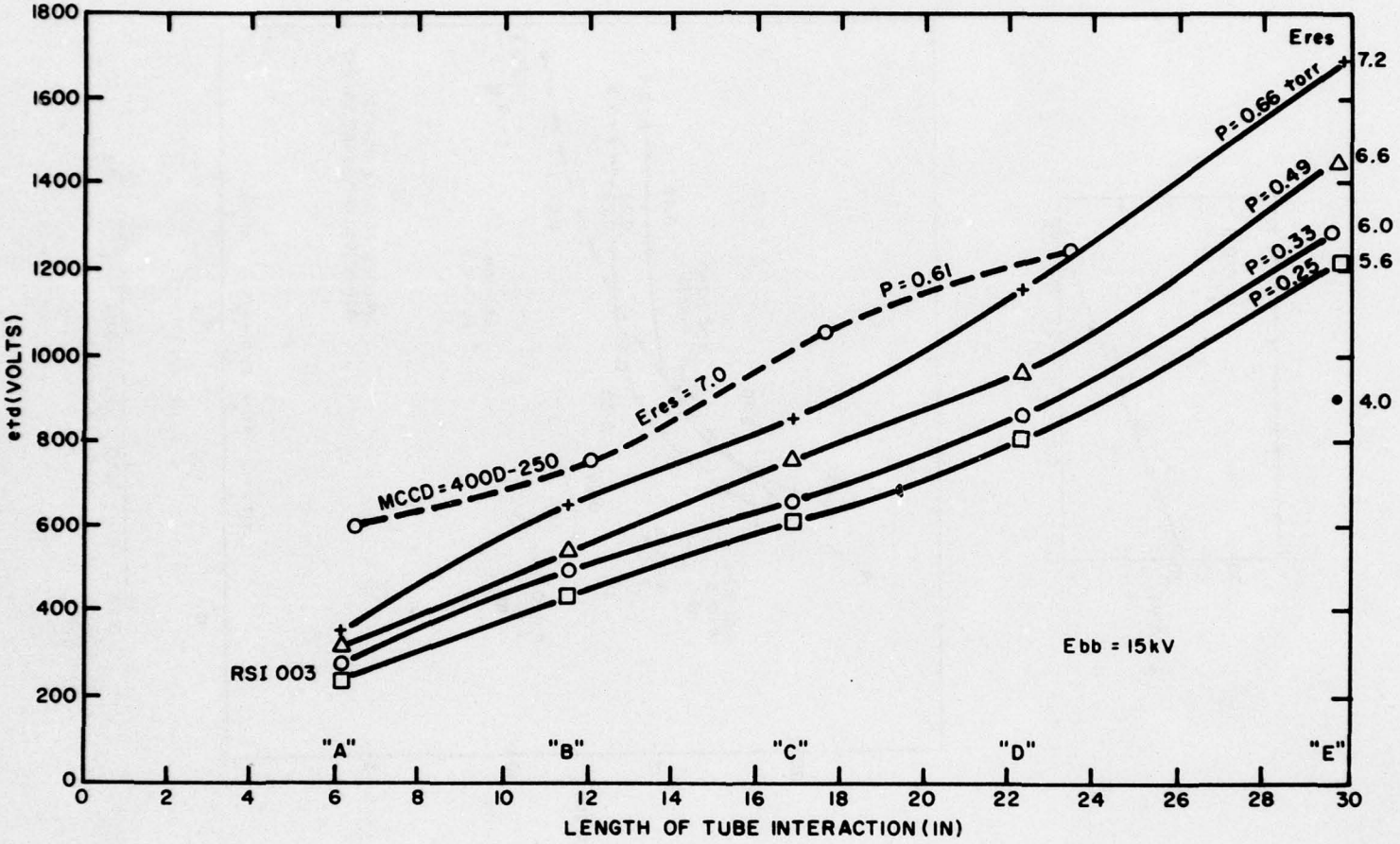

Figure 49. Voltage drop versus length and pressure.

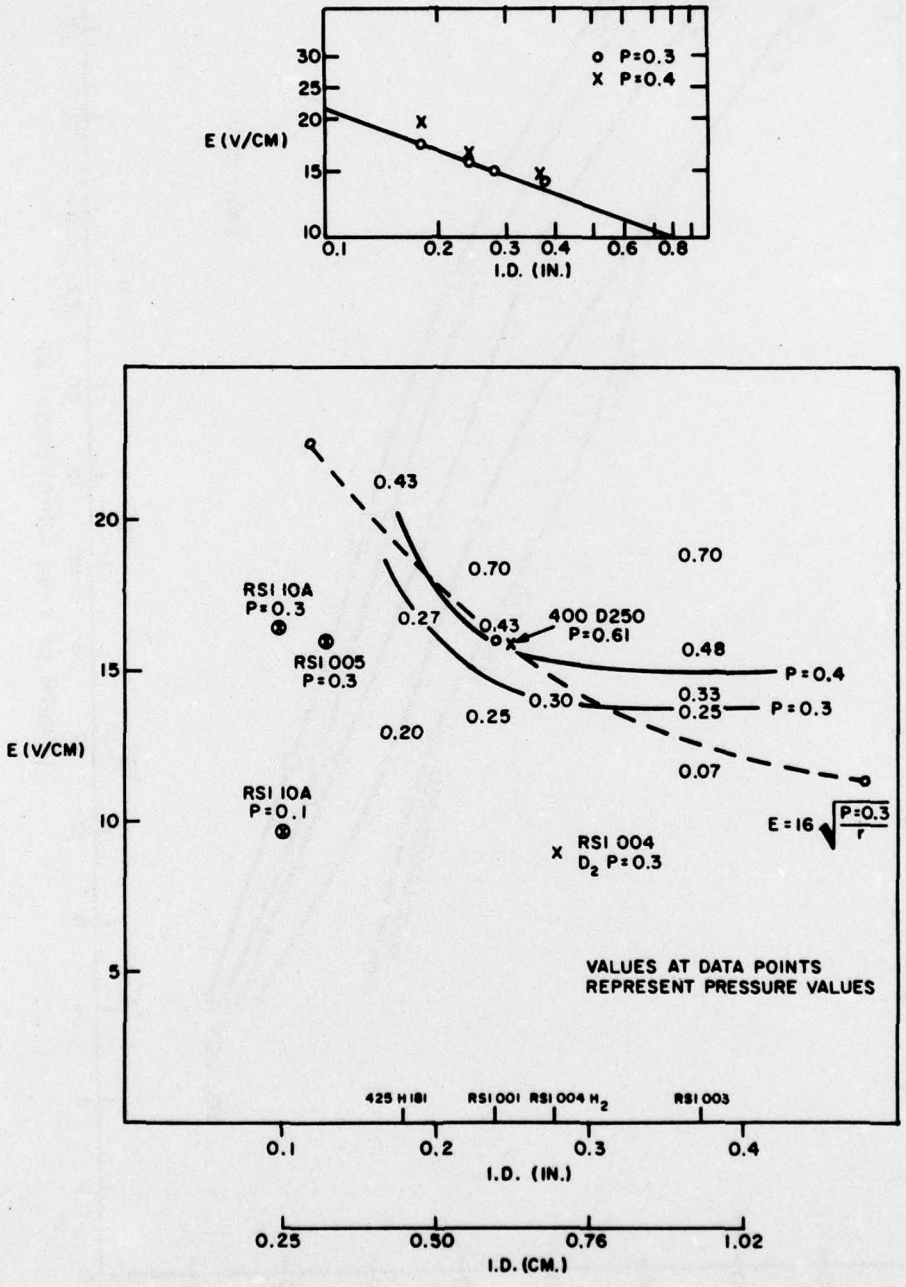

Figure 50. Discharge channel voltage drop versus tube I.D., pressure.

Full dependence of the interaction channel voltage drop upon channel parameters under 25-ampere pulse conditions is given by Breusova[1] to be $E = 16\ (p/r)^{0.5}$ (section 4.a). Figure 50 includes a plot of this curve at p = 0.3 which details a moderate agreement with experimental data. Data from the RSI 003, however, indicate a relationship closer to $E \alpha p^{+0.36}$ (Figures 51 and 52).

The voltage drop in chuted wall interaction channels was expected to be somewhat higher than that for uniform channel tubes by virtue of the increased wall surface area and the requirement for the formation of plasma double sheath structures at interfacing irregularities in the discharge channel. Robinson[10] has demonstrated that positive columns devised in channels of alternating thin and wide diameter bore segments have voltage drops higher than channels of diameter equal to the smaller diameter of the irregular channel. This effect was not seen in the RSI 005 (Figure 50) or the RSI 10 tubes tested to date, where discharge channel voltage drops are lower than expected.

Voltage drop in the interaction channel decreases as a function of increasing current (see section 4.a). This effect is particularly seen during fault current conduction, where tube current levels are considerably higher than during pulse operation. The drop in voltage with respect to current is not expected to be important in the pulse current conditions under which the RSI is designed to operate. Interaction channel voltage drop in the RSI 10E1 is approximately 300 volts (Figure 53).

Voltage drop between anode and grid can represent a substantial portion of the total tube drop in the RSI, particularly at low pressure. Figures 54 and 55 demonstrate the total tube drop in the RSI 10A and the RSI 10E1 as a function of epy in a conventional grid structure. A total tube drop of 800 volts at p = 0.4 torr is apparent, of which 50% is caused by the grid-grid baffle-anode region. Reworking of the anode-grid structure will be necessary to reduce this portion of the total tube voltage drop. Anode-grid voltage drop can be reducible to under 100 volts, as demonstrated in the 1951 hydrogen thyratron study (EG&G[19]).

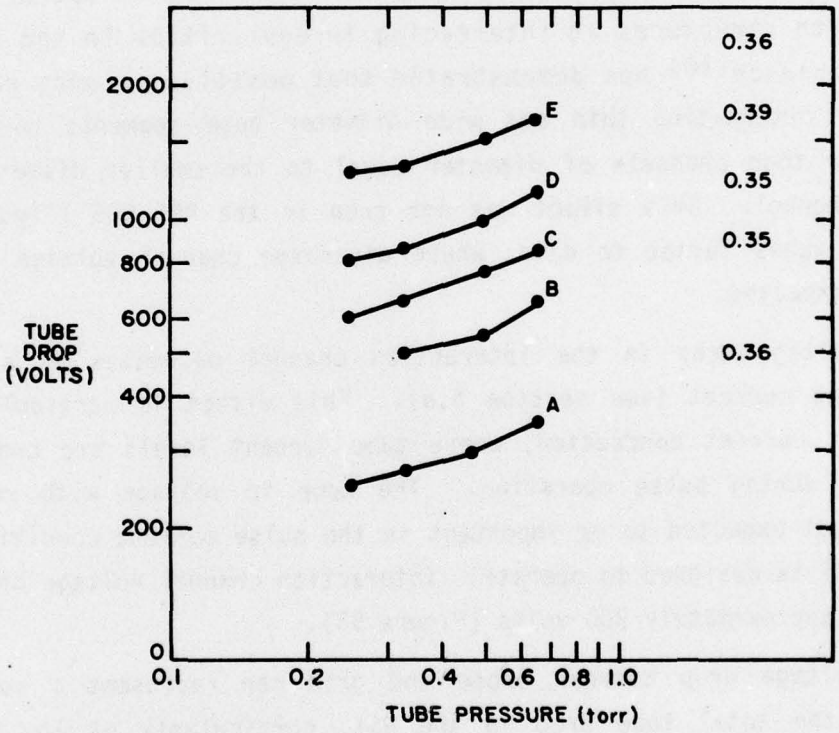

Figure 51. Tube voltage drop versus pressure for the RSI 003.

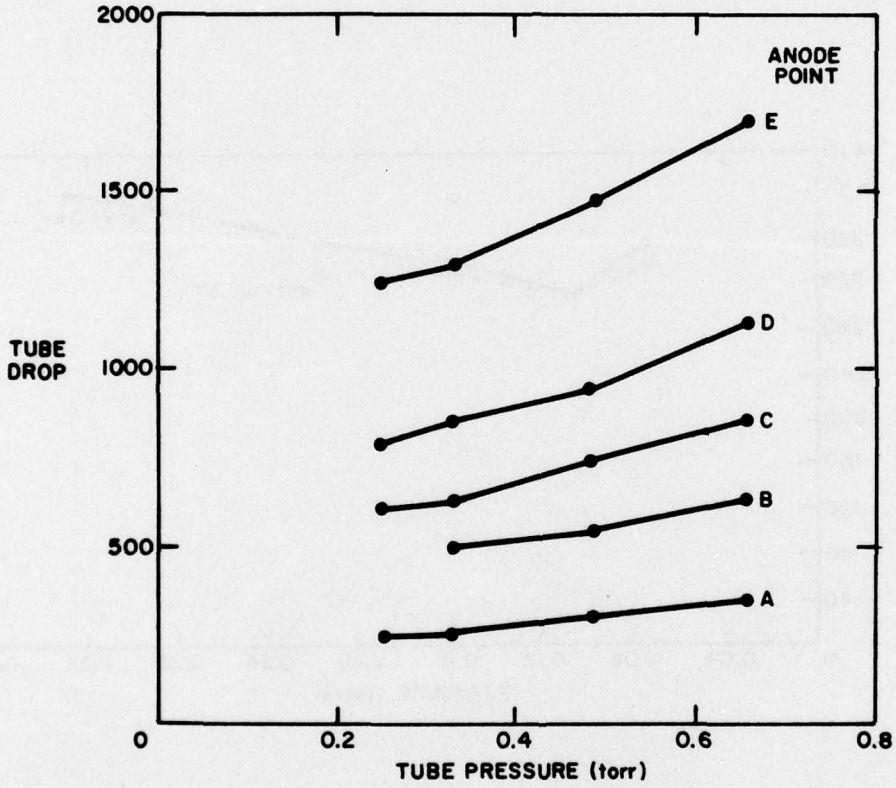

Figure 52. Tube voltage drop versus pressure for the RSI 003.

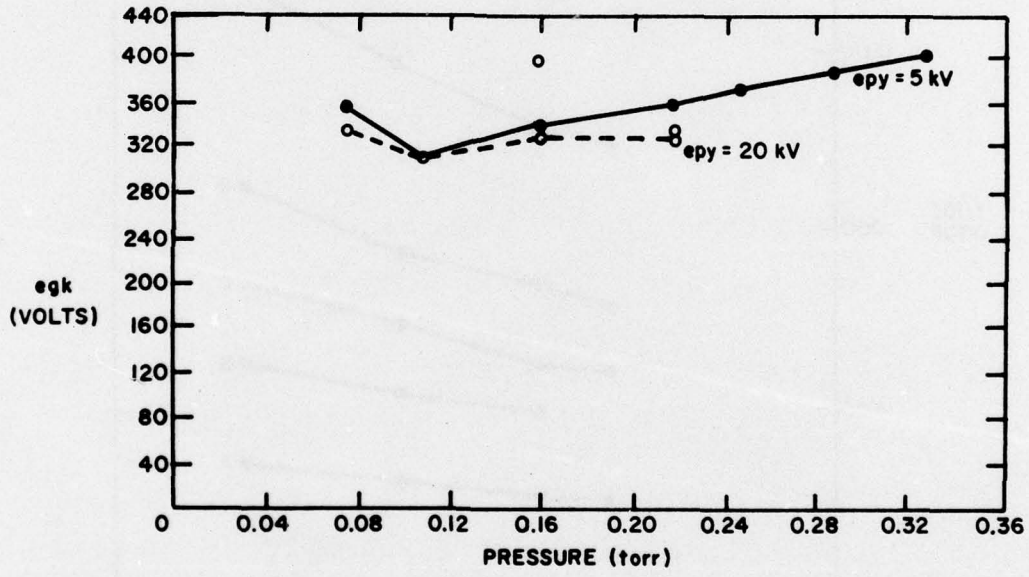

Figure 53. Interaction section voltage drop versus pressure for RSI 10E1.

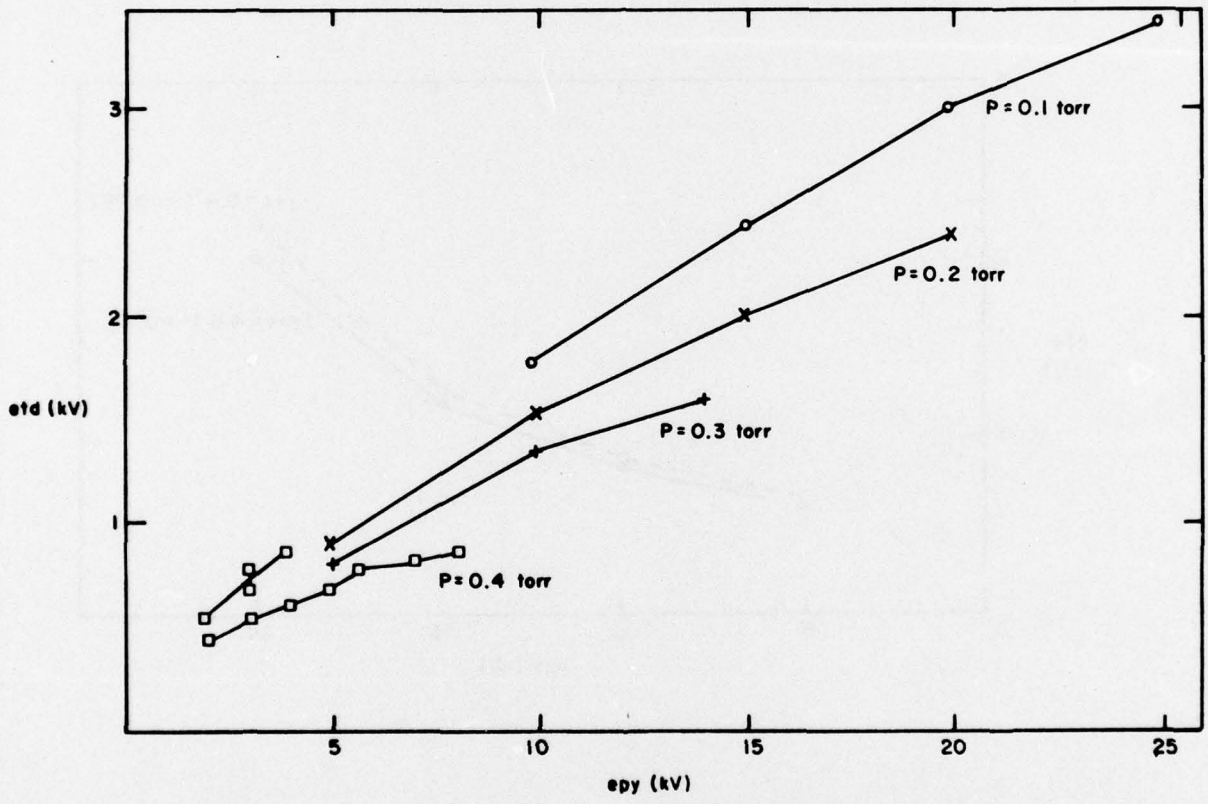

Figure 54. etd versus epy for RSI 10A (including anode-grid structure).

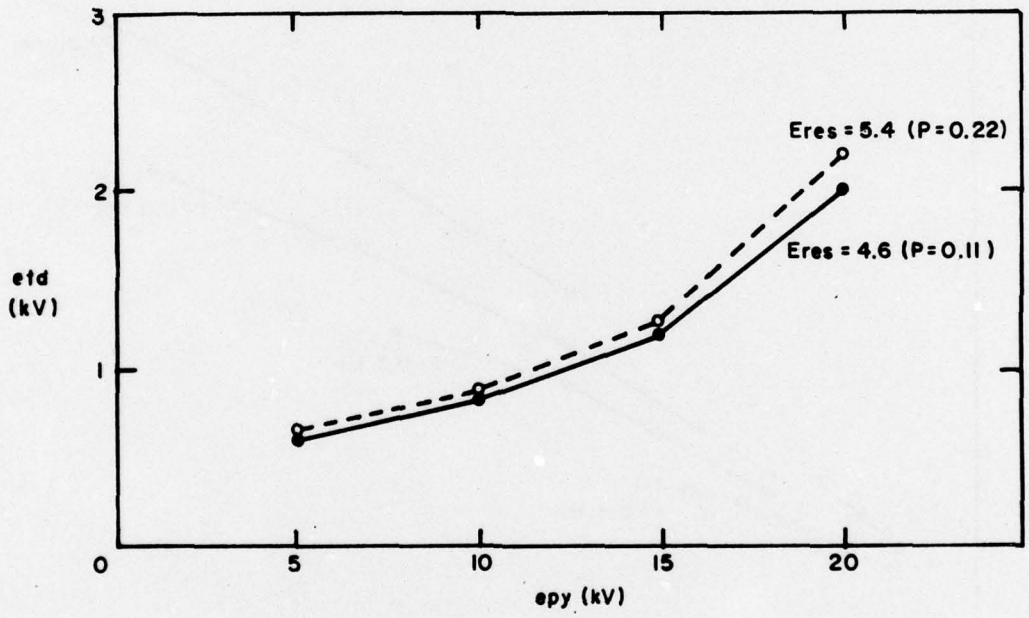

Figure 55. Total tube drop versus plate voltage for RSI 10E1.

The use of a keep-alive discharge in the RSI interaction channel has been shown in the RSI 003 to have no effect on tube voltage drop, irrespective of current level or length of the keep-alive discharge path.

(3) Pulse Stability and Triggering

Due to the added length of the interaction channel, pulse stability in RSI operation is not as good as that of normal thyratron operation, but it has been demonstrated to be possible to hold tube jitter to under 5 to 10 nsec under optimum conditions. Firing delay times were of the order of 1 μsec. Operation at high tube voltage and relatively high tube pressure improves both tube jitter and delay.

The tubes which operated most satisfactorily included the 400 D 250, the RSI 003, 004, 7-2, and 10 series. Earlier post-anode design tubes operated with difficulty; the 380 D 250 had high voltage drop, poor firing consistency, high tube jitter, and extremely poor Δtad (5 - 25 μsec).

Application of a high impedance keep-alive discharge to the RSI tubes assists in reducing firing delays and somewhat improves tube jitter. RSI 003 firing delay is reduced from 0.8 - 1.9 μsec to 0.45 - 1.6 μsec by the use of a keep-alive discharge. A keep-alive current of a few milliamperes and a keep-alive voltage of 2 - 10 kV is required.

Some difficulty has been observed in stabilizing the keep-alive discharge at the grid structure. This is presumably due to interaction between source and keep-alive power supply systems and is reducible.

Tube jitter associated with RSI triggering has been observed at the nanosecond level, increasing at low pressure and source voltage.

The RSI devices can be operated in two modes, either with a keep-alive discharge through the high voltage holdoff structure (as demonstrated by Weiner[17]) or with a trigger applied to the RSI grid. Application of the keep-alive through the interaction section requires the use of additional external circuitry to assure interruption of the keep-alive current after fault interruption.

Trigger requirements for the RSI tubes are somewhat high due to the length of the interaction channel, particularly at low pressure. Figure 56 demonstrates the trigger voltage requirement for the RSI 7-3.

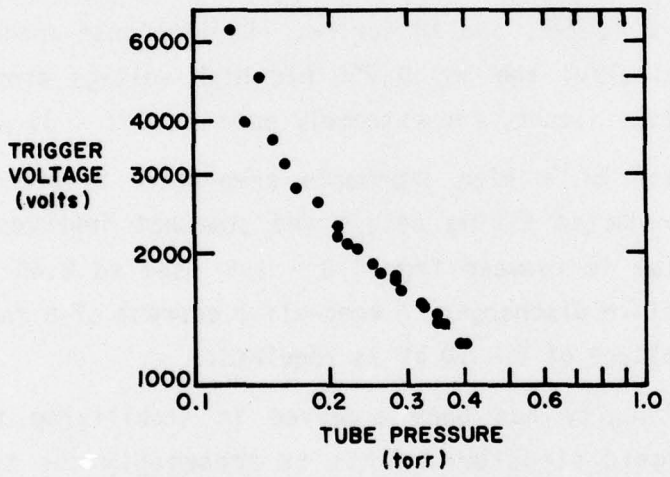

Figure 56. Trigger voltage versus tube pressure for RSI 7-3.

Work previously reported (Turnquist[15]) suggested that the location of the grid-controlling region relative to the interaction region had an effect on the stability of the tube during normal operation. Present work tends to confirm that location of the interaction region between the high voltage anode-grid holdoff region and the cathode decreases triggering delay and instability.

Placement of the high voltage holdoff region between the interaction section and the cathode has the disadvantages of: (1) adding an additional baffled transition region to the plasma column; (2) constructing an unnecessary additional cavity for the plasma discharge; and (3) disturbing the optimum hold-off section geometry.

e. Magnetic Field Energy - RSI Voltage Drop Relationship

(1) ξj - etd Relationship

A relationship basic to RSI design is the tradeoff between low magnetic field switching energy and low tube voltage drop. The requirement for Bq has been determined empirically to be $Bq = \varepsilon_0\ \varepsilon_1\ Ebb^{1.25}\ ib^{0.25}\ L^{-0.75}\ H(p)$, where

ε_0 = reduction factor due to the use of chuted interaction walls

ε_1 = reduction factor due to decrease in tube radius below 0.1 inch

$H(p)$ = correction factor for pressure, normalized at p = 0.3 torr

An exponent of -0.75 is used for L on the consideration that a final tube design will require a folded channel design to minimize magnetic fringe field losses; discharge channel folding appears to result in $m < 1$ (subsection 3.c(3)(c)).

The switching magnetic field energy is determined by

$$\xi j = \frac{1}{2} \int \vec{B} \cdot \vec{H}\, dV = \frac{1}{80\pi}\, Bq^2\, V = \frac{1}{20\pi} \varepsilon_0^2 \varepsilon_1^2\, Ebb^{2.5}\, ib^{0.5}$$

$$L^{-0.5}\, H(p)^2\, (r + \delta)^2 \varepsilon_3\,,$$

where

δ = interaction channel wall thickness

ε_3 = correction factor for increased channel volume required by use of a chuted wall surface

The tube drop is given by: $etd = e_0 + \varepsilon_2 L \cdot 16 (p/r)^{0.5}$,

where

e_0 = anode and cathode voltage drop = $e_0(p)$

ε_2 = correction for increased channel voltage drop due to chuted wall surface

Setting:

ε_0 = 0.4 (based on RSI 005, RSI 10A performance)

ε_1 = 1 (assuming no improvement of Bq at low r)

H(p)= 1 (assuming operation near p = 0.3 torr)

Ebb = 15 kV

ib = 300 amps

δ = 0.25 cm

ε_2 = 1 (based on RSI 005, RSI 10A results)

ε_3 = 2 (assuming a chute depth equal to 2 (r + δ).

The primary relationships become:

$$\xi j = 75.8 (r + 0.25)^2 L^{-0.5}$$

$$etd - e_0 = 8.8 L r^{-0.5}$$

Eliminating L as a parameter results in

$$(etd - e_0) \xi j^2 = 5.06 \times 10^4 \frac{(r + 0.25)^4}{r\ 0.25}$$

where it is apparent that $(etd - e_0)$ and ξj cannot be mutually minimized.

Several curves of ξj, L and Bq versus $(etd - e_0)$ and r are shown in Figure 57. A requirement for $(etd - e_0)$ results in the option of choosing small L or high r. Selection toward low L reduces ξj but increases Bq, which is an important parameter if the use of a magnet core is desired.

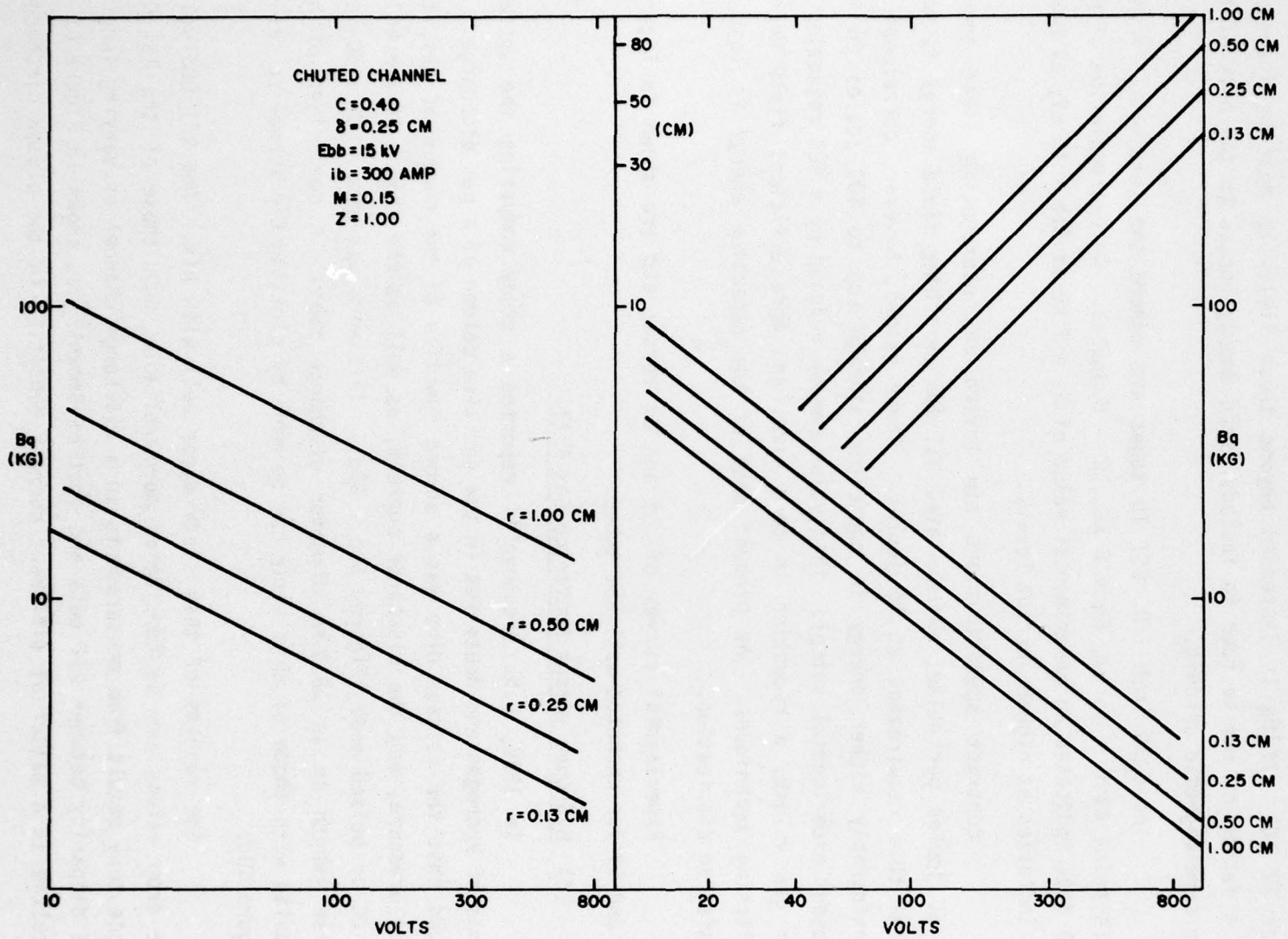

Figure 57. Calculated dependence of Bq, ε_β, and L upon the parameter e_{ic}.

Maximum Bq with the use of a core is 15 kG, but the onset of saturation occurs near 12 kG. If Bq is increased beyond these limits, ξj must be increased by a factor of two to four to include field energy losses in the bulk of the air core magnetic circuit.

The 0.30 inch I.D. RSI 10 tubes aim toward the (etd - e_0) = 240-volt point at L = 15 cm, Bq = 6 kG, $\xi\beta$ = 6 joules. An extrapolation of RSI 10A data indicates an experimental value of Bq = 7 kG at Ebb = 15 kV, although ε_0 increases at higher current levels.

Contract specifications aim toward an interrupting field energy of 50 joules per pulse; extrapolated RSI 10A switching field energy is well below this requirement at 16 joules. These values, however, correspond to considerably higher energy in capacitor storage (up to 400 joules in the present experimental setup). This value can be reduced by a 50% reduction in air gap volume, a reduction in core size, and more efficient field energy switching techniques. At present most of the capacitor energy is lost in resistive dissipation.

Experimental curves of ξj and Bq versus etd are shown in Figures 58 and 59 for unchuted-wall RSI tubes.

(2) Hydrogen versus Deuterium Gas Fill

In 1969, L.N. Breusova[1] reported a study comparing the voltage drops of hydrogen and deuterium in the positive column of a gas discharge. He found that the voltage drop was a strong function of the choice of gas, the tube pressure, and the discharge current, as well as the choice of operation in DC or pulsed mode (Figures 60a - 60d). This work was done with a 30-μsec pulse length in an 18.5-mm diameter discharge tube. A comparison of his results with those of this study can be made by plotting E/p versus rp, as in Figure 60d.

The results of this study agree well with his. The RSI 003 voltage drop values can be considered more reliable than those of the RSI 001 since they result from measurements in a discharge channel of varying length. The disparity between RSI data and that of Brown[3] as shown in Figure 61 is resolved as a matter of different current densities in the plasma discharge.

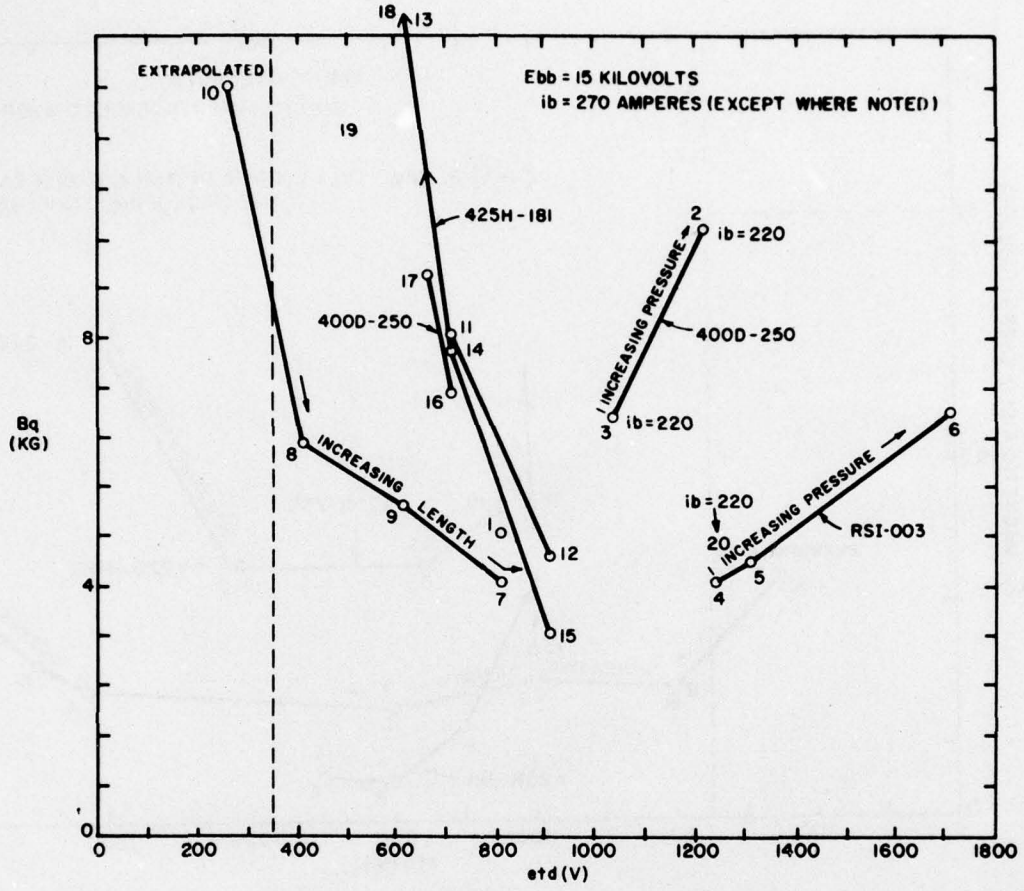

No.	Tube	Eres	Electrode Anode	Interaction Length (in.)
1	425H-181	5.6	B	12.0
2	400D-250	6.5	D	23.4
3	400D-250	6.0	D	23.4
4	RSI 003	5.6	E	31.75
5	RSI 003	6.0	E	31.75
6	RSI 003	7.2	E	31.75 (Extrapolated)
7	RSI 003	5.6	D	23.0
8	RSI 003	5.6	B	11.5
9	RSI 003	5.6	C	17.3
10	RSI 003	5.6	A	5.8 (Extrapolated)
11	425H-181	5.6	B	12.0
12	425H-181	5.6	C	17.5
13	425H-181	5.6	A	6.5
				Off scale for Bq
14	425H-181	5.2	B	12.0
15	425H-181	5.2	C	17.5
16	400D-250	6.0	D	23.4
17	425H-181	6.0	C	17.5
18	Bifilar Tube (Thomas[13])	P = 0.14		11.0
19	Diode C (Thomas[13])	Er = 4.5		
20	ITT Coaxial Tube	P = 0.45		21.0

Figure 58. Quenching field strength versus tube voltage drop for several tubes.

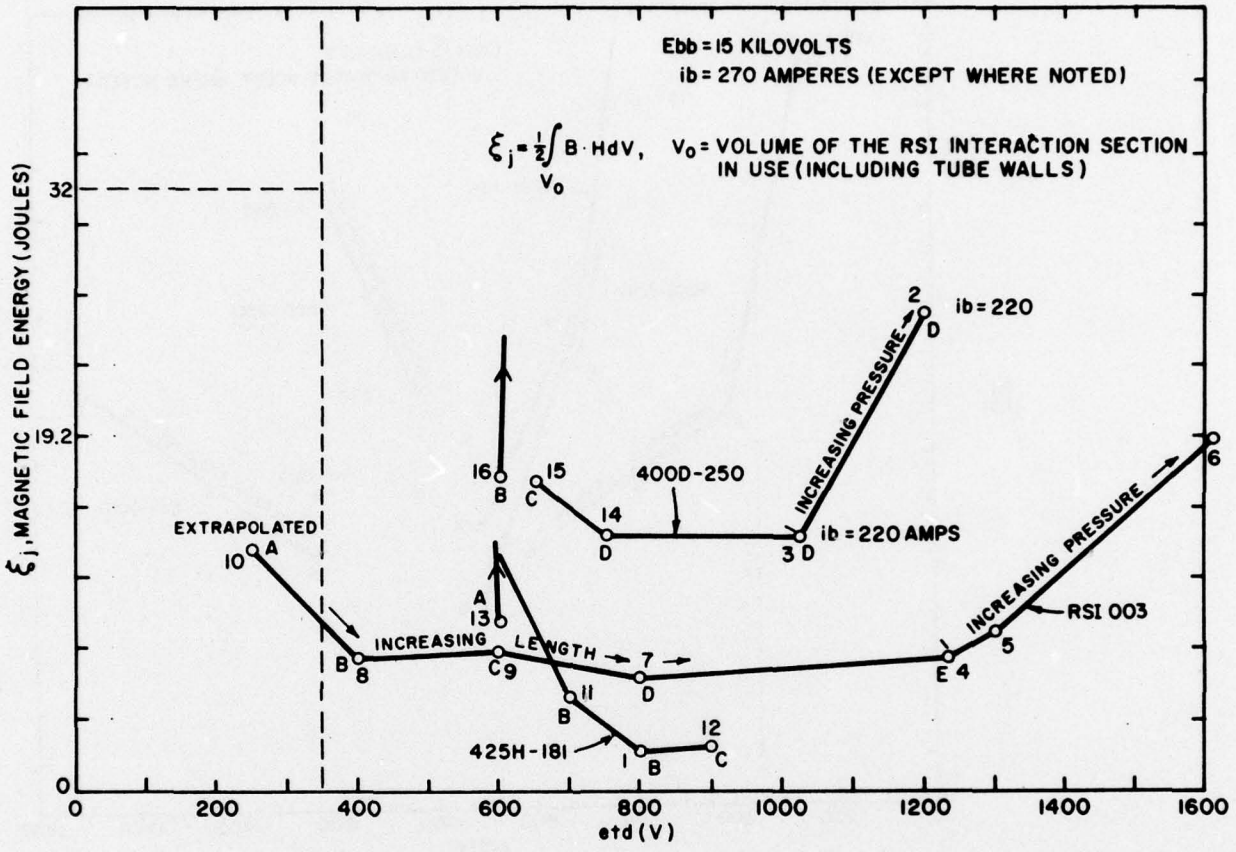

No.	Tube	Eres	Electrode Anode	Interaction Length (in.)
1	425H-181	5.6	B	12.0
2	400D-250	6.5	D	23.4
3	400D-250	6.0	D	23.4
4	RSI 003	5.6	E	31.75
5	RSI 003	6.0	E	31.75
6	RSI 003	7.2	E	31.75
7	RSI 003	5.6	D	23.0
8	RSI 003	5.6	B	11.5
9	RSI 003	5.6	C	17.3
10	RSI 003 (Extrapolated)	5.6	A	5.8
11	425H-181	5.6	B	12.0
12	425H-181	5.6	C	17.5
13	425H-181	5.6	A	6.5
14	400D-250	6.0	D	23.4
15	400D-250	6.0	C	17.5
16	400D-250	6.0	B	12.0

Figure 59. Quenching field energy versus tube voltage drop for several tubes.

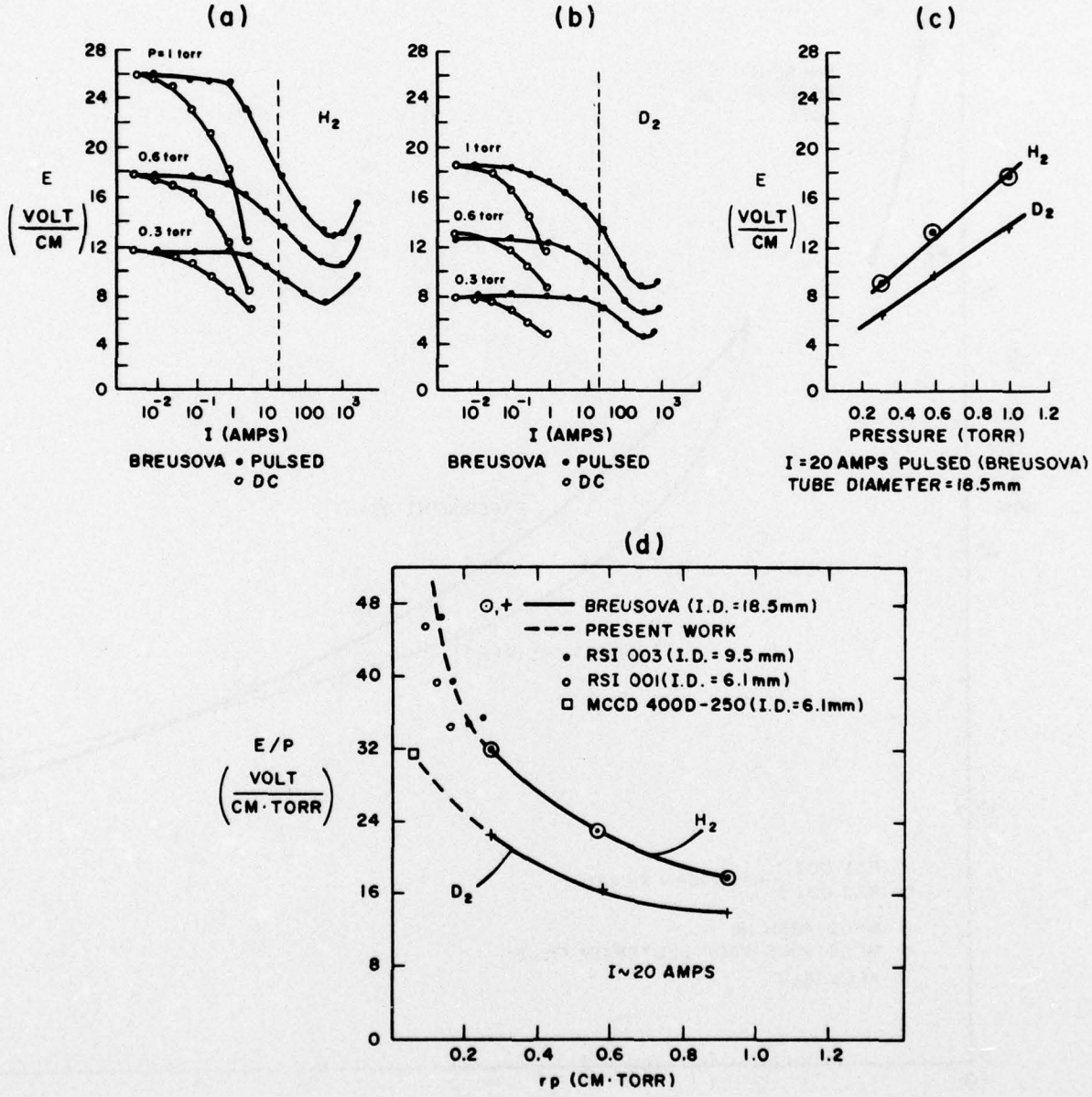

Figure 60. Voltage drop versus current and pressure: comparison of results.

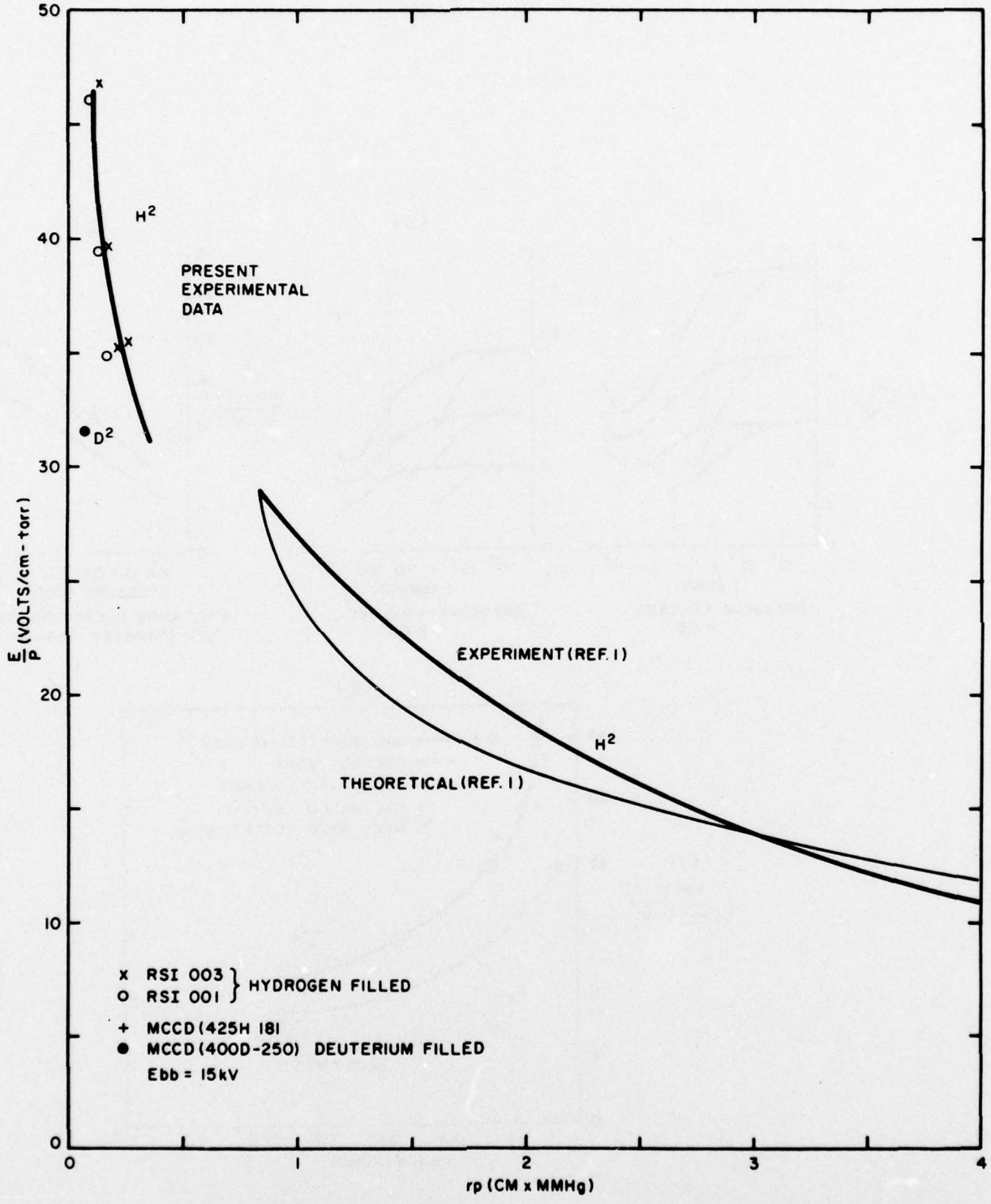

Figure 61. Comparison of present and previous tube voltage drops (experimental and theoretical).

The results of the Breusova study suggest that deuterium or a still heavier gas might prove valuable for use in RSI tubes, since the tube drop appears to diminish somewhat as the reciprocal of the square root of the ion mass. However, problems arise with magnetic interruption in heavier gases, since the heavier gases have a greater inertial resistance of the positive ions to the magnetic-field-induced transverse diffusion, thereby slowing plasma movement to the plasma wall surface. To determine the effects of deuterium on current interruption, the RSI 004 was filled with deuterium and tested, with the results shown in Figure 21. Values of the ratio of interrupting field in deuterium to that in hydrogren [$Bq(D_2)/Bq(H_2)$] for various voltage and current levels are shown in Figure 62. The average of these values is 1.67

A second set of data points is included in Figure 62 which represent the ratio of interruption in the deuterium-filled 400 D 250 to that of interruption in the hydrogen-filled RSI 003. The tube pressures under test were slightly different (RSI 003: p = 0.25 torr; 400 D 250: p = 0.33 torr), but this has been compensated for by the use of a multiplying factor of 0.9 against the Bq ratio. The difference in tube I.D. (RSI 003: 0.375 inch; 400 D 250: 0.250 inch) is not compensated, considering the results of subsection 3.c(3)(d). The ratios shown average 1.62.

The voltage drop advantage of deuterium over hydrogen in the positive column was determined by Breusova to be a reduction of approximately 1/1.4. Results from our tests indicated a ratio of about 1/1.5. To achieve the same tube drop, then, a hydrogen tube could be lengthened by a factor of about 1.5 when filled instead with deuterium. Using previous results, that $Bq \propto L^{-0.75}$, the ratio of quenching fields of deuterium to hydrogen would equal approximately $1.67/(1.5^{-0.75})$. The magnetic field energy, proportional to Bq^2L, would give a ratio for the two tubes of $(1.35)^2$ 1.5 = 2.3. Therefore, the use of deuterium offers no advantage to the RSI application, since the reduced tube drop is counter-balanced by an increased switching energy requirement. Deuterium filling would be advised only in applications where tube voltage drop was of paramount importance.

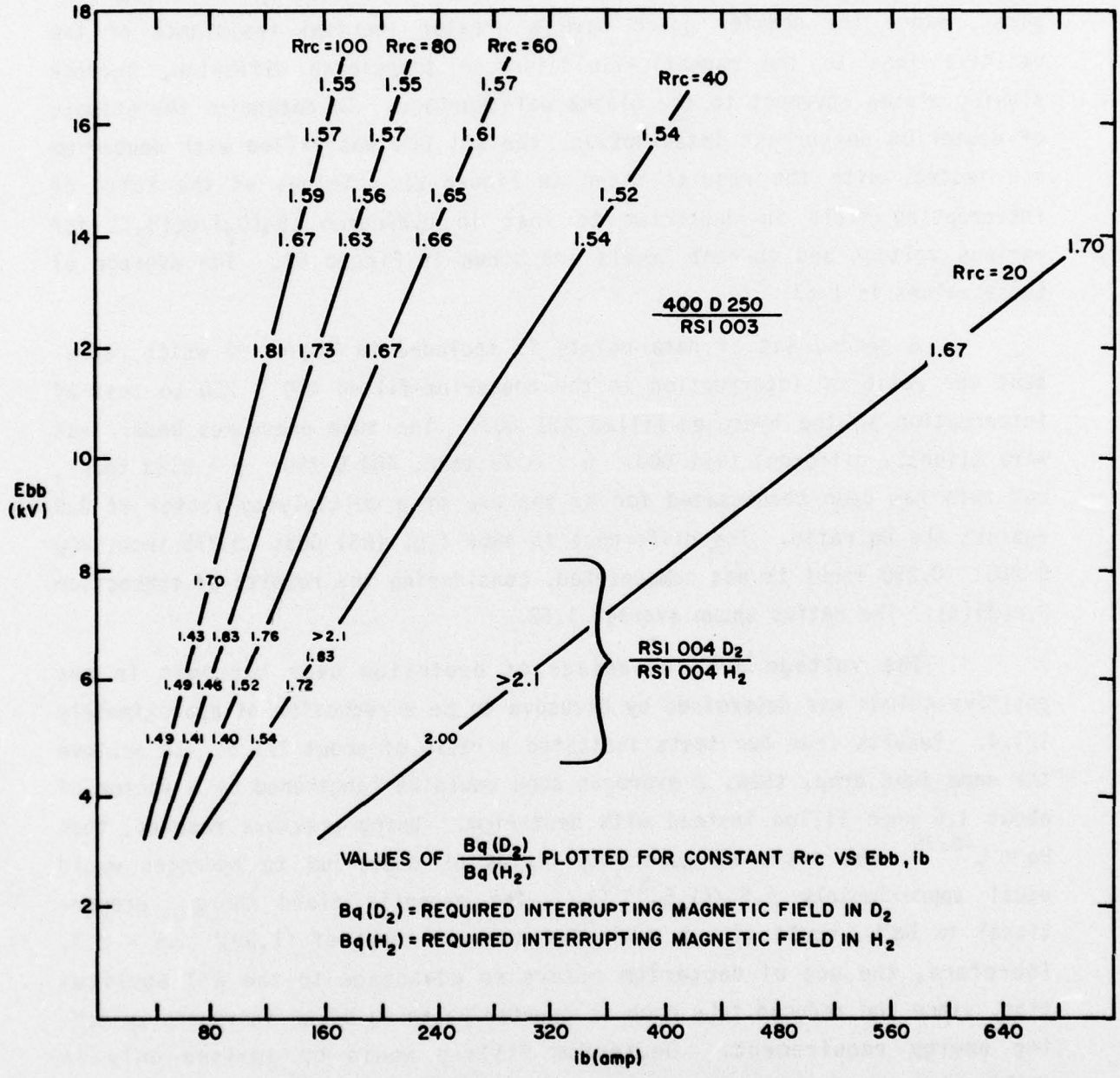

Figure 62. Interrupting magnetic field in deuterium versus hydrogen as a function of Ebb, ib for RSI 004, and for 400 D 250/RSI 003.

Hydrogen is thus the gas of choice for the RSI application. Heavier gases or metal vapors are expected to detract from current interruption capability. Low concentration impurities in the discharge may for the same reason impair current interrupting capability.

f. Test Results: Image Converter and Spectrometer Studies

(1) Optical Instrumentation for Tube RSI 004

Two experimental arrangements used in the optical studies are shown in Figure 63. Since the $\vec{I}\vec{X}\vec{B}$ force on the plasma is perpendicular to the magnetic field, observation of the motion of the plasma during current interruption must be made in a direction parallel to the magnetic field. To do this, while retaining the tube position in the field, the arrangement shown in Figure 63a was used. In this configuration, the tube is subject to a non-homogeneous fringe field somewhat weaker than that within the core gap, and at an angle to it. However, transverse plasma motion, although somewhat obscured, would still be expected to be visible. A reference grid was placed in front of the tube and a mirror was used to reflect the light path for the convenience of the experimental arrangement.

Spectroscopic measurements were made with direct tube observation, as shown in Figure 63b. Noise from firing the RSI and the magnet had an effect on experimental measurements, including a noticeable shift of the beam within the image converter tube. These errors were separated from the data presented in this report.

(2) Image Converter Observations

An image converter containing a Mullard ME-1202 AA tube was obtained for optical use. The image converter trigger circuit is shown in Figure 64. An adjustable pulse width PFN is discharged by a KN-6B krytron through a transformer to provide an enabling 6-kV pulse to the image converter grid. The krytron is triggered from a second delay unit, after the magnet time delay, so that the image converter is gated for observations of short periods of the RSI discharge interruption time.

It was observed, with the RSI 004, that the plasma discharge narrowed and was directed toward one side of the discharge channel during application of the magnetic field. Examination of field directions indicated that

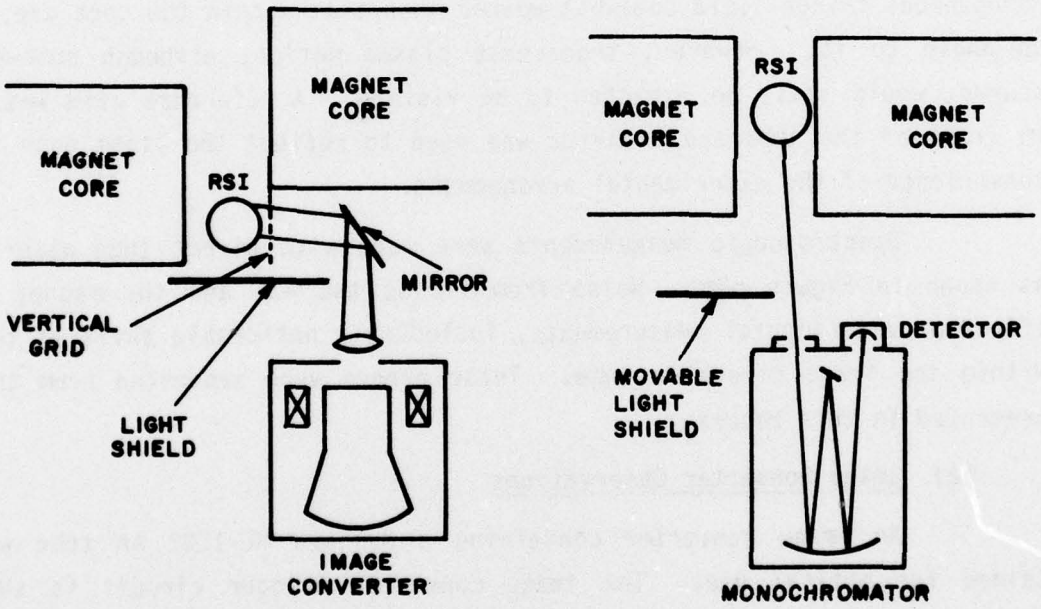

Figure 63. Optical arrangement for observing RSI 004.

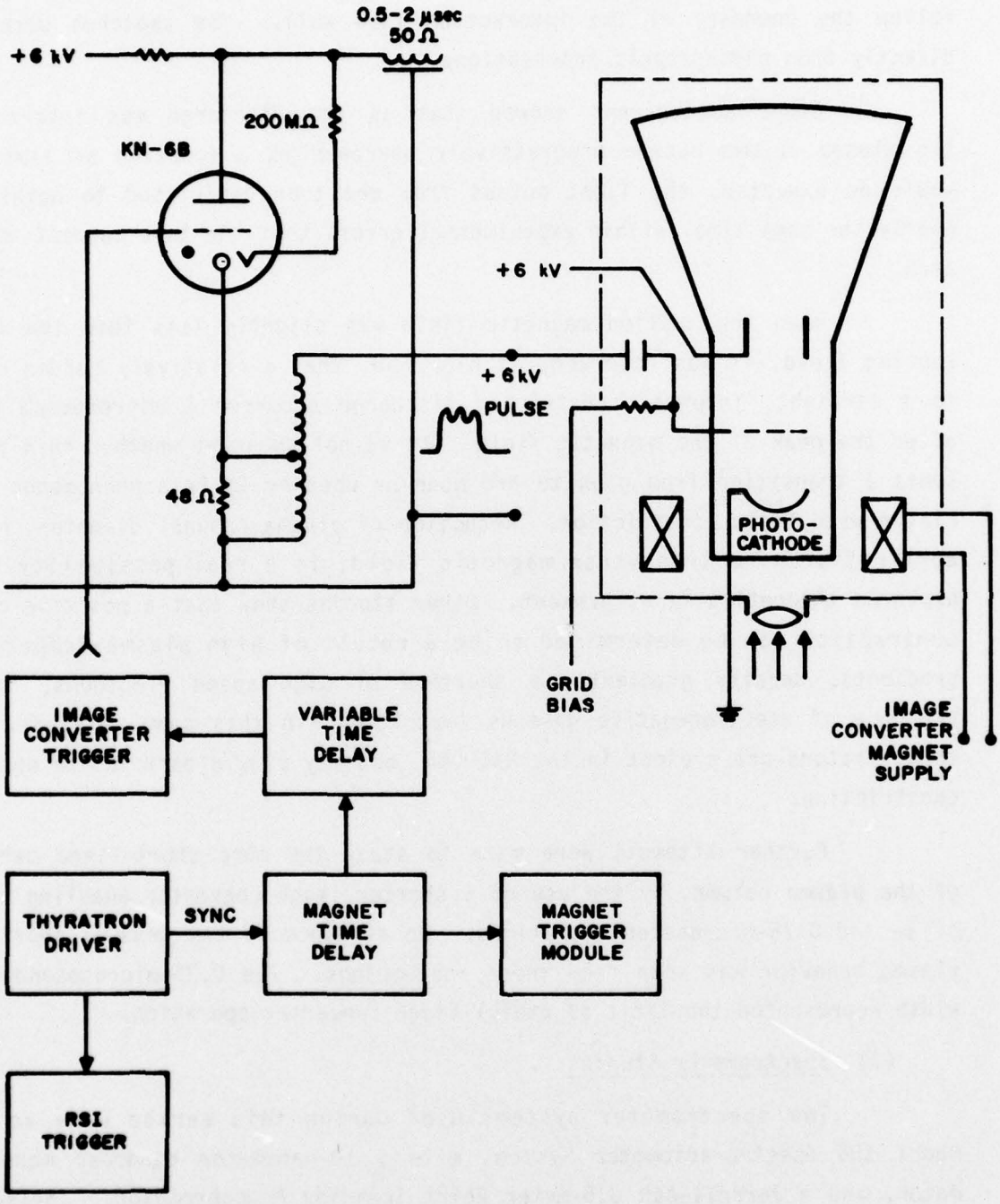

Figure 64. Image converter trigger circuit.

the plasma acted as it should for $\vec{I}\times\vec{B}$ behavior. Figure 65 shows some examples of the motion of the plasma column, where the light intensity is seen to follow the boundary of the interaction tube wall. The sketches were made directly from photographic observations.

Other photographs showed that as the discharge was interrupted, the plasma column became progressively narrower as a function of time. As would be expected, the light output from the tube diminished to nothing at nearly the same time (within experimental error) that the tube current went to zero.

When the applied magnetic field was slightly less than the interrupting field, it was observed, at high Ebb, that a relatively sudden change to a straight, intense, constricted discharge occurred 1 microsecond or so after the peak of the magnetic field. It is not apparent whether this represents a transition from glow to arc mode or whether it is a phenomenon associated with field constriction. Reduction of plasma channel diameter, by the application of a transverse magnetic field, is a real possibility being explored theoretically at present. Other studies show that a positive column contraction can be determined to be a result of high plasma temperature gradients, density gradients, a shortage of high speed electrons, or the presence of electronegative gaseous impurities (in this case, oxygen). All these factors are present in the RSI 004, and may play a part in the observed constriction.

Further attempts were made to study the more short-lived behavior of the plasma column, by the use of a shorter image converter enabling pulses of 1- and 0.25-microsecond durations. No evidence of any unusual short-time plasma behavior was seen from these photographs. The 0.25-microsecond pulse width represented the limit of useful image converter operation.

(3) Spectrometer Studies

Two spectrometer systems used during this period were an EG&G Model 585 Spectroradiometer System, with a 10-nanometer bandpass monochromator, and a Jarrell-Ash 0.5-meter Ebert Scanning Monochromator. These were used in conjunction with EG&G detector heads or with an S-1 photomultiplier tube. Two somewhat different modes of operation were used: for the high

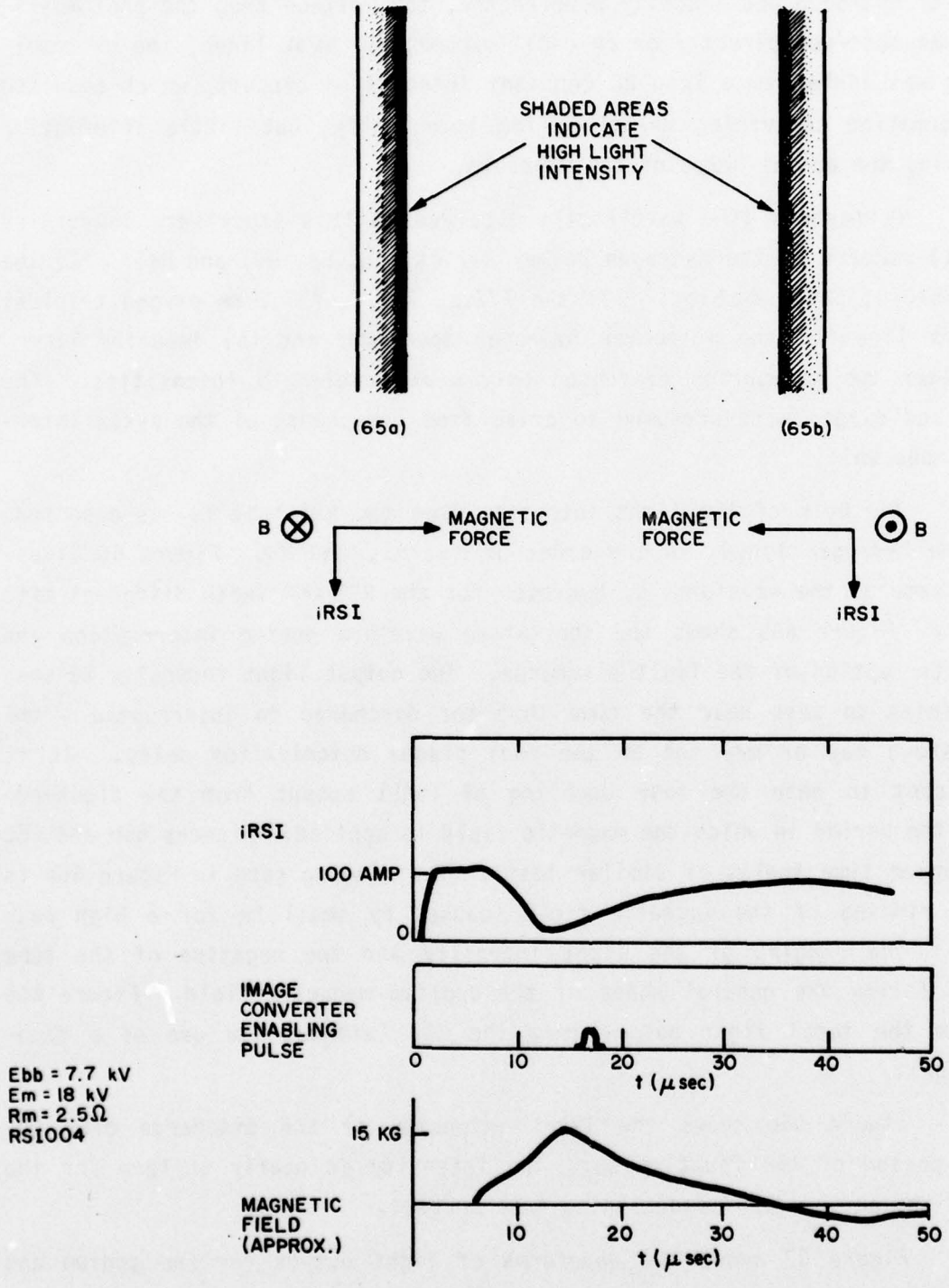

Figure 65. RSI 004 light intensity and current and magnetic field waveforms during magnetic field interaction.

intensity hydrogen and impurity wavelengths, the voltage from the photomultiplier was observed directly on an oscilloscope; for weak lines, the photomultiplier was linked to a long RC constant integrating circuit, which resulted in information concerning relative line intensities, but little information concerning the actual shape of the waveform.

Pronounced line wavelengths observed in this study were identified as: (1) members of the hydrogen Balmer series ($H\alpha$, $H\beta$, $H\gamma$, and $H\delta$); (2) the sodium 589.0, 589.6 doublet; (3) the 777.1, 777.4, 777.5 nm oxygen triplet; (4) many lines of the molecular hydrogen spectrum; and (5) impurity lines. The latter two categories evidenced only weak wavelength intensities. The sodium and oxygen were presumed to arise from components of the pyrex interaction tube wall.

The bulk of the light intensity from the RSI tube is, as expected, from the hydrogen lines, in the order of $H\alpha$, $H\beta$, and $H\gamma$. Figure 66 illustrates some of the waveforms of hydrogen for the RSI 004 (with different time scales). Figure 66a shows the short-term waveform during interruption and near interruption of the fault discharge. The output light intensity is seen to diminish to zero near the time that the discharge is interrupted - the delay shown may or may not be the real plasma deionization delay. It is significant to note the near doubling of light output from the discharge during the period in which the magnetic field is applied. Figures 66b and 66c show longer time scales of similar tests. The ringing seen in Figure 66b is due to ringing of the magnetic field (caused by small Rm for a high peak field). The ringing of the light intensity and the negative of the tube current follow the general shape of the applied magnetic field. Figure 66b reflects the total light output from the RSI (without the use of a monochromator).

Figure 66c shows the light intensity of the discharge over the entire period of the fault pulse. The intensity is nearly uniform for the body of the pulse, despite declining tube current.

Figure 67 shows the waveforms of light output for the sodium and oxygen lines. Both the sodium and oxygen lines first appear after application of the magnetic field. The sodium lines persist considerably longer than the

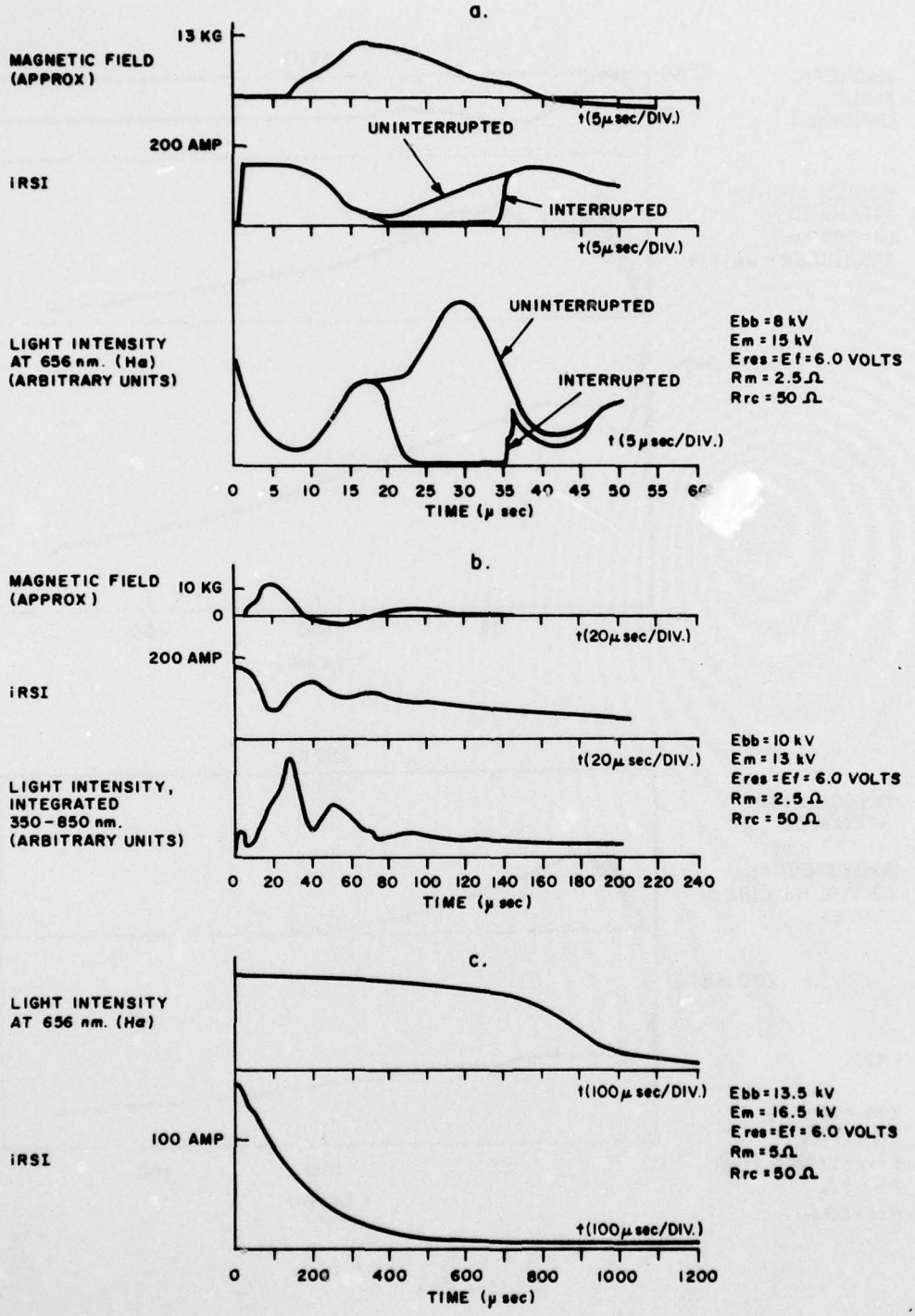

Figure 66. Hydrogen light intensity during fault conduction - RSI 004.

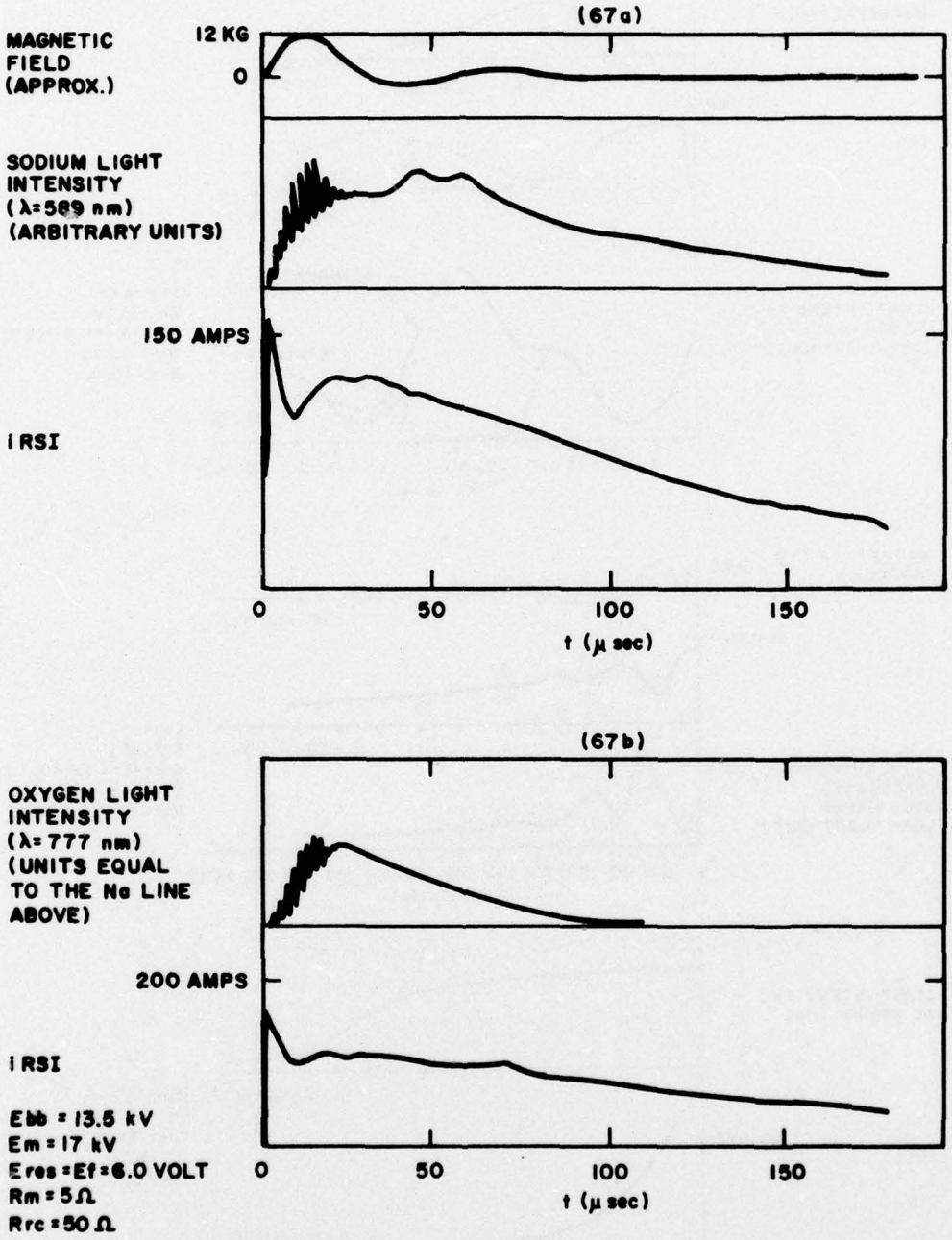

Figure 67. Sodium and oxygen light intensities during fault conduction - RSI 004.

oxygen lines, which appear to diminish to zero shortly after ringing of the magnetic field ceases. These lines arise from neutral sodium and oxygen atoms, which suggests that wall heating may cause the presence of the sodium line. Oxygen contamination of the plasma is a possibility, although decay of the oxygen line intensity during the fault pulse suggests otherwise.

Another test showed that the intensities of the sodium and oxygen lines were stronger by factors of 150 and 15, respectively, when the quenching field was applied (compared with a zero field condition), while the intensity of the major hydrogen lines integrated over the entire pulse changed relatively little. It could be concluded that the plasma-wall interaction is responsible for the introduction of the sodium and oxygen lines to the light output from the plasma.

Weaker lines were observed with the Jarrel-Ash monochromator, many of which were attributable to the complex molecular hydrogen spectrum. A 345.3-nanometer line was also seen, which is likely due to cobalt (345.4) which arises from the Kovar alloy (17.5% cobalt) used to seal the ends of the glass interaction tube. Visual examination of the tube after operation showed that this seal did undergo some slight melting at the point of plasma interaction.

g. Interaction Channel Wall Damage

(1) Energy Dissipation at the Channel Wall

Considerable power is generated in the RSI interaction channel during current interruption. Peak power is generated midway through the interruption process, at a rate, P_{max}, equal to 1/2 Ebb · 1/2 ib, which equals 1125 kilowatts at Ebb = 15 kV, ib = 300 amperes. It is important to minimize the time duration of this dissipation.

Average power dissipation during interruption occurs at a rate of less than 1/2 P_{max}, dependent upon the specific voltage and current waveforms. For $P = 0.4\ P_{max} = 0.1$ Ebb ib, the energy transferred to the channel walls, ϵ_w, is 0.1 Ebb ibΔt = 450 X $10^3 \Delta t$. An interruption time of 10 μsec results in an energy dissipation of 4.5 joules at the wall surface.

Waveforms of epy, iRSI, and P during an interruption and an incomplete interruption are shown in Figure 68. Energy dissipation to the channel wall in the uninterrupted pulse is seen to be three times the dissipation during the interrupted pulse.

The temperature rise of the wall surface can be calculated from

$$\Delta T(^{o}C) = \frac{2}{\pi}\sqrt{\frac{\Delta t}{\lambda\sigma}}\,F_o$$

where λ = wall thermal conductivity; σ = wall heat capacity; F_o = incident power density = P/A; A = wall surface area. For alumina ceramic, λ = 0.25 j/cm · sec · ^{o}K, and σ = 1.8 j/cm^3 · ^{o}K. This results in:

$$\Delta T = 0.95\sqrt{\Delta t}\,\frac{P}{A} \cong 0.1\sqrt{\Delta t}\,\frac{Ebb\ ib}{A} \quad .$$

At $\Delta T = 1000^{o}C$ maximum, at Ebb = 15 kV, ib = 300 amps: $A = 450\ (\Delta t)^{0.5}\ (cm^2)$. A 10-μsec interruption time, therefore, requires that the dissipating wall surface area equal 1.4 cm^2.

The eroded surface of the RSI 005 was localized at a strip along the central channel (see subsection 3.g(2)). The total surface area along this line equals approximately 0.7 cm^2. This tube was tested at an average Ebb = 8.5 kV, which corresponds to a surface temperature rise of 1900^{o}C, which explains the extent of the damage noted (subsection 3.g(2)). The maximum working temperature of alumina ceramic is 1600^{o}C.

The dissipation surface area of the RSI 10 series is calculated to be 1.5 cm^2, which corresponds to a 900^{o}C local temperature increase. At Δt = 20 μsec, $\Delta T = 1270^{o}C$.

(2) Channel Wall Damage Assessment

RSI thyratrons tested were subject to damage to the interaction channel wall in varying degrees of severity. The glass channel RSI 004 and the chuted RSI 005 suffered the greatest degree of damage; the RSI 003 was

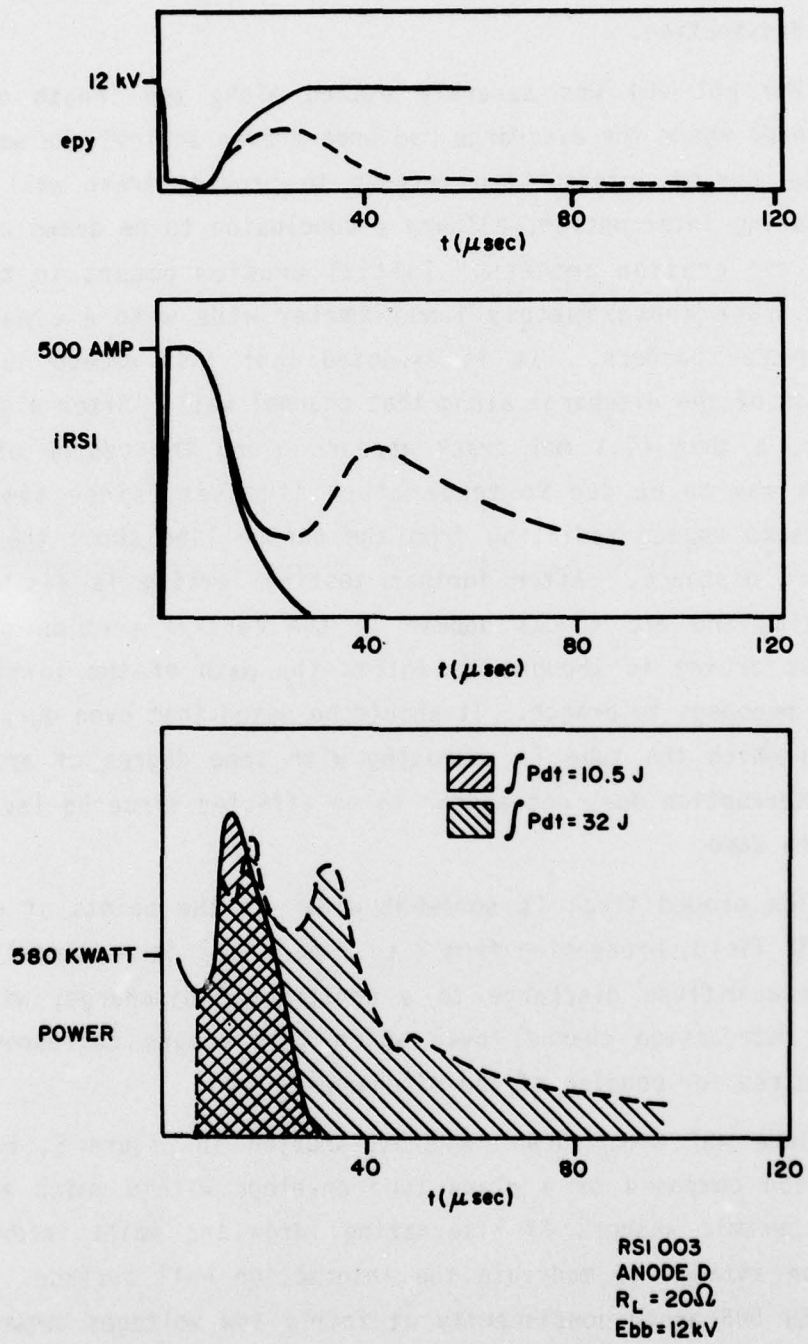

Figure 68. Energy dissipation at the interaction channel wall during an interrupting and a non-interrupting field pulse.

relatively undamaged. The cause for this disparity is due to the relative temperature tolerance of the wall material and the degree of localization of energy dissipation.

The RSI 004 was severely etched along the length of the interaction channel where the discharge had been driven against the wall. Rotation of the tube during interruption testing to provide fresh wall surfaces for exposure during interruption, allowed a conclusion to be drawn concerning the nature of the erosion process. Initial erosion occurs in the form of a discharge track approximately 1-millimeter wide with a clear center and parallel darker borders. It is expected that this damage is caused by a constriction of the discharge along that channel wall. After a greater period of testing, a thin (0.1 mm) crack appears along the center of this track. This crack may to be due to temperature stresses, since similar perpendicular cracks appear radiating from the center line about the channel axis for a short distance. After further testing, arcing is visible along the channel axis, and arc tracks appear in the central portion of the eroded zone. This arcing is thought to follow the path of the initial crack but afterwards proceeds to branch. It should be noted that even during the period of time in which the tube is operating with some degree of arc occurrence, current interruption does not appear to be affected since Bq levels appear to be about the same.

The eroded track is somewhat wider at the points of entrance into the magnetic field, broadening from 2 to 3 mm. This is presumably caused by a shift from a diffuse discharge to a constricted discharge, with the short length of interaction channel over which this occurs corresponding to the length required for bending of the discharge column.

Tube RSI 005, shown in cross-section in Figure 5, has an interaction region composed of a glass tube envelope within which are stacked a series of ceramic washers of alternating large and small internal diameter base, in an attempt to modulate the interaction wall surface. As reported earlier, RSI 005 arced consistently at fairly low voltages between the glass envelope and the ceramic washers. An attempt to alleviate this problem by shrinking the glass onto a portion of the ceramic washer surface was not

successful, because the glass fractured due to the difference in thermal expansion rates between glass and ceramic. Repair of the tube was not considered worthwhile, and an examination was made of the damage sustained by the ceramic washers.

Most of the damage to the ceramic occurred on the side of the washers facing the cathode, suggesting that erosion was caused by electron bombardment of the surface. The length of apparent plasma penetration into the washer-to-washer gap is also significant, since the 1 - 1.5 millimeter penetration depth (as determined from the extent of surface damage) into the plasma chute indicates an increase in the total discharge length by a maximum factor of only 1.7, as shown in Figure 69. The mechanism of improvement of tube interruption probably stems, therefore, from direct electron surface energy losses rather than from a radical bending and folding of a narrowed discharge column.

Also apparent from a visual observation of the washers was a difference in the degree of erosion depending upon the position of the washer in the interaction tube. Washers near the cathode end suffered a greater amount of "burning" than those near the anode end. In addition, the erosion near the cathode end was more diffuse, from one to several millimeters wide, whereas the anode end washers revealed "burning" to but 1 millimeter in width. Possible explanations for this behavior include longitudinal plasma density gradients, a nonlinear electric field distribution, a gas pressure gradient, high energy electron beaming, or a shift from a diffuse to a constricted discharge caused by interaction with the washer edges.

The ceramic washers removed from the tube were eroded radially for approximately 1 mm from the central plasma bore, in the expected $\vec{I}\times\vec{B}$ direction of magnetic force. An SEM (Scanning Electron-Microprobe) X-ray analysis was performed on the eroded surface (Figures 70 and 71), looking particularly for possible electrode metal contamination. The analytical report indicated weak concentrations of Fe, Ni, Ta, and Mn in only a small portion of surface area. Most of the surface damage appears to have been caused by wall heating by the hydrogen plasma.

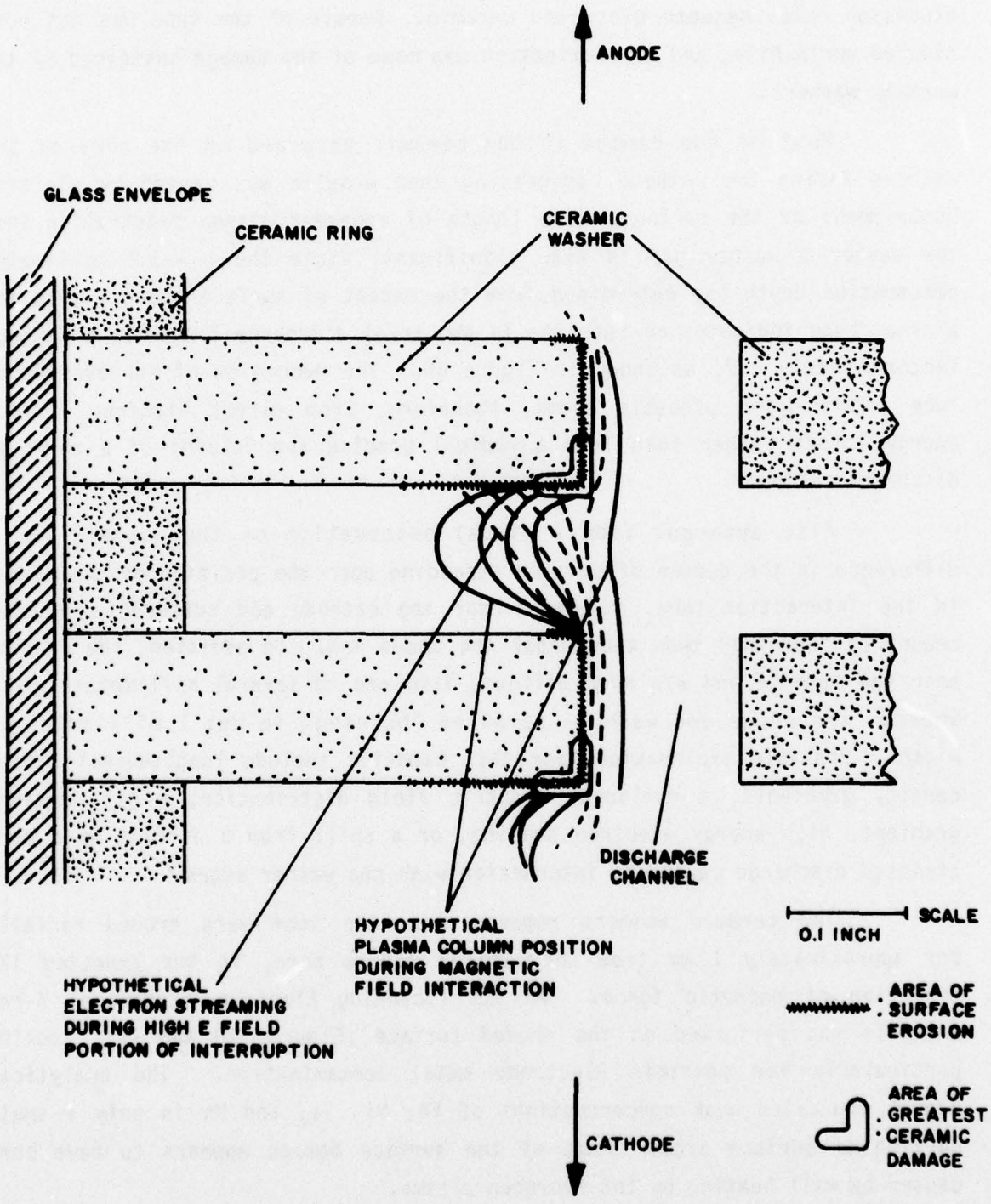

Figure 69. RSI 005 during magnetic field interaction.

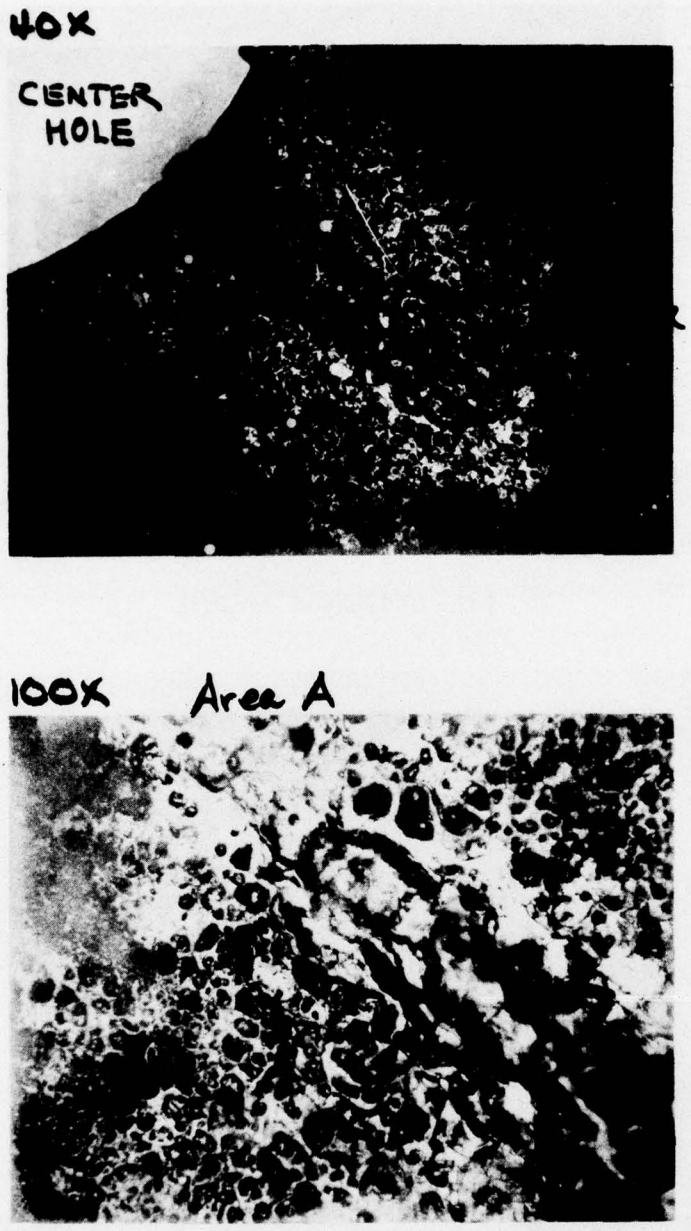

Figure 70. Surface damage to RSI 005 ceramic washer.

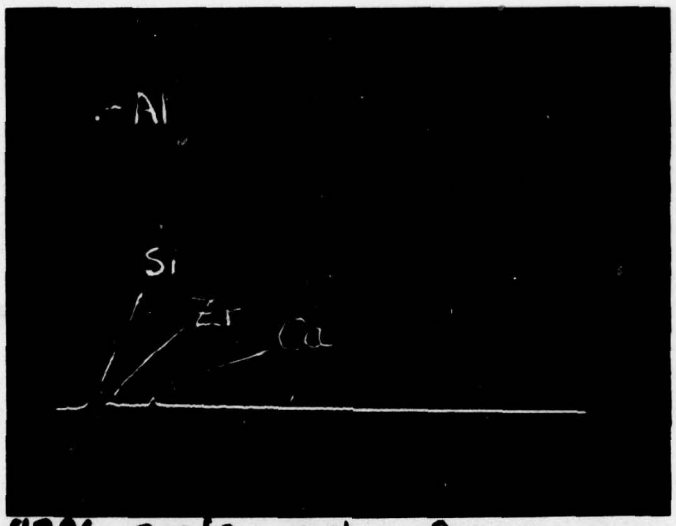

(a) Undamaged ceramic

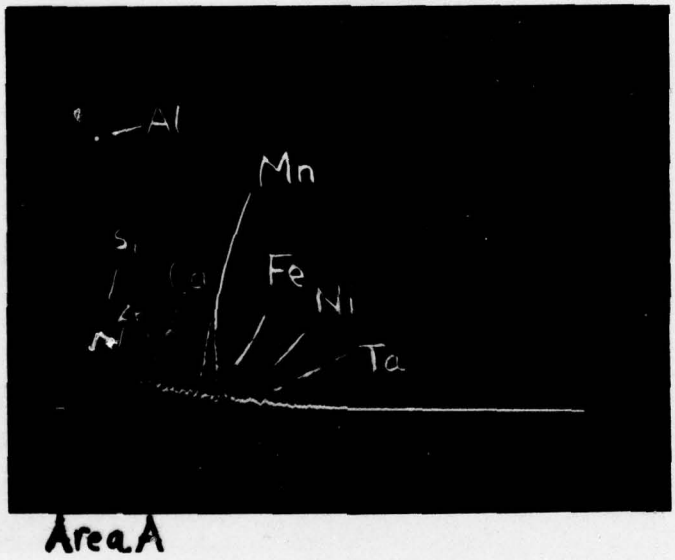

(b) Eroded surface (expanded scale)

Figure 71. SEM analysis of RSI 005 ceramic washer surface.

The analysis was made in the magnesium to uranium mass range, using Ortec spectrum X-ray fluorescence detector equipment.

The concern that large amounts of metal vapor might contaminate the plasma was unsubstantiated, probably due to the distance between the interaction region of high magnetic field strength and the glass-metal seals.

The RSI 005 was tested at an average voltage of 8 kV, at an average current of 160 amp. A power dissipation calculation can be made, utilizing the assumptions of: an average 10 μsec interruption time, an average penetration depth of 1 mm into the washer-to-washer gap, and an average discharge column width during interruption at the ceramic surfaces of 1 mm. The result indicates an average short time scale wall surface heating of about 900°C, which suggests that ceramic erosion could be occurring during the higher power testing phase. At the peak power level, Ebb = 7.5 kV, ib = 375 amp, and the calculated surface temperature is approximately 2000°C.

A damage assessment of the RSI 7-2 reveals some information regarding the incapability of the magnetic field to displace the discharge column against a high sustaining electric field. During interruption, the plasma column does not follow the curvature of the wall, but shortens its path as shown in Figure 72. These conclusions are drawn from the location of wall damage to the glass channel. Heaviest plasma tracking is observed at points A, C, E, G, and I, and these points display a wider plasma channel tracking. Point A displays the heaviest damage and some narrow branched tracking which could be caused by local arcing. Point B does not present obvious evidence of arc damage, but rather a somewhat wider (0.5 mm) and more uniform track mark. The turn-edged damage of differing width is probably due to a constricted discharge pressed against the interaction wall to a greater degree at points A, C, E, G, and I than at B, D, F, and H, flattening it and causing increased wall heating at the former points. The hotter central portion of the discharge presumably serves to "clean" the wall at that point, causing a two-sided outline.

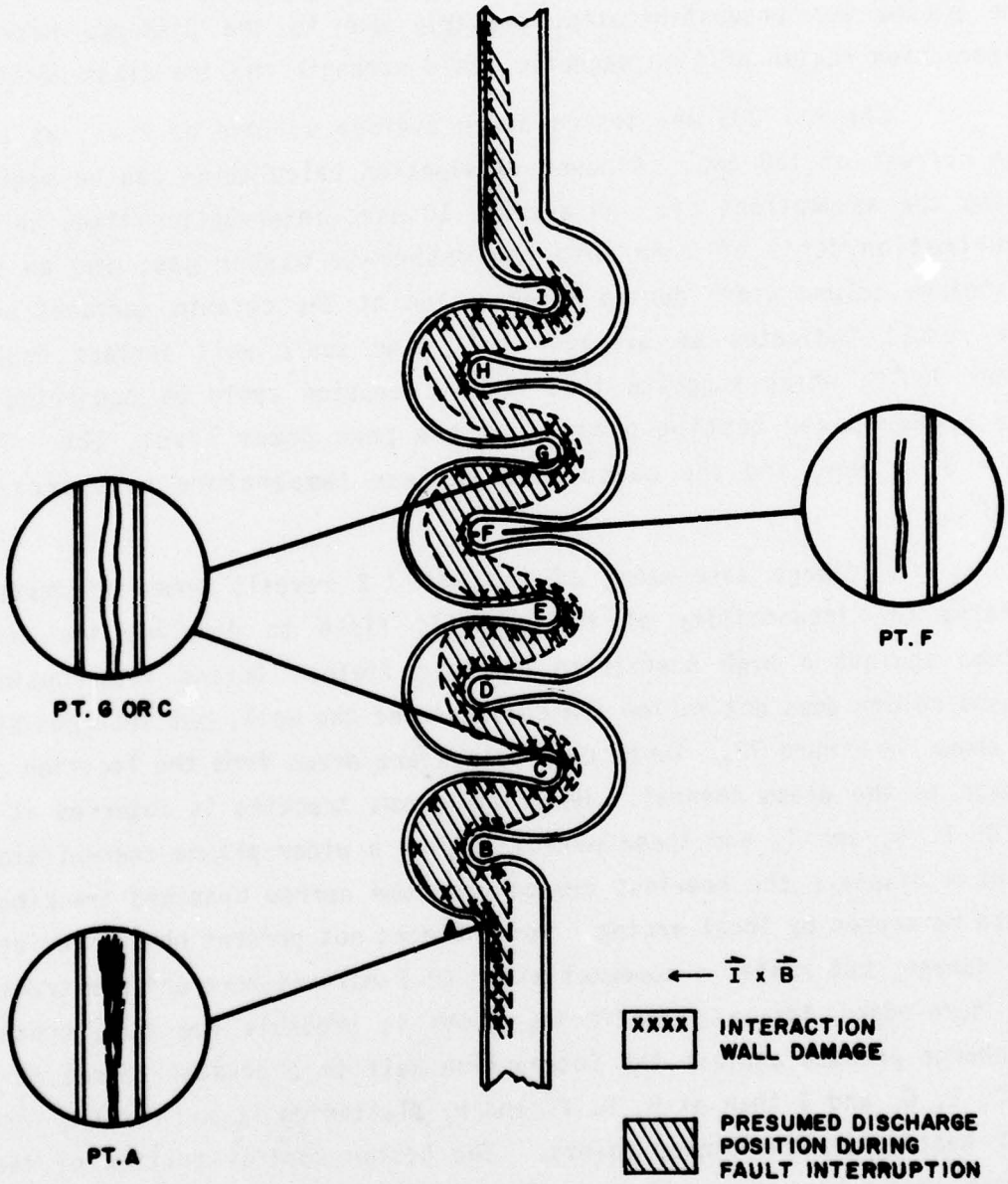

Figure 72. RSI 7-2 damage survey.

4.0 COURSE OF THE INVESTIGATION: THEORETICAL ANALYSIS

a. Voltage Drop in a Positive Column

A theory for voltage drop in the positive column of a gas discharge was developed by Von Engel and Steenbeck[16] and reported in Brown[3]. A relationship for the average electron energy, $\bar{u}$, is determined as a function of pr by balancing gas ionization and ambipolar diffusion losses to the channel walls for a Maxwellian electron velocity distribution. The electric field required to support the discharge is determined by the use of f = fraction of energy lost by an electron in a neutral particle collision to be $E = 1.41 f^{0.5} \bar{u} 1^{-1}$ where 1 = electron mean free path. The result is plotted in Figure 61 as E/p versus rp.

L.N. Breusova[1] reports corrections to the potential gradient which are current and time dependent, and which are explained as being caused by resistive gas heating. His data are shown in Figures 60a-60c, which indicate a relationship similar to $E \alpha (p/r)^{0.5}$.

A comparison with RSI tube drop measurements, shown in Figure 60d, shows that agreement is good despite the compensated difference in channel diameters and pressure range.

b. Plasma Discharge in a Transverse Magnetic Field

When a strong magnetic field is applied transverse to a plasma discharge, several physical processes take place which contribute to the eventual interruption of the discharge:

1. plasma energy is lost to the channel wall by electron and ion bombardment;
2. plasma particle loss is greatly increased by recombination at the wall surface;
3. the wall structure is heated, increasing outgassing and secondary electron emission; and
4. plasma density is effected by a reduction in discharge volume and a consequent reduction in gas available for ionization.

Statements equivalent to the first statement above are:

5. the plasma resistance is increased according to the equation:

$$R = \frac{Lm_s}{An_e e^2} \nu_{ce} \left(1 + \frac{\Omega_e^2}{\nu_{ce}^2}\right); \text{ and}$$

6. the plasma-column-sustaining electric field is increased by a constriction of the effective discharge radius.

A theoretical study was made of the properties of the plasma column in a transverse magnetic field. A rectangular cross-section discharge column is used, with coordinates and field directions as shown in Figure 73. MKS units are used throughout. The following assumptions are made:

1. the plasma is a weakly ionized hydrogen plasma with electron temperature less than 5 eV;
2. all parameters are independent of the longitudinal direction $(\frac{\partial}{\partial z} = 0)$;
3. the risetime of the magnetic field is sufficiently slow, compared with plasma time constants, so that the plasma can be considered to be in a steady state $(\frac{\partial}{\partial t} = 0)$;
4. lower-order electron and ion temperature gradient and mass terms are neglected; and
5. charge neutrality $(n_i = n_e)$ exists throughout the plasma.

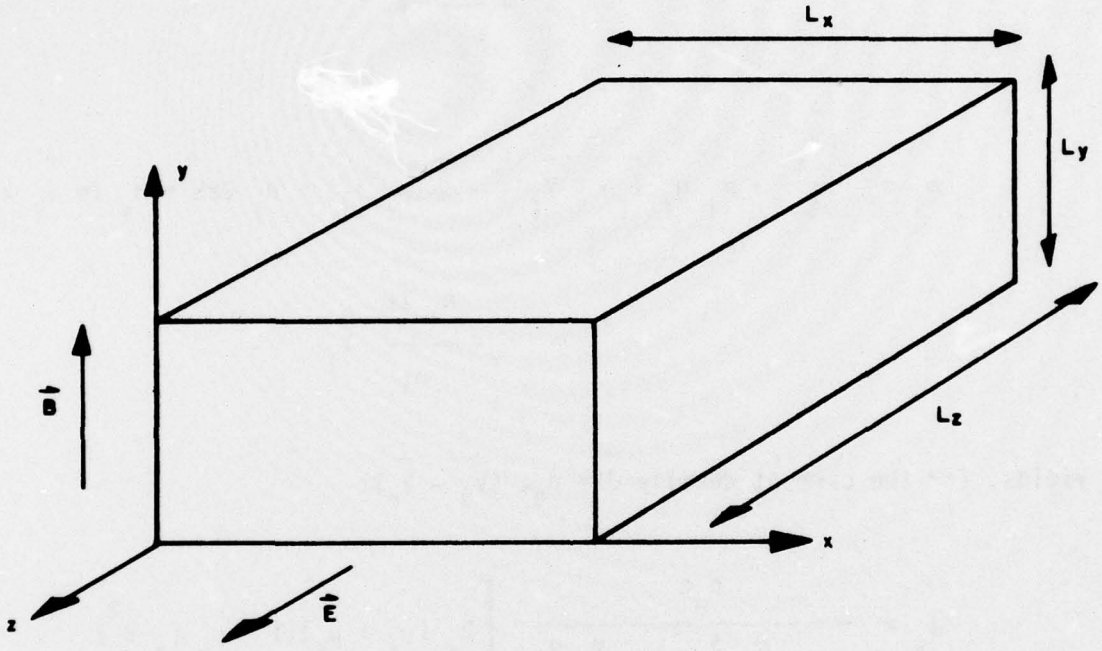

Figure 73. Geometry for positive column analysis.

Then, solution of the momentum conservation equations:

$$m_e n_e \frac{\partial \vec{V}_e}{\partial t} + m_e n_e \vec{V}_e \cdot \nabla \vec{V}_e = -\vec{\nabla}(n_e T_e) - n_e e \vec{E} - n_e e \vec{V}_e \times \vec{B}$$

$$- \frac{n_e e}{\mu_e} \vec{V}_e$$

$$m_i n_i \frac{\partial \vec{V}_i}{\partial t} + m_i n_i \vec{V}_i \cdot \nabla \vec{V}_i = - \vec{\nabla}(n_i T_i) + n_i Ze\vec{E} + n_i Ze \vec{V}_i \times \vec{B}$$

$$- \frac{n_i Ze}{\mu_i} \vec{V}_i$$

yields, for the current density $\vec{J} = n_e e (\vec{V}_i - \vec{V}_e)$:

$$J_x = \frac{n_e e}{(1 + \mu_e^2 B^2)(1 + \mu_i^2 B^2)} \left[E_x (\mu_e + \mu_i)(1 + \mu_e \mu_i B^2) \right.$$

$$+ E_z (\mu_e^2 - \mu_i^2) B + \frac{k T_e}{e} \mu_e \frac{1}{n_e} \frac{\partial n_e}{\partial x} (1 + \mu_i^2 B^2 - \frac{\mu_i}{\mu_e} \frac{T_i}{T_e}$$

$$\left. - \mu_e \mu_i B^2 \frac{T_i}{T_e}) \right]$$

$$J_y = n_e e \left[E_y (\mu_e + \mu_i) + \frac{k T_e}{e} \mu_e \frac{1}{n_e} \frac{\partial n_e}{\partial y} \left(1 - \frac{\mu_i}{\mu_e} \frac{T_i}{T_e}\right) \right]$$

$$J_z = \frac{n_e e}{(1 + \mu_e^2 B^2)(1 + \mu_i^2 B^2)} \left[- E_x (\mu_e^2 - \mu_i^2) B \right.$$

$$+ E_z (\mu_e + \mu_i)(1 + \mu_e \mu_i B^2) - \frac{k T_e}{e} B \frac{1}{n_e} \frac{\partial n_e}{\partial x} (\mu_e^2 + \mu_i^2 \frac{T_i}{T_e}$$

$$\left. + \mu_e^2 \mu_i^2 B^2 (1 + \frac{T_i}{T_e})) \right]$$

Let

$f_i = f_i(T_e, n_o)$ = ionization rate per electron.

In the steady state:

$$\vec{\nabla} \cdot \vec{J} = 0;$$

$$\vec{\nabla} \cdot (n_e \vec{V}_e) = n_e f_i.$$

These two equations provide solutions for the two unknowns n_e (x, y), E(x, y), with the boundary conditions at the walls:

$$\vec{J} = 0;$$

$$n_e = 0.$$

An analytical solution to the above equations is not attainable, which suggests further simplification. For both B = 0 and B very large, the above equations require that $J_x = J_y = 0$. Furthermore, J_x, J_y are not zero only when circulatory currents develop in the transverse direction in the plasma. Because the principal electrically and magnetically induced plasma motion occurs in the longitudinal planes, any transverse circulatory current must be necessarily second-order, and can be neglected. This is particularly appropriate since the plasma time constants are short compared to the B time, and since this represents the steady state assumption previously made.

Setting $J_x = J_y = 0$, therefore, yields equations for E_x and E_y as functions of n_e and E_z. From these, a solution for J_z can be determined:

$$J_z = \frac{n_e(x,y)e}{1 + \mu_e \mu_i B^2} \left[E_z (\mu_e + \mu_i) - \frac{k T_e}{e} \frac{1}{n_e} \frac{\partial n_e}{\partial x} \mu_e \mu_i B \left(1 + \frac{T_i}{T_e}\right) \right]$$

as well as for the transverse electron velocities. These velocities, substituted into the equation $\vec{\nabla} \cdot (n_e \vec{V}_e) = f_i n_e$ yield:

$$\frac{\partial^2 n_e}{\partial x^2} + (1 + \mu_e \mu_i B^2) \frac{\partial^2 n_e}{dy^2} + \frac{(\mu_e + \mu_i) Be E_z}{k (T_e + T_i)} \frac{\partial n_e}{\partial x}$$

$$+ f_i \frac{e}{k (T_e + T_i)} \frac{\mu_e + \mu_i}{\mu_e \mu_i} (1 + \mu_e \mu_i B^2) n_e = 0$$

Assuming that the y dependence for n_e is proportional to $\sin\left(\frac{\pi}{L_y} y\right)$ yields:

$$\frac{\partial^2 n_e}{\partial x^2} + \alpha \frac{\partial n_e}{\partial x} + \beta n_e = 0$$

where

$$\alpha = (\mu_e + \mu_i)\, B\, \frac{e}{k(T_e + T_i)}\, E_z$$

$$\beta = \left[f_i \frac{e}{k(T_e + T_i)} \frac{\mu_e + \mu_i}{\mu_e \mu_i} - \frac{\pi^2}{L_y^2} \right] \quad (1 + \mu_e \mu_i B^2) \,.$$

This result contains the assumption that

$$\frac{\nu_i}{D} > \frac{1}{\Lambda^2} \,,$$

or that the electron ionization be greater than the electron diffusion loss.

Boundary conditions of the form $n_e(0) = n_e(L_x) = 0$ define the solutions to the differential equation in n_e. For $n_e(0) = 0$, and for

$$\beta - \frac{\alpha^2}{4} < 0,$$

the solution for n_e is a hyperbolic sine function which cannot meet the second boundary condition. Therefore, for $\beta < \frac{\alpha^2}{4}$, no discharge can exist, and

$$\beta - \frac{\alpha^2}{4} > 0$$

represents the breakdown condition for the plasma, and the solution for n_e is:

$$n_e = n_{eo} e^{-\frac{\alpha}{2}x} \sin \sqrt{\beta - \frac{\alpha^2}{4}}\, x$$

and the electron ionization condition must accept the scale length $\Lambda \text{eff} \simeq \frac{2}{\alpha}$. Applying the boundary condition gives

$$\beta - \frac{\alpha^2}{4} = \left(\frac{\pi}{L_x}\right)^2$$

and

$$n_e = n_{eo} e^{-\frac{\alpha}{2}x} \sin \frac{\pi x}{L_x}$$

where the electron density profile appears as in Figure 74, and the electron density maximum occurs at

$$x = x_* = \frac{L_x}{\pi} \tan^{-1} \left(\frac{2\pi}{\alpha L_x}\right)$$

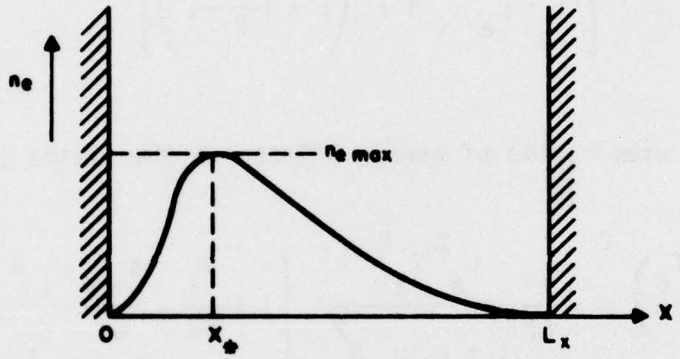

Figure 74. Solution form for electron density versus x for a positive column in a transverse magnetic field.

The peak electron density and average electron density are readily determined, and are seen to reduce to the standard positive column for $B = 0$.

Integrating J_z over the cross-section gives the total current:

$$I = \frac{L_x L_y \mu_e n_{eo} eE_z \frac{2}{\pi^2} \left(1 + e^{-(\frac{\alpha L_x}{2})}\right)}{\left[(1 + \mu_e \mu_i B^2)\left(1 + (\frac{\alpha L_x}{2\pi})^2\right)\right]}$$

A final examination of energy balance in the plasma yields the equation:

$$\left(\frac{k T_e}{e}\right)^2 = \frac{1}{6f} \frac{L_e^2 E_z^2}{1 + \mu_e \mu_i B^2} \left[1 + \frac{\mu_i}{\mu_e} - \frac{k T_e}{e} \mu_i B \frac{1}{E_z} \frac{1}{n_e} \frac{\partial n_e}{\partial x} \left(1 + \frac{T_i}{T_e}\right)\right]$$

As long as the last term in the brackets is small, a simple expression is derived for $T_e = T_e (E_z)$. Should this not be the case, the calculations must be repeated, including ∇T_e terms.

The foregoing theory has been further considered to compare its results with the available experimental data.

For our conditions, the reduced discharge radius, x_*, can be approximated with the use of

$$\tan^{-1}\left(\frac{2\pi}{\alpha L_x}\right) = \frac{2\pi}{\alpha L_x},$$

for $\alpha L_x >> 1$.

With $\alpha \cong \mu_e \frac{BE_z}{\left(\frac{KT_e}{e}\right)}$, and $\mu_e\ (m^2/v\cdot sec) \cong \frac{49}{p_o(torr)} \frac{1}{\sqrt{\frac{KT_e}{e}}}$

then

$$x_* \cong \frac{2}{\alpha} = \frac{T_e^{\frac{3}{2}} p_o}{25\ B\ E_z} \quad (m, eV, torr, T, V/m)$$

or, at $p_o = 0.3$ torr, $T_e = 4$ eV:

$$x_*(cm) = \frac{0.14\ T_e^{\frac{3}{2}}}{B(Kgauss)\ E(volt/cm)} \approx \frac{1.1}{B\ E}$$

To determine the predicted interrupting field, the voltage drop in a channel of radius x_* should be made equivalent to the applied electric field; that is, the magnetic field should be seen as a mechanism of constricting the plasma column, and thereby increasing the electric field in the plasma to the point at which the electric potential can no longer support the discharge energy losses.

Data for E/p versus rp at very low rp, however, are not available, and it becomes necessary to extrapolate from data four orders of magnitude higher, as shown in Figure 75.

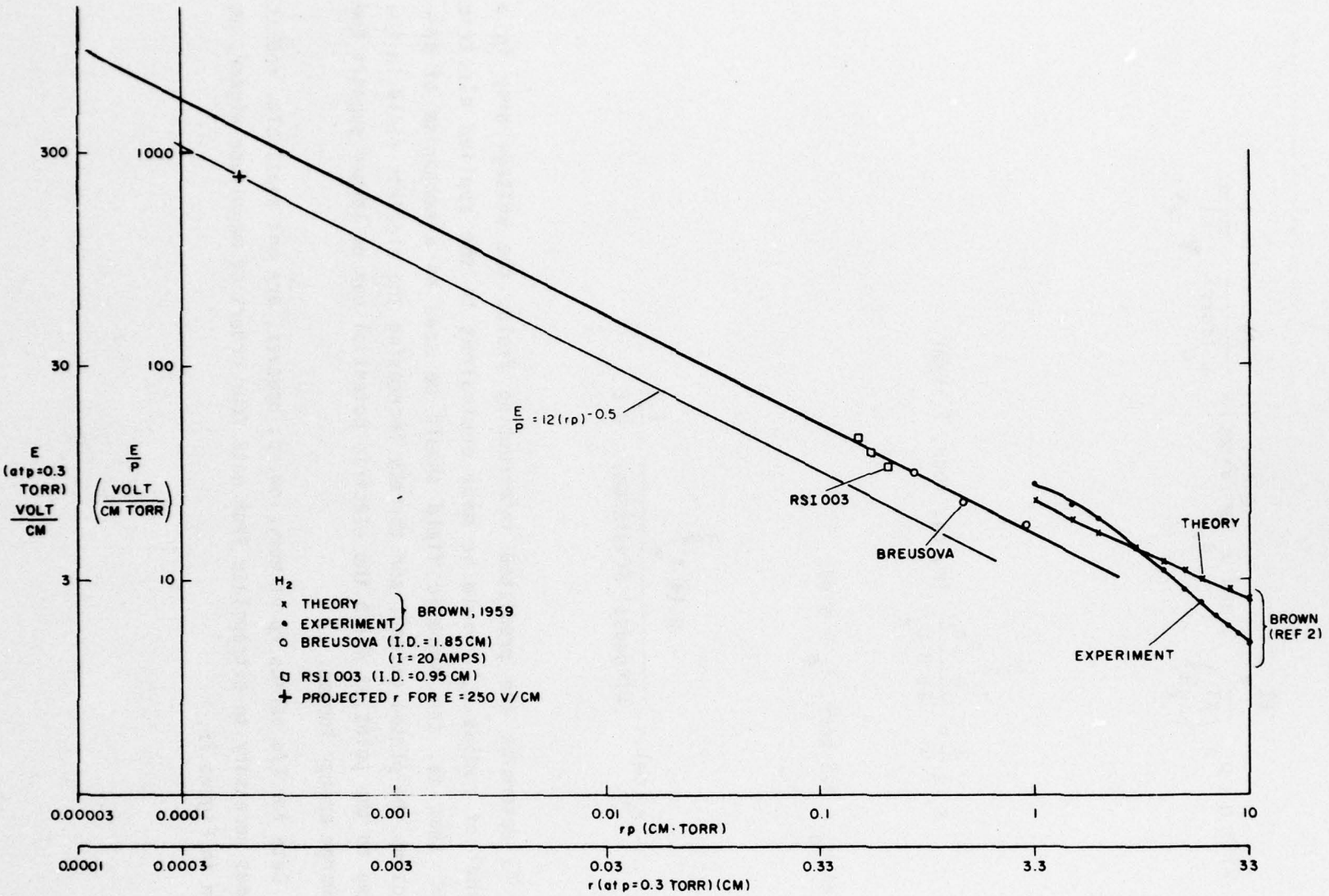

Figure 75. E/p versus rp: an extrapolation of etd.

Experimental data at $0.1 < rp < 10$ suggest that $\frac{E}{p} \cong 16\ (rp)^{-0.5}$, under 20-amp pulsed discharge conditions. An extrapolation of this formula to 300-amp pulses can be made from Figure 60a data, suggesting that $\frac{E}{p} \cong 12\ (rp)^{-0.5}$, or that

$$E \cong 12 \sqrt{\frac{p}{r}}$$

Since $x_* \equiv r$, we find that at $B = Bq$:

$$Bq = \frac{0.14\ T_e^{\frac{3}{2}}}{E} \cdot \frac{E^2}{144p} \cong 0.001\ \frac{T_e^{\frac{3}{2}} E}{p} \quad \text{(Kgauss, eV, volt/cm, torr)}$$

at $p_o = 0.3$ torr, $T_e = 4$ eV we predict that $Bq = 0.025\ E$.

These results can be compared with our experimental observations. The RSI 003 tube was observed at Ebb = 15 kV, ib = 300 amps, L = 60 cm, p = 0.30 torr, and E = 250 volt/cm to require an interrupting field, Bq, equal to 5 kilogauss, while the predicted interrupting field is 6.25 kilogauss. The RSI 004 tube (at Ebb = 10 kV, ib = 200 amps, L = 16 cm, p = 0.35 torr, and E = 625 volt/cm) required a field of 9.5 kilogauss, while the predicted value equals 13.6 kilogauss.

Considering the number of approximations made in our calculations, the agreement between theory and experiment is remarkably good, although the predicted dependencies of

$$Bq \propto \frac{E}{p} T_e^{\frac{3}{2}}$$

do not agree with the empirical formula of:

$$Bq \propto Ebb^{1.25}\ L^{-0.75}\ ib^{0.25}\ p^{0.23-0.77}.$$

This deviation may be explainable in that the electron temperature of a positive column is a nonanalytical inverse function of rp.

T_e can be evaluated by the use of $T_e = 1.9 \times 10^{-16}\ v_e^2$. Lawson[7] presents a relationship between v_e and E/p:

$$v_e = 4.4 \times 10^7\ (E/p)^{0.29} \qquad (E/p \text{ in the range 0-80 volt/cm} \cdot \text{torr})$$

This relationship must be extrapolated to E/p values as high as 3000 v/cm · torr. The relationship which results is $T_e = 0.37\ (E/p)^{0.58}$ and $Bq = 0.0063\ E^{1.87}\ p^{-0.87}$, which differs from experimental data:

Tube	Ebb (kV)	ib	L (cm)	E	p	Predicted Bq	Observed Bq
RSI 003	15	300	60	250	0.3	547	5
RSI 004	10	200	16	625	0.35	2650	9.5

and from the empirically derived relation:

$$Bq \propto Ebb^{1.25}\ L^{-0.75}\ ib^{0.25}\ p^{0.5\pm0.27}.$$

However, significant extrapolations of data have been made to obtain this result. Furthermore, low T_e may still occur as the result of cooling action of the interaction wall on the discharge, or as the result of a significant amount of low energy secondary electrons. These effects eliminate the high predictions for Bq and cast doubt on the validity of the derived predictions for Bq dependence on Ebb and tube pressure.

A further test of the theory can be made by comparing the predicted values for x_* with the width of the surface damage to the RSI discharge channel walls, and with the image converter observations of discharge column

light intensity during interruption. Figure 76 depicts the cross-sectional geometry of the RSI 003 discharge channel with an approximate contour (presumed) for the plasma column during magnetic constriction. Wall damage along the arc $\widehat{AC}$ can be used to provide an estimate of the average discharge diameter (a) during the energy dissipative portion of the discharge (for $a \ll b$, $a \cong R_1 - \sqrt{(R_1)^2 - (\widehat{BC})^2}$).

For RSI 003 (R_1 = 4.7 mm), slight wall damage occurred along an arc $\widehat{AC}$ of approximately 2 mm, which indicates an $x_* = a/2 \cong 0.05$ mm. At Bq = 6.25 kilogauss, E = 250 volt/cm, our theory predicts that $x_* = 0.07$ mm. Maximum energy dissipation to the wall surface will occur midway through interruption, at which time $B \cong \frac{1}{2}$ Bq, $E \cong \frac{1}{2}$ Ebb, $iRSI \cong \frac{1}{2}$ ib, and $x_* = 0.03$ mm. This latter approaches the theoretical prediction.

For RSI 004 (R_1 = 3.5 mm), heavy wall damage occurred along $\widehat{AC}$ = 2 mm, indicating an $x_* = a/2 = 0.08$ mm. Our theory predicts an $x_* = 0.002$ mm at Bq = 9.5 kilogauss, E = 625 volt/cm, or $x_* = 0.008$ mm at maximum power. Definite fine structure is observable in the wall damage to this tube at AC = 0.13 mm and 0.5 mm, corresponding to $x_* = 0.005$ mm and 0.018 mm, which range close to the predicted x_*. Since both RSI 003 and RSI 004 were operated at lower values of Ebb and Bq, some wider damage tracking would be expected by theory. Therefore, damage assessment observations agree with theoretical calculations within experimental limits.

Image converter observations taken earlier are not as accurate an asessment of discharge diameters as are wall damage assessments due to: (1) light scattering by the channel walls, (2) thermal retention by the wall surfaces during the interrupted pulse, (3) neutral hydrogen afterglows, and (4) the limited quality of the photographs obtained. Results confirm the qualitative nature of the constriction of the discharge during interruption.

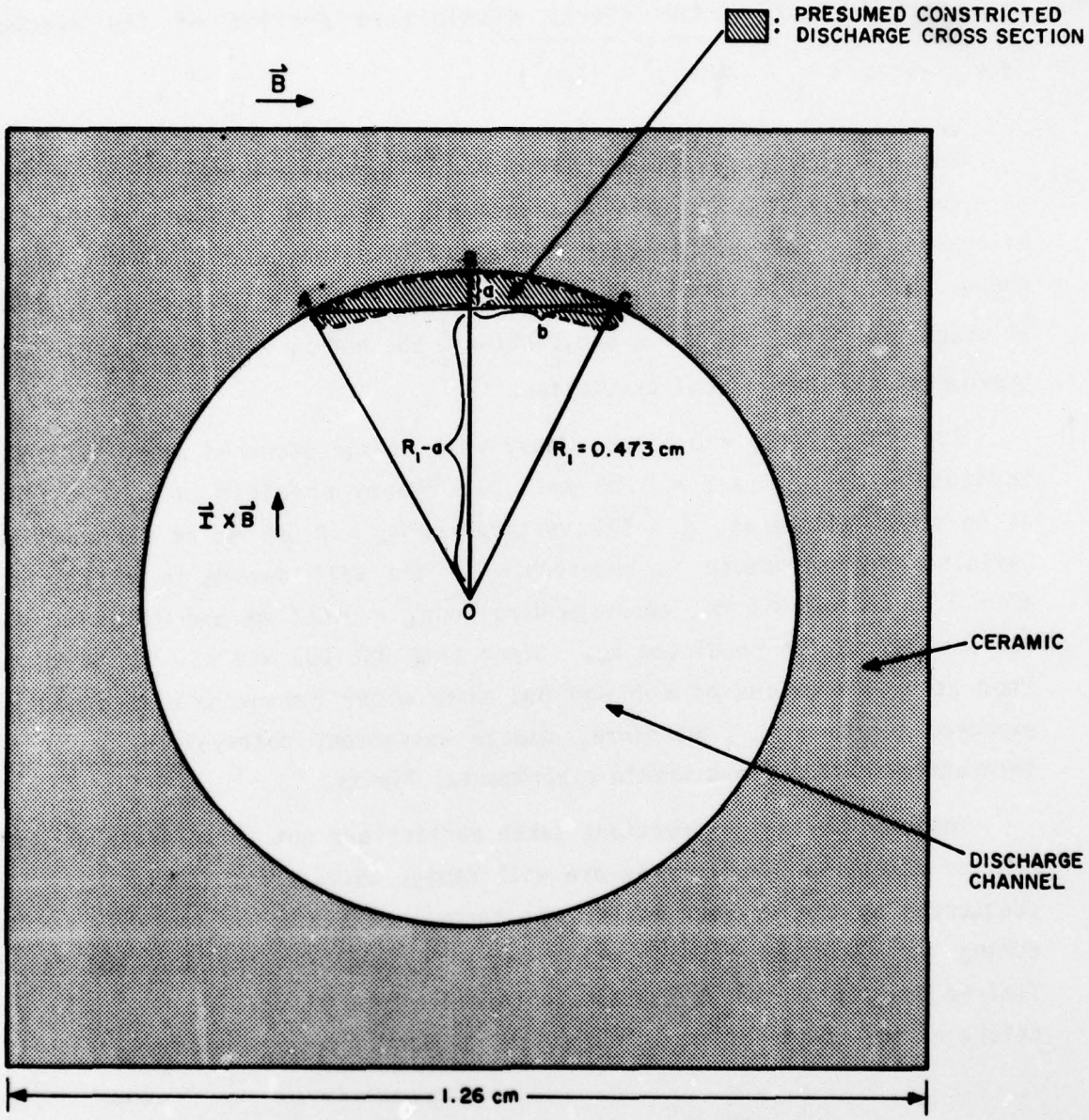

Figure 76. RSI 003 tube and discharge cross-section dimensions.

c. Discharge Instability

Noise and oscillations often appear at varying amplitude levels on the voltage and current waveforms of the RSI tube during interruption. These oscillations appear across the interaction column of the tube at frequencies near 5-10 mHz. This frequency is suspiciously close to the ion cyclotron frequency:

$$\Omega_{H^+}\ (\text{Hz}) = \frac{1}{\pi 2}\ \frac{e\ B}{m_{H^+}} = 15.2 \times 10^6\ B\ (\text{Tesla})$$

Furthermore, the oscillations often appear to act in a beating mode, which could be explained by the superposition of cyclotron frequencies from H^+, H_2^+, H_3^+, etc. (H_3^+ and H_5^+) have been observed at high concentrations in hydrogen discharges (McDaniel[9]).

The observed noise appears at high operating voltages and is not caused by noise pickup by the oscilloscope. Also, the noise appears to contribute to tube current interruption which suggests that an instability or wave is present in the discharge column. This instability appears only under fault conditions and appears to be more important in nonuniform discharge channels.

d. Degree of Ionization of a Discharge Column

A calculation can be made of the degree of ionization of a positive column as a function of column current and channel radius. Assuming that tube current is carried principally by electrons; that $v_e \cong 10^6\ E^{0.5}\ p^{-0.5}$ (Brown[4]); and that $E = 12\ p^{0.5}\ r^{-0.5}$ (subsection 4.b), then the result is obtained:

$$\frac{n_e}{n_{H_2}} = 1.6 \times 10^{-5}\ I^{+1}\ r^{-1.75}\ p^{-0.75} \qquad \text{(amps, cm, torr)}$$

At p = 0.4 torr, I = 300 amperes, this ratio equals $9.5 \times 10^{-3}\ r^{-1.75}$. A plot of this equation at p = 0.4 torr is shown in Figure 77. It is apparent that at I = 300, the discharge column becomes well ionized for r less than 0.1 cm.

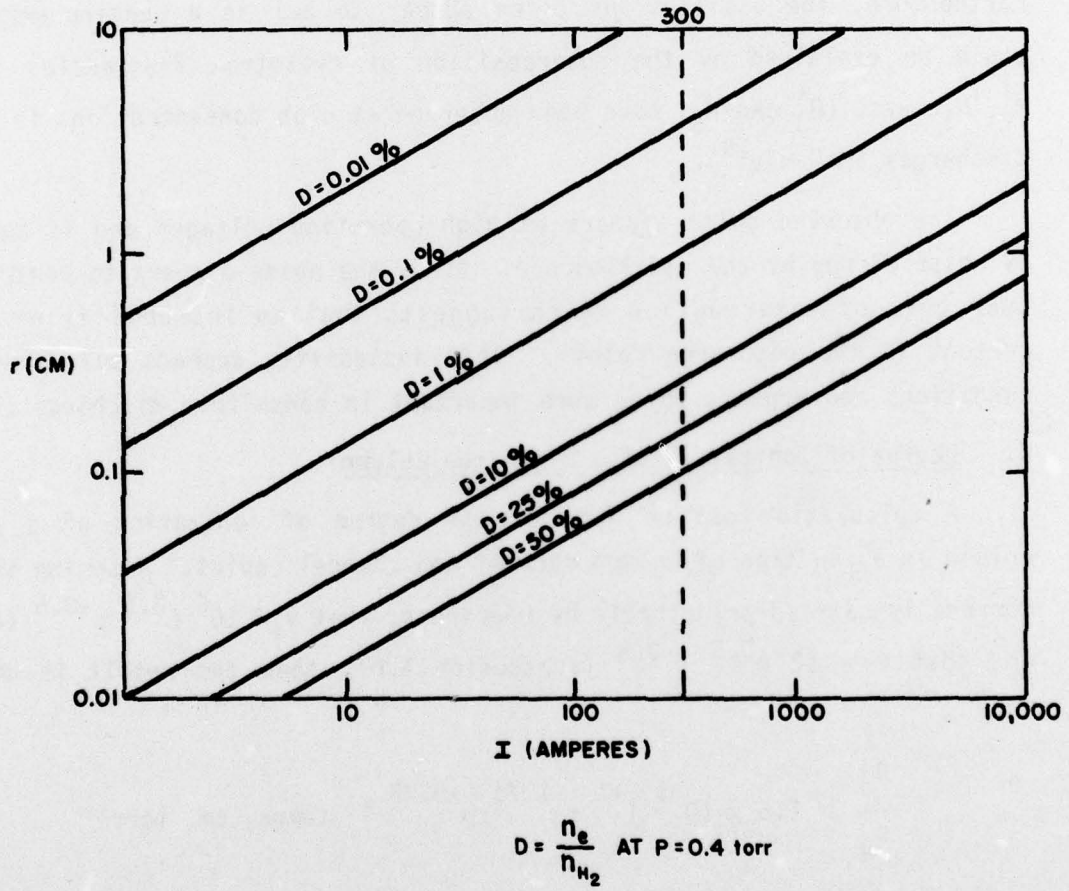

Figure 77. Degree of ionization of a discharge column versus channel radius and current.

This relationship casts some doubt on the validity of previous extrapolations of E/p to low values of rp and suggests that alternative explanations be given to the agreement between theory and experiment as previously reported.

5.0 COMPARISON WITH PREVIOUS EXPERIMENTAL RESULTS

A comparison of the results obtained in the parametric portion of this investigation indicates substantial agreement with previous experimental results. The nature of the interruption process as determined by the current and voltage waveforms appears to be similar to results seen in the 1967 and 1974 studies (Thomas et al.[13], Shackleford[11]). Several data points from these studies are plotted in Figure 58 to demonstrate the apparent relative effectiveness of interruption. Earlier EG&G work indicated a more difficult interruption (Bq levels are considerably higher than those reported here); this may be due to incorrect magnetic field measurements (performed by calculation rather than by measurement), as performed in that study. If the mirror coils used in that study were less effective than theoretically predicted, correlation between experimental results would improve.

The ITT results agree well with results obtained with the RSI 003. This agreement suggests that the coaxial tube design used in that study is not necessary to improve interruption performance, but rather it adds increased magnetic field volume, which reduces the efficiency of the interrupter. The increased voltage drop reported in that study relative to the etd level shown for the RSI 003 is due to the added consideration of anode-grid drop in ITT's figure, which is not included in the RSI 003 series of figures.

6.0 CONCLUSIONS AND RECOMMENDATIONS

a. Conclusions

This program has demonstrated the feasibility of magnetically induced current interruption and has explored the effects of the various tube design parameters on interruption. The important conclusions reached in the course of this study are:

1. The influence of the magnetic field on a discharge column is to propel the plasma in correspondence with the $\vec{I}\times\vec{B}$ force against the channel wall and, if the magnetic field is of sufficient intensity, to thereby cause interruption of the current flowing through the discharge channel. Image converter studies indicated neither retrograde motion of the plasma nor any serious convolutions or disturbances in the column.

Optical studies and damage assessments indicate that a discharge mode exists which represents a constricted glow discharge pressed against the interaction channel wall. Arcing does occur in the discharge column but represents a separate mode recognizable from the former. Arcing appears to occur after current interruption, at times in conjunction with restrike activity.

The use of a chuted-wall interaction channel surface reduces the magnetic field requirement for interruption by one-half to two-thirds.

2. Currents as high as 300 amperes at 15 kV can be successfully interrupted with magnetic field switching energies as low as 5 joules. The total charge transferred during such an interruption is less than 0.003 coulomb, which value is sufficiently low as to preclude damage to the series device being protected.

3. An interaction column voltage drop as low as 300 volts is achievable at the required normal peak tube current, but the total tube drop, which consists of the sum of the column drop and the anode-grid drop, is the factor of real importance if the interrupting and holdoff sections are to be incorporated into a single tube. Further work is required to reduce the total tube drop in order to reduce the power dissipated in the RSI at high average current levels.

4. Hydrogen is the gas of choice for use in an interruptible thyratron due to its reduced resistance to control by the transverse magnetic field.

5. An extrapolation of present data indicates that the magnetic interruption of fault discharges of 1000 amperes at 50 kV is feasible while simultaneously meeting the various other requirements of the technical guidelines as established for Phase II.

b. Recommendations for Further Work

1. Restrike elimination. A primary goal of the continuing work will be the elimination of restriking after a current interruption. Present results show that restriking is eliminated at low plate voltages and low tube pressure with the use of grid bias and magnetic field bias techniques. Efforts will be made to completely eliminate restriking, particularly at high Ebb. Toward this end, work will be done to precisely identify each mode of restrike occurrence to determine whether its cause is internal or external to the RSI, with considerable care taken to prevent external signals from influencing tube performance after interruption.

2. Tube drop. Work will be done to establish the voltage drop of holdoff structures in normal thyratron service and a comparison made with the drop of such structures when they are appended to an interaction column. It may be desirable to modify standard grid-anode structures such that they are specifically suited to RSI usage, although preliminary results obtained during Phase II show that operation at high tube pressure (which reduces the anode-grid voltage drop) may be possible without materially affecting the interaction column drop or the probability of a restrike. Further work will thus be expended to minimize the total tube drop consistent with operation at higher voltage levels.

3. Magnetic field requirements. Efforts will continue to reduce the magnetic field required for interruption consistent with operation at higher power levels. The performance of the RSI 10 series shows that switching performance improves (lower Bq) with the use of irregular wall surfaces (chutes) and shows further that long chute depths are not advantageous as a means of reducing Bq. Varying the dimension of the chute opening and the

angle of attack that the chuted wall presents to the discharge (Figure 78) and altering of the cross-sectional geometry of the channel (Figure 79) may decrease field requirements below those presently encountered. Various combinations of these parameters will be investigated to ensure that the interrupting field is kept to a minimum, particularly as higher voltage tube designs are evolved.

4. Operation at higher voltages. As shown in Table 8, interest in the RSI is directed toward operation at higher voltages (up to 50 kV). Operation at voltages above about 40 kV implies the addition of a gradient grid to the high voltage holdoff structure and also folding of the interaction channel to ensure efficient use of the magnetic field (Figure 80). The performance of 50 kV designs will be investigated at current levels up to 1000 amperes.

5. Triggering requirements. Further testing of the RSI 10 series will be performed to determine how triggering requirements and stability are influenced by forward voltage, impedance level, and the use of a keep-alive system.

6. Life testing. The most successful of the developmental models will be tested at realistic pulse repetition rates and evaluated in terms of hours of operation under non-fault conditions as well as the achievable number of fault interruptions.

The electrical requirements for the RSI development have been extended for the second phase of this program to the specifications presented in Table 8.

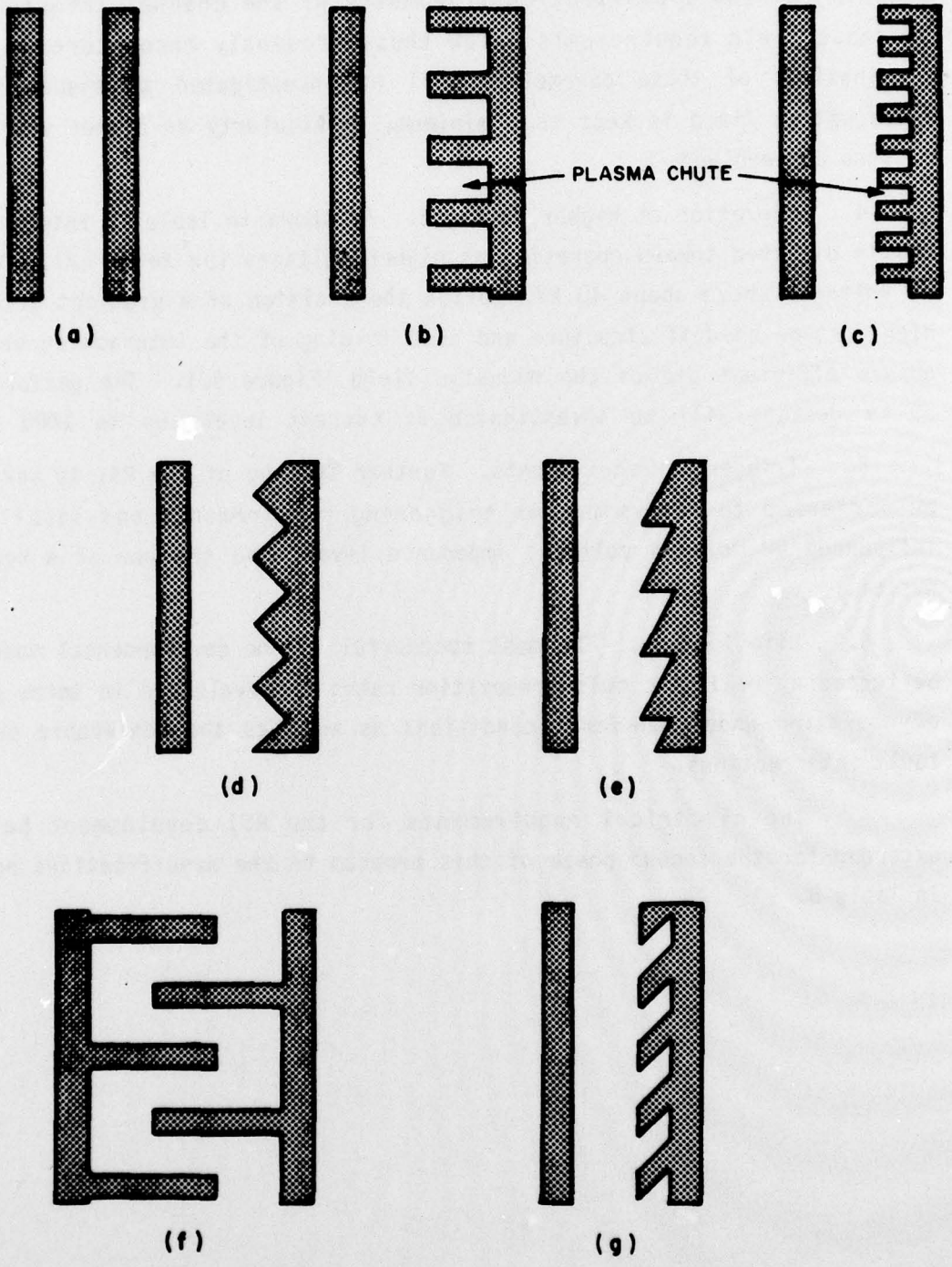

Figure 78. Nonuniform interaction channel longitudinal cross-sections.

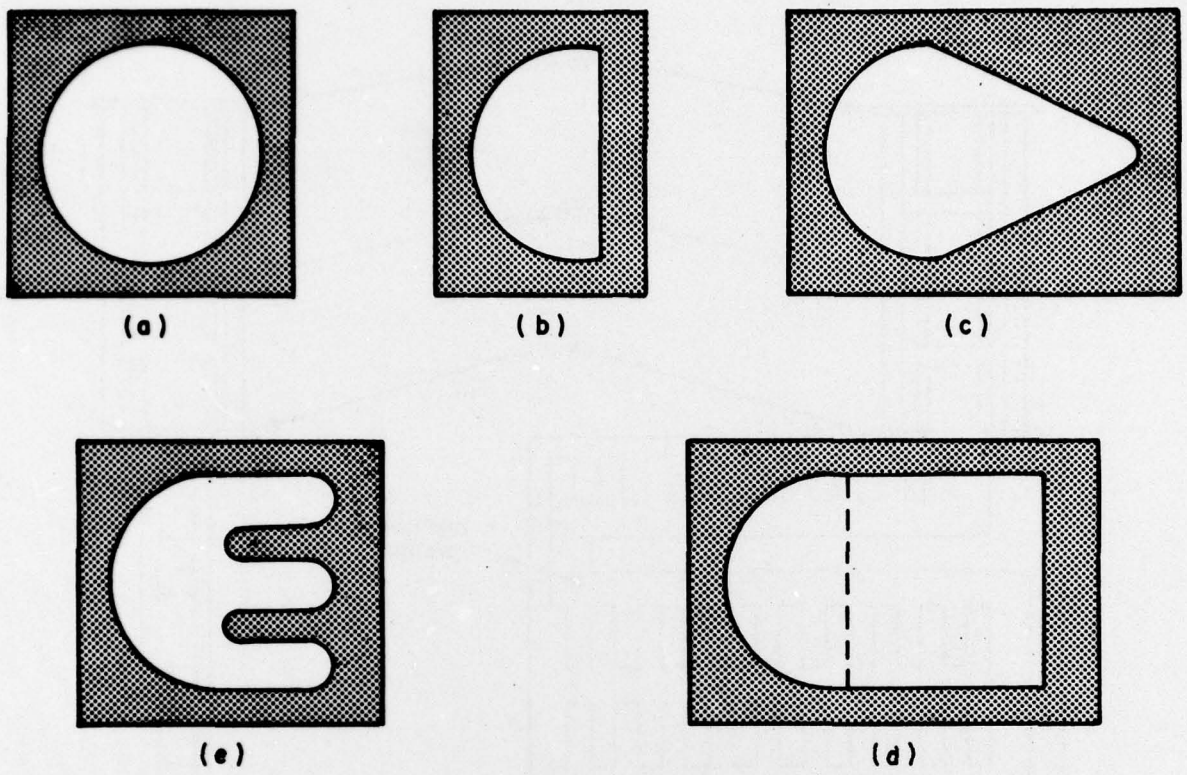

Figure 79. Nonuniform interaction channel lateral cross-sections.

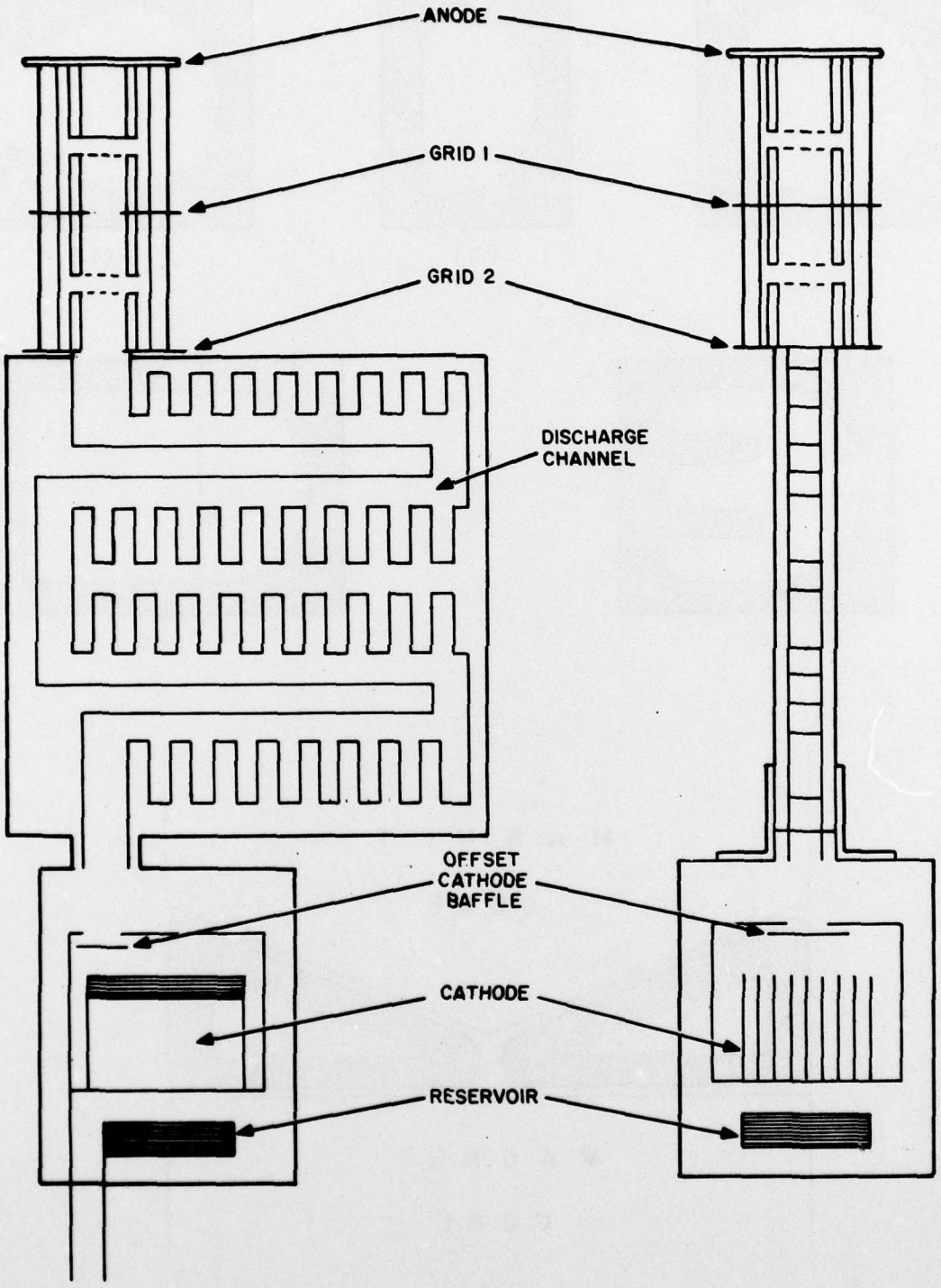

Figure 80. Possible 50 kV RSI design.

Table 8. Amended Specifications for RSI Development.

Open circuit holdoff voltage	Ebb	50 kV minimum
Normally closed voltage drop	etd	500 V maximum
Peak fault current	iRSI	1000 A maximum
Normal average current	Ib	0.7 A maximum
Normal peak current	ib	17 A maximum
Repetition rate	prr	1.0 kHz to 20 kHz (burst mode)
Lifetime		1000 hours, minimum
Operating mode		Normally closed
Opening actions		20,000 minimum
Magnetic field energy		50 joules
Keep-alive power		200 watts

7.0 REFERENCES

1. Breusova, L.N., "Longitudinal Potential Gradient in a Positive Column in H_2 and D_2," Soviet Physics - Technical Physics, Vol. 14, No. 6, December 1969.

2. Breusova, L.N., Radiotekhnika i Elektronika, 10, No. 10, 1865 (1965).

3. Brown, S.C., Basic Data of Plasma Physics, 1959 MIT - Technology Press.

4. Brown, S.C., Basic Data of Plasma Physics, 1966, MIT - Technology Press, p. 80.

5. Goldberg, S., Research Study on Hydrogen Thyratrons, Vol. II, 1956, EG&G, Boston, Mass.

6. Harvey, R. J., and Lutz, M.A., "High Power On-Off Switching with Crossed Field Tube," IEEE Transactions on Plasma Science, Vol. PS-4, No. 4, December 1976, p. 210.

7. Lawson, P.A., and Lucas, J., Proceedings, Physical Society, London, Vol. 85, p. 177.

8. Lutz, M.A., and Hofmann, G.A., "The Gamitron - A High Power Crossed Field Switch Tube for HVDC Interruption," IEEE Transactions on Plasma Science, Vol. PS-2, No. 1, March 1974, p. 11.

9. McDaniel, E.W., Collision Phenomena in Ionized Gases, 1964, Wiley, p. 472.

10. Robinson, T.S. et al, "Current Limitation and Pressure Gradients in the Nonuniform Long Positive Column," Journal of Physics D: Applied Physics (Great Britain), Vol. 3, p. 69.

11. Shackleford, C., "Repetitive Series Interrupter," Technical Report ECOM-73-0320-F, September 1974.

12. Simon, R. and Turnquist, D., "Repetitive Series Interrupter II," Technical Reports ECOM-76-1301-2; ECOM-76-1301-3; ECOM-76-1301-4; ECOM-76-1301-5.

13. Thomas, J., Vanden Brink, H., and Turnquist, D., "New Switching Concepts," Technical Report ECOM-00123-F, October 1967, pp. 75-128.

14. Turnquist, D., "Magnetic Field Control of a Gas Discharge Switch," Proceedings Ninth Modulator Symposium, U.S. Army Electronics Command, May 1966, p. 108.

15. Turnquist, D., "Repetitive Series Interrupter II," Technical Report ECOM-76-1301-1.

16. Von Engel, A., and Steenbeck, M., Elektrische Gasentladungen, Vol. II, J. Springer, Berlin, 1932, p. 82.

17. Weiner, M., "Repetitive Series Interrupter," IEEE Twelfth Modulator Symposium, 1976, p. 224.

18. Wheldon, R.J., "A Thyratron with Magnetic Interruption," Proceedings IEEE, Twelfth Modulator Symposium, 1976, p. 219.

19. EG&G, Research Study on Hydrogen Thyratrons, Report SCL-2471, U.S. Army Signal Corps, 1953.